INVESTIGATION OF ELECTROCHEMICAL PROPERTIES OF PPY/RGO/NICOFE$_2$O$_4$ AS AN ACTIVE ELECTRODE MATERIAL FOR SUPERCAPACITOR APPLICATIONS

Thesis Submitted for the Award of the Degree of

DOCTOR OF PHILOSOPHY

in

Physics

By

Ansari Novman Nabeel Mohammad Haroon

Registration Number: 42000281

Supervised By

Prof. (Dr.) Alok Jain

(Associate Professor)

Department of Physical Sciences

Lovely Professional University

Co-Supervised by

Dr. Kailash Chandra Juglan

(Professor and Associate Dean)

Department of Physical Sciences

Lovely Professional University

LOVELY PROFESSIONAL UNIVERSITY, PUNJAB

2025

Dedicated to my loving parents, wife, and my daughter

Dr. Haroon, Ansari Parveen, Ansari Ammara Firdaus, and Arhama Firdaus

DECLARATION

I, hereby declared that the presented work in the thesis entitled "Investigation of electrochemical properties of PPy/rGO/$NiCoFe_2O_4$ as an active electrode material for supercapacitor applications" in fulfilment of the degree of **Doctor of Philosophy (Ph. D.)** is outcome of research work carried out by me under the supervision of Dr. Alok Jain, working as Associate Professor and Head at Examination, in the School of Chemical Engineering and Physical Sciences of Lovely Professional University, Punjab, India. In keeping with general practice of reporting scientific observations, due acknowledgments have been made whenever work described here has been based on findings of other investigator. This work has not been submitted in part or full to any other University or Institute for the award of any degree.

(Signature of Scholar)
Name of the scholar: Ansari Novman Nabeel
Registration No.: 42000281
Department/school: School of Chemical Engineering and Physical Sciences
Lovely Professional University,
Punjab, India

CERTIFICATE

This is to certify that the work reported in the Ph. D. thesis entitled "Investigation of electrochemical properties of PPy/rGO/$NiCoFe_2O_4$ as an active electrode material for supercapacitor applications" submitted in fulfillment of the requirement for the award of the degree of **Doctor of Philosophy (Ph.D.)** in in the School of Chemical Engineering and Physical Sciences, is a research work carried out by Ansari Novman Nabeel, 42000281, is bonafide record of his original work carried out under my supervision and that no part of thesis has been submitted for any other degree, diploma or equivalent course.

(Signature of Supervisor)
Name of Supervisor: Dr. Alok Jain
Designation: Associate Professor and Head at Examination
Department/School: School of Chemical Engineering and Physical Sciences
University: Lovely Professional University

(Signature of Co-Supervisor)
Name of Co-Supervisor: Dr. Kailash Chandra Juglan
Designation: Professor & Associate Dean
Department/School: School of Chemical Engineering and Physical Sciences
University: Lovely Professional University

Abstract

The study of supercapacitors, a cutting-edge technology with a high-power density, extended lifespan, and quick charge-discharge time. They could be used in renewable energy storage systems, electric cars, and portable electronics. The characteristics of the electrode materials, which must have remarkable conductivity, stability, and efficient charge storage, have a major influence on the effectiveness of supercapacitors. Among the many options, their complementary electrochemical properties have drawn a lot of attention for transition metal oxides, including the polypyrrole (PPy), reduced graphene oxide (rGO), and nickel-cobalt ferrite ($NiCoFe_2O_4$).

This doctoral thesis focuses on developing efficient electrode materials for supercapacitor applications by exploring different composite formulations of PPy, rGO, and $NiCoFe_2O_4$. The synthesis was carried out using cost-effective and scalable methods, including the Modified Hummers' method for rGO, sol-gel auto-combustion for $NiCoFe_2O_4$, and chemical oxidative polymerization for PPy. Initially, rGO was synthesized using the Modified Hummers' method, while $NiCoFe_2O_4$ nanoparticles were produced via Sol-gel auto-combustion. To obtain binary composites, rGO was incorporated during the $NiCoFe_2O_4$ synthesis process. In the next step, polypyrrole monomers were introduced into the binary composite using chemical oxidative polymerization to form ternary composites. Additionally, a PPy/rGO composite was synthesized by adding rGO during the polymerization of PPy. The composites were developed with varying nickel content (0, 20, 40, 60, 80, and 100%) to gain insight into how composition affects electrochemical performance.

Structural and morphological characteristics of the synthesized materials were investigated using X-ray diffraction (XRD), Fourier-transform infrared spectroscopy (FTIR), and field emission scanning electron microscopy (FESEM). Moreover, electrochemical study was examined using cyclic voltammetry (CV), galvanostatic charge-discharge (GCD), and electrochemical impedance spectroscopy (EIS) revealed. All electrochemical tests were conducted using 3M KOH as the electrolyte.

In the cyclic voltammetry experiment, the PPy/rGO composite electrode generates a specific capacitance (C_P) of 365.1 F/g at a scan rate of 10 mV/s. In the Galvanic Charge Discharge investigation, the C_P for 2 Ag^{-1} was 375 Fg^{-1}. The binary rGO/$NiCoFe_2O_4$ composite has a C_P of 216.5 F/g, while the ternary composite system showed a significant improvement in performance with a C_P of 664.98 F/g. The C_P values of the binary and ternary composites are around 275 F/g and 720 F/g, respectively, according to an additional GCD investigation. Furthermore, the ternary composite displayed much improved values at 90 Wh/kg and 1167.14 W/kg. However, the binary composite displayed a power density (P_d) of 1135.15 W/kg and an energy density (E_d) of 34.37 Wh/kg. Among all the composites, PRNC80 (Ppy/rGO/$NiCoFe_2O_4$ 80%) had the greatest electrochemical performance, with a C_P of 742.85 F/g in CV measurements and a P_d of 1234.6 W/kg in GCD tests. It had an E_d of 32.19 Wh/kg. PRNC80 may find application in supercapacitors due to its superior electrochemical efficiency compared to other composites.

Acknowledgments

I begin by expressing my gratitude to the Almighty Allah for blessing me with the gift of learning and fostering a spirit of knowledge-seeking. May this acquire wisdom guide not only myself but also those connected to me on the righteous path, both in this world and the hereafter.

I extend my heartfelt appreciation to my research supervisor, Dr. Alok Jain, and Co-Supervisor, Dr. Kailash Chandra Juglan, for their unwavering attention, guidance, and invaluable insights that helped me navigate challenges and overcome obstacles. Their expertise and thoughtful suggestions have truly enriched the significance of this work.

My sincere thanks go to the Head of the Department (HOD), Dr. Kailash C. Juglan, and all faculty members of the Physics Department for their unwavering support. Gratitude is also extended to research scholars, technical and non-technical staff, and friends who have played pivotal roles in this journey.

Special thanks go to my dear friends Ammara Firdaus, Shoaib Khan, Dr. Prabhpreet Kaur, Rauf Khan, Anuj Garg, and Asha Saini Mam for their unwavering encouragement.

Lastly, my profound gratitude to my parents, whose unwavering support—financially, morally, and inspirationally—made this work possible. I am forever indebted to them, and I pray for their happiness and good health, bestowed by the Almighty.

Ansari Novman Nabeel

Table of Contents

List of Tables

List of Figures

CHAPTER 1

CHAPTER 2

Figure 2.2: The specific capacitance of the as-synthesized PPy coated fabric (a), and the fabric after being stretched to 100% for 1000 times (b) at different scan rates

Figure: 2.3 (a) Cycling tests of flexible polypyrrole electrodes for 3000 cycles in different electrolyte environments (v ¼ 50 mV s¡1). (b) Galvanostatic charge-discharge curves for polypyrrole film against bare graphite at current density 0.2 mA cm¡2 in different electrolyte environments. c) Photograph of symmetric polypyrrole electrodeposited on graphite based flexible tape electrodes in Reline deep eutectic solvent

Figure 2.4. Electrochemical performance of supercapacitors made of e-PPy and c-PPy. (a) CV curves at scan rates of 1 mV/s and 5 mV/s. (b) GCD curves at different charging/discharging specific currents of 1 A/g and 0.16 A/g. (c) Capacitances as functions of scan rates. (d) Capacitances as functions of charging/discharging specific currents

Figure 2.5. (a) Cyclic voltammetric curves at a scan rate of 100 mV/s; (b) Specific capacitance per gram of active material. (c) Galvanostatic charge/ discharge profiles of the PPy-AC 50 mV at different current densities. (d) Cycling stability of PPy-AC 50 mV measured by galvanostatic charge/ discharge at current density of 10 A/g. (e) SEM images of PPy-AC 50 mV collected before and after testing 1000 cycles. All measurements were performed by 3-electrode system in 0.5 M H2SO4 aqueous electrolyte

Figure 2.6: preparation steps for Flexible all-solid-state supercapacitors composed of reduced graphene oxide/polypyrrole films

Figure 2.7: TEM images of (a) PPy nanowires and (b) GO/PPy composites, (c) The specific capacitances of GO, PPy and GO/PPy composites at different scan rates

Figure 2.8: (a) Representative galvanostatic charge–discharge curves at 0.5Ag−1, (b) rate performance with current density variation from 0.5 to 5Ag−1, and (c) charge–discharge cycling performance at the current density of 1.0Ag−1 of PPy, Hy-RGO/PPy,

CHAPTER 4

CHAPTER 5

CHAPTER 6

CHAPTER 1

Introduction

1.1 Introduction

The cost of non-renewable energy sources like coal, uranium, natural gas, and oil has gone up recently, and the requirement is that the development of alternative energy sources, especially renewable energy, be given top priority in all countries. The use of non-renewable energy resources poses serious environmental issues. Moreover, the depleted non-renewable energy resources can't be restored in a short period of time. Renewable energy sources, such as solar, wind, water, geothermal heat, and biomass, produce energy. The technologies associated with renewable energy harness these resources to produce electricity, heat, chemical compounds, or mechanical power. Additionally, there is an increasing demand for storage solutions with enhanced capacity to store energy during surplus periods and release it as needed. Non-renewable energy sources like coal, petroleum, and fossil fuel cannot be regenerated in a short period once exhausted. Renewable energy will be the alternate energy resource that will safeguard the citizens from environmental pollution. However, the main disadvantage of renewable energy is that it is seasonal and not available continuously. Recently, a higher amount of energy has been produced from solar and wind. But the electricity generated from these resources cannot be stored easily. Electrical energy produced by non-renewable resources such as coal, diesel, etc., can be controlled, and around 10 to 20% of it can be stored through efficient energy storage devices. So, it is crucial to develop and improve the capacity of energy-storage devices with high efficiency to overcome the energy storage problem in the coming years.

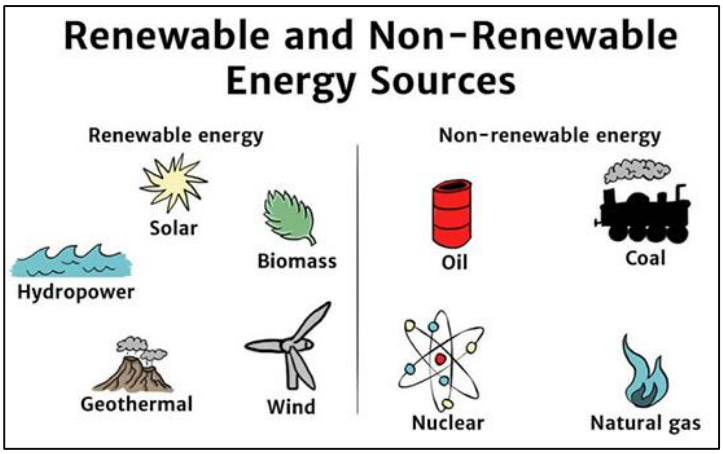

Figure 1.1: Renewable and Non-Renewable Energy Sources

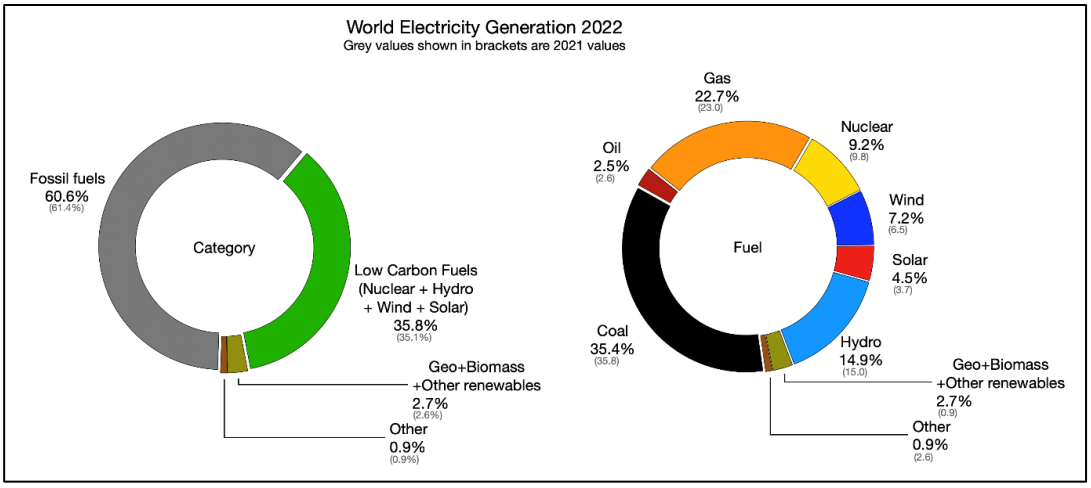

Figure 1.2: World electricity generation data (Source: https://www.worldenergydata.org/world-electricity-generation/)

In fact, the charge is normally stored to some extent in batteries, super capacitors, fuel cells, etc. In the subsequent sections, the basics of energy-storing mechanisms and their salient characteristics are discussed

1.2 Fuel cells

Fuel cells are modern and innovative devices that convert chemical energy directly into electricity and thermal energy without being subjected to the normal charging procedures. Only in a case when fuel is properly fed and with necessary regularity, the cells have to pursue the principle of constant reaction. This feature makes it possible

for them to work non-stop without the need for replacement, hence reliability. Because the fuel cells are more effective than the traditional methods of thermomechanical conversion because of processes requiring combustion, the energy conversion efficiency highly increases to range between 40% and 60%.

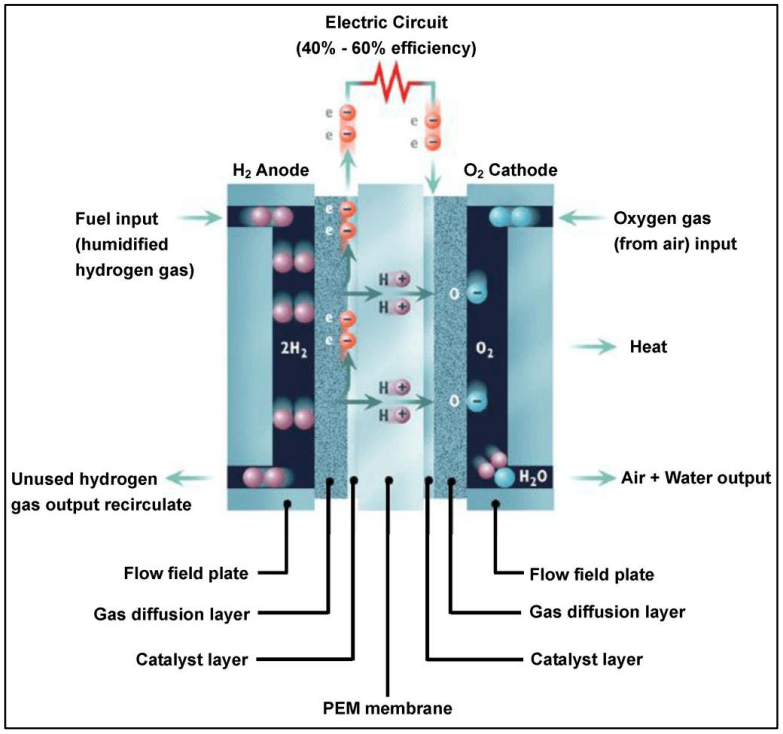

Figure 1.3: Fuel cell (PEM) working principle (Source: https://www.fuelcellstore.com/blog-section/fuel-cell-characterization)

This, along with high efficiency, leads to by-products of an environmentally benign nature, like water and heat; hence, fuel cell technology evolves as one of the most sustainable and cost-efficient reliable solutions to power generationOne of the most powerful energy storage technologies available today is the fuel cell, rated at an extremely high energy density (E_d) exceeding 500Wh/kg. In this sense, its power density is relatively low in applications that have high energy. Their use is relatively poor. Simply put, a fuel cell has three major elements: the anode, the cathode, and the electrolyte, which may vary from one kind to another. The main cause of this variation is the electrolyte, of which some options include aqueous alkaline solutions, polymer membranes, and ceramic oxides.

A particularly prevalent design in fuel cell technology is the hydrogen proton exchange membrane (PEM) fuel cell. This design uses hydrogen gas at the anode, on which a

catalyst is placed that helps in the oxidation reaction of hydrogen, producing protons (hydrogen ions) and electrons [1]. This PEM has an exclusive engineering in such a way that it allows only the protons to get through to the anode side; hence, electrons accumulate at the cathode. Such electrons, when connected through an outer circuit, get attracted to the cathode, where they come together again with protons and oxygen to yield water. Thus, the energy conversion cycle is complete. This will, however, form an underlying possibility through which fuel cell technology opens doors for the future, which would be more helpful toward a cleaner and energy-efficient world.

1.3 Battery

By permitting electrons to go from an anode to a cathode in a circuit, A battery turns chemical energy into electrical energy, which is an energy storage device. The three fundamental parts of a battery are the electrolyte, cathode, and anode. Batteries are categorized into primary and secondary based on their working principle. They come in different sizes as well as different material compositions.

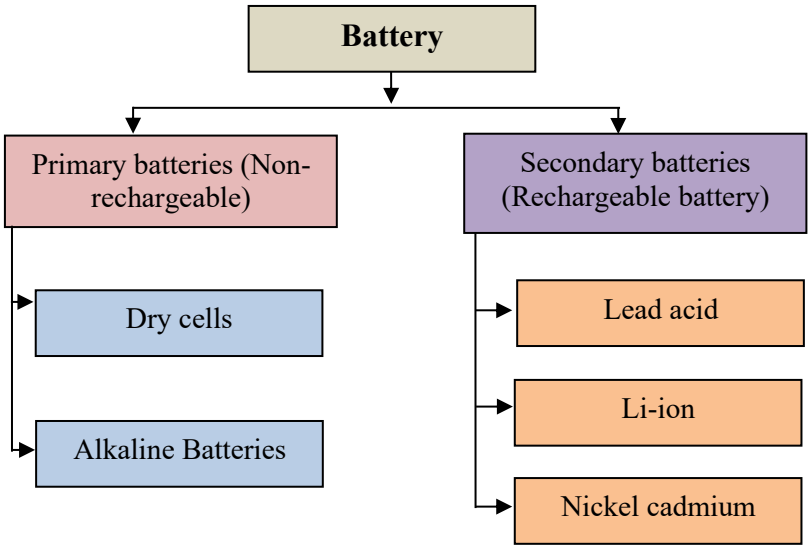

Figure 1.4: Different types of batteries

Dry cell Leclanche is an example of a primary battery. A dry cell is comprised of Zinc, Carbon, MnO_2, $ZnCl_2$, NH_4Cl, where Zinc acts as a negative terminal and the positive terminal consists of MnO_2, $ZnCl_2$, NH_4Cl, C powder, and a limited level of water pasted over a C rod. During a chemical reaction, Zn undergoes oxidation and

releases electrons, which flow to the other negative terminal. The potential developed in the dry cell is about 1.5V. However, the dry cell has some disadvantages, such as leakage issues and spontaneous chemical reactions when the cell is not in use, which reduces the life span and efficiency of the dry cell.

Figure 1.5: Dry cell components and commercial dry cell

The chemical reaction occurs in dry cell as follows,

The overall reaction occurring in the dry cell produces **1.5 volts**:

anode			$Zn(s)$	⟶	$Zn^{2+}(aq)$	+	$2e^-$	
cathode	$2\ e^-$	+	$2\ NH_4^+(aq)$	⟶	$2\ NH_3(g)$	+	$H_2(g)$	
	$2\ NH_3(g)$	+	$Zn^{+2}\ (aq)$	⟶	$[Zn(NH_3)_2]^{2+}(aq)$			
	$H_2(g)$	+	$2\ MnO_2(s)$	⟶	$Mn_2O_3(s)$	+	$H_2O(l)$	
$Zn(s)$	+ $2\ NH_4^+(aq)$	+	$2\ MnO_2(s)$	⟶	$[Zn(NH_3)_2]^{2+}(aq)$	+	$Mn_2O_3(s)$	+ $H_2O(l)$

The alkaline battery is also an example of a dry battery discovered in the year 1950, The alkaline cell also has a leakage issue as it uses potassium hydroxide as an electrolyte. The following figure shows an example of alkaline battery components and commercial alkaline batteries in the market.

Figure 1.6: Dry cell (Alkaline battery) components and commercial alkaline battery

An alkaline battery generally consists of a MnO_2 cathode and Zn anode, which undergo a chemical reaction spontaneously. The chemical reaction of an alkaline battery is as follows:

First half reaction,

$Zn\ (s) + 2HO^-\ (aq) \rightarrow Zn(s) + H_2O\ (l) + 2e^-\ (e^o = -1.28\ V)$

Second half reaction,

$2MnO_2\ (s) + H_2O\ (l) + 2e^- \rightarrow Mn_2O_3\ (s) + 2HO^-\ (aq)\ (e^o = +0.15V)$

Overall reaction,

$Zn\ (s) + 2MnO_2\ (s) \rightleftharpoons Mn_2O_3 + Zno\ (s)\ (e^o = 1.43\ V)$

One type of secondary battery is the lead acid battery. which comprises cells attached in series and produces a voltage of around 2 V. The lead acid battery is constructed using Pb (cathode) and PbO (anode) submerged in a sulphuric acid electrolyte solution. The general chemical reaction that occurs in the lead acid battery is as follows:

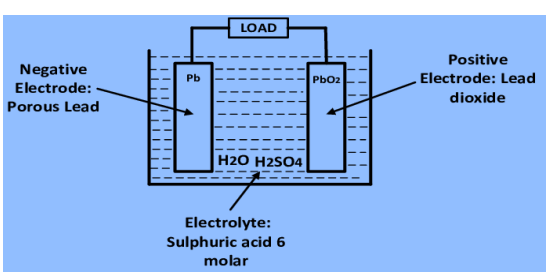

Figure 1.7: Lead acid battery construction (left) and commercial battery (right)

Lead acid battery chemical reaction during discharging

Negative:

$Pb(s) + HSO_4^- + H_2O(l) \rightarrow 2e^- + PbSO_4(s) + H_3O^+(aq)$ (oxidation)

Positive:

$PbO_2(s) + HSO_4^-(aq) + 3H_3O^+(aq) + 2e^- \rightarrow PbSO_4(s) + 5H_2O(l)$ (reduction)

Lead acid battery chemical reaction during recharging

Negative:

$2e^- + PbSO_4(s) + H_3O^+(aq) \rightarrow Pb(s) + HSO_4^- + H2O(l)$ (reduction)

Positive:

$PbSO_4(s) + 5H_2O(l) \rightarrow PbO_2(s) + HSO_4^-(aq) + 3H_3O^+(aq) + 2e^-$ (oxidation)

Normally, the electrolyte is added to the acid from 20% to 40%. Thereafter, the anode and the cathode, together with the electrolyte, respond, initiating a chemical reaction in such a way that lead sulfate forms, and the release of electrical energy takes place during the discharge of the battery. The chemical reaction is reversible and can be recharged. Lead acid battery construction is very simple, yet can be recharged and discharged at very high speeds, hence allowing for a huge output of power. These are the characteristics that make lead-acid batteries an ideal choice for delivering that surge of power required in vehicles like cars and bikes. On the other side, the lead acid battery has some disadvantages such as a short life span, toxic Pb as electrode, and occupying large space. The lead acid battery is replaced with a new one after its damage.

Secondary batteries include, for instance, lithium-ion batteries; they were first discovered in 1990. Lithium-ion batteries have been used in almost all electronic gadgets due to their unique characteristics, like being lightweight, having a low self-discharge rate of just 1.2% per month, having long cyclic stability, and possessing high operating voltage and power density. The more advanced lithium-ion batteries display 5000 charge-discharge cycles and exhibit high stability [2]. The Li ion battery consists of the cathode ($LiCoO_2$, $LiNiO_2$, $LiFePO_4$) and an anode (stacked graphite), which are coated over respective current collectors. The $LiPF_6$ salt dissolved in carbonate is used as an electrolyte, which is sandwiched between two electrodes with the help of a separator [3]. During discharging, because of a minimal variation in the concentration of the electrolyte, the lithium ions in the anode get ionized. The electrolyte transports the ionized ions to the cathode, and then the lithium atoms get deposited on the cathode, gaining an external electron.

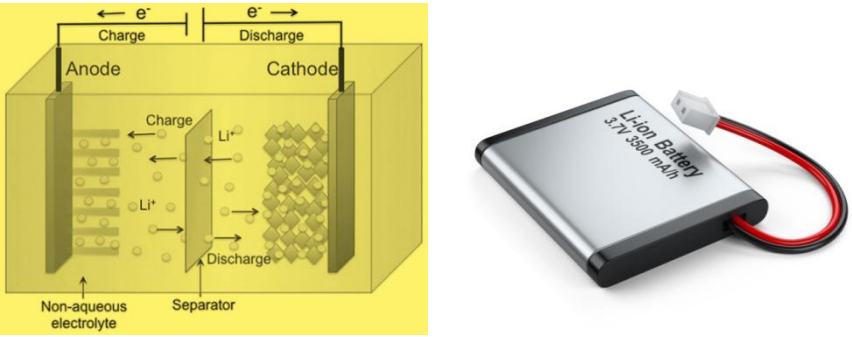

Figure 1.8: Working principle of Lithium-ion battery and commercial Li ion Battery

In the anode, due to the mobility of lithium ions, free electrons are generated that flow towards the cathode and recombine with lithium ions. Similarly, the reversible mechanism takes place during charging. The operating procedure of the Li-ion battery is displayed in Figure 1.7, and the chemical reactions that occur in the Li-ion batteries are provided below:

At anode:

$$Li_{1-x}CoO_2 + xLi^+ + xe^- \leftrightarrow LiCoO_2$$

At cathode:

$$Li_xC_6 \leftrightarrow xLi^+ + xe^- + C_6$$

Overall chemical reaction:

$$LiC_6 + CoO_2 \leftrightarrow C_6 + LiCoO_2$$

Ni-Cd battery is yet another example of a secondary battery which consists of NiOOH (+ve), metallic cadmium (-ve), and KOH electrolyte. The electrodes are isolated by a nylon divider that controls the direct charge transmission between the electrodes. The charge-storing capacity is based on the redox reaction that takes place between two electrodes. The charging and discharging process of Ni-Cd battery is shown in figure.

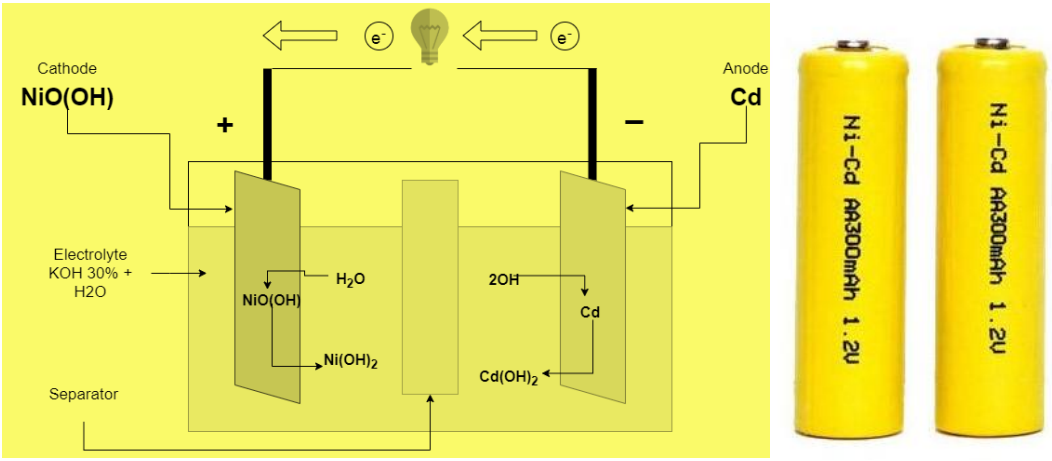

Figure 1.9: Ni-Cd battery charging/discharging process and commercial battery

The chemical reaction of Ni-Cd battery and over all reaction is given below.

At anode:

$$Cd + 2OH \leftrightarrow Cd(OH)_2 + 2e^-$$

At cathode:

$$NiOOH + H_2O + 2e^- \leftrightarrow Ni(OH)_2 + OH$$

Overall chemical reaction:

$$2NiOOH + Cd + 2H_2O \leftrightarrow 2Ni(OH)_2 + Cd(OH)_2$$

However, Ni-Cd battery is not environmentally friendly and Cd used as electrode is toxic metal which is polluting the environment severely.

1.4 Supercapacitor

Energy demand has increased in modern times, creating an urgent need to develop sustainable solutions to meet these demands. Although they are thought to be a potential alternative, rechargeable batteries' power density and cycling life restrict their ability to meet energy demands. A supercapacitor is an energy storage system that boasts high P_d and specific capacitance (C_P). Supercapacitors release energy quickly and with high density over short periods. Such devices are essential for a variety of uses, from supplying electricity to portable electronics to helping integrate renewable energy sources into the electrical grid. [4].

Another name for supercapacitors is electrochemical capacitors are a type of energy storage devices that offer an advantage over conventional batteries and capacitors. Supercapacitors fill the void left by traditional capacitors as they possess fast charge/discharge with short time and high energy storage capacity. These properties make supercapacitor application into a wide range of electronic items. Following Ragone's plot, illustrate the E_d and power of different electrical energy storage devices. [5]. Supercapacitors replace batteries used in e-vehicles, as the e-vehicle needs high power in a short time during acceleration. Even though a supercapacitor has some advantages towards many high-energy required devices, it has disadvantages like low energy density [6]. The low E_d of a supercapacitor could be improved by selecting the right materials with proper engineering. As is well known, a supercapacitor's C_P and cell voltage determine its energy density using the following formula:

$$E_d = \frac{1}{2} CV^2 \qquad 1.1$$

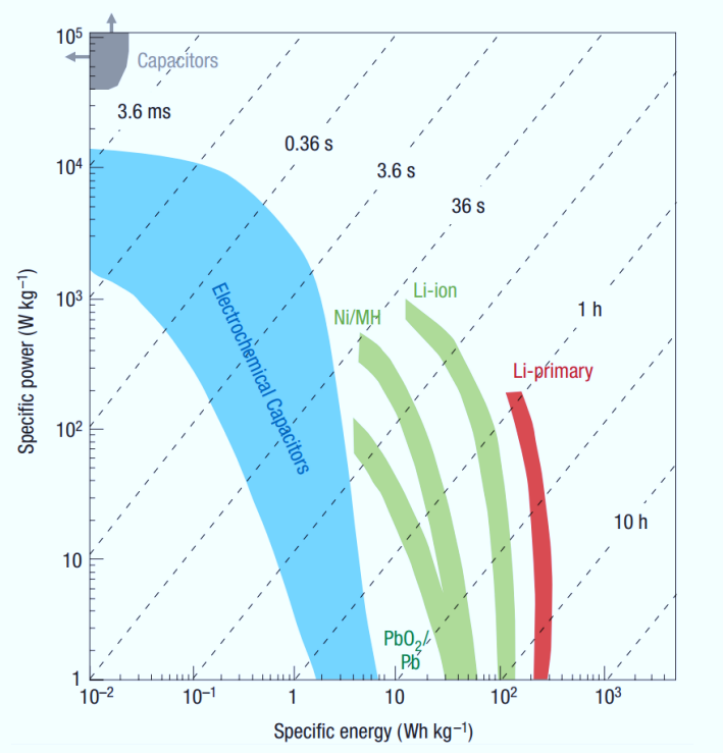

Figure 1.10: Specific power against specific energy, also called a Ragone plot, for various electrical energy storage devices (Source: [5])

1.5 Classification of Supercapacitors

Depending on how they store energy, the supercapacitors are classified as hybrid capacitors, electrochemical double-layer capacitors, and Pseudocapacitors. The pictorial representation depicts the classification of supercapacitors.

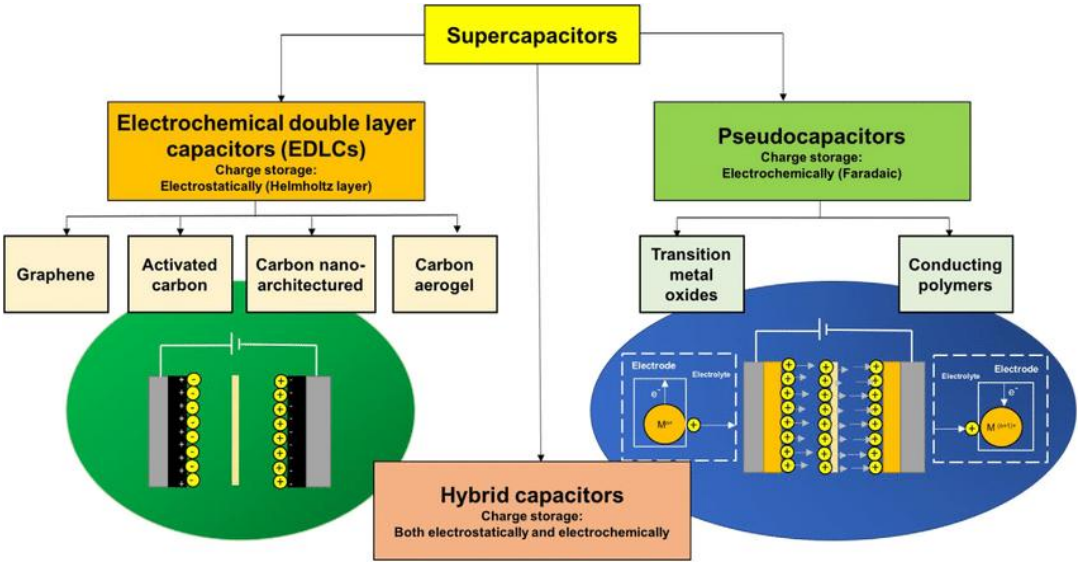

Figure 1.11: Classification of supercapacitors (Source: [7])

1.5.1 Electric Double-Layer Capacitor

Electrochemical double layer capacitance (EDLC) stores charge on the electrode electrostatically, therefore producing great energy density and fast charge/discharge rates. Because of this fundamental idea, EDLCs may provide high power and exceptional cycling stability, which makes them appropriate for electronic devices that need long-term stability and quick energy transfer. The following figure illustrates the charge storage principle of EDLC.

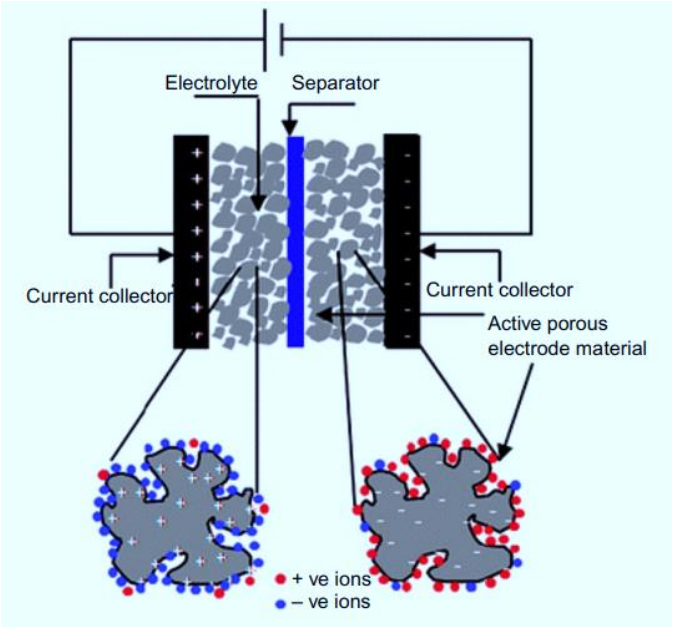

Figure 1.12: Charge storage process in EDLC

A supercapacitor based on EDLC is constructed using graphene, activated carbon, and carbon aerogel, where charge accumulation occurs at the electrode/electrolyte contact by ion adsorption and desorption [8]–[10]. The electrochemical storage process in Electric Double-Layer Capacitors (EDLCs) mirrors the dielectric characteristics seen in traditional capacitors, as it proceeds without any chemical changes (faradaic reactions) contributing to the storage of energy. The appeal of EDLC materials lies in their significantly high surface area, commendable electrical conductivity, and robust mechanical strength, though they are limited by their relatively modest C_P.

1.5.2 Pseudocapacitors

Pseudocapacitors, Faradaic capacitors, or redox capacitors distinguish themselves through the storage of energy by means of fast and reversible chemical reactions at the material's surface. The charge storage mechanism of a Pseudocapacitors is schematically represented in the following figure. Faradaic capacitors or Pseudocapacitors are different from electrostatic or EDLC capacitors. When a potential is applied to an FS, quick and reversible A Faradaic current flows through the supercapacitor cell as a result of Faradaic reactions (redox reactions) that occur on the electrode materials and entail the transport of charge across the double layer, similar to

the processes that batteries use to charge and discharge. Research is vigorously underway to identify optimal materials for Pseudocapacitors. Transition Metal Oxides (TMOs) are notable for their high C_P and energy levels, whereas Conductive Polymers (CPs) are recognized for their excellent conductivity, positioning them as ideal choices for advanced supercapacitor applications [11]–[13]. However, CPs are hindered by their limited cycle life, attributed to the polymers' dimensional changes with each charge and discharge cycle. TMOs, in contrast, are challenged by their low electrical conductivity, which impedes their ability to achieve maximum capacitance values.

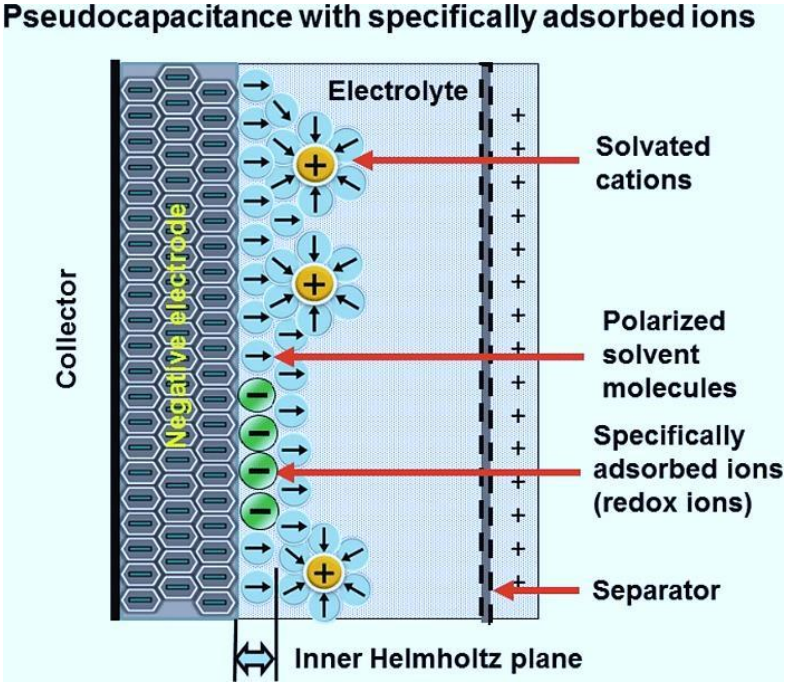

Figure 1.13: Charge storage mechanism of pseudo capacitors

1.5.3 Hybrid supercapacitors

Hybrid supercapacitors integrate the features of pseudocapacitors and electrical double-layer capacitors, allowing both Faradaic and non-Faradaic charge storage processes to occur. Generally, one electrode undergoes redox reactions while the other accumulates charge electrostatically. This combination can improve the energy density and cycling stability compared to using either type alone. Nevertheless, maintaining a balanced interaction between the two electrode materials is still a major challenge. In the present study, a PPy/rGO/$NiCoFe_2O_4$ composite was developed to achieve a strong synergistic effect between these mechanisms and thereby enhance overall electrochemical

performance. The electrochemical performance would be enhanced when combined with both EDLC and pseudocapacitive behaviour. This type of hybrid supercapacitor could increase E_d as well as P_d without compromising the structure and stability of the system [14]–[16].

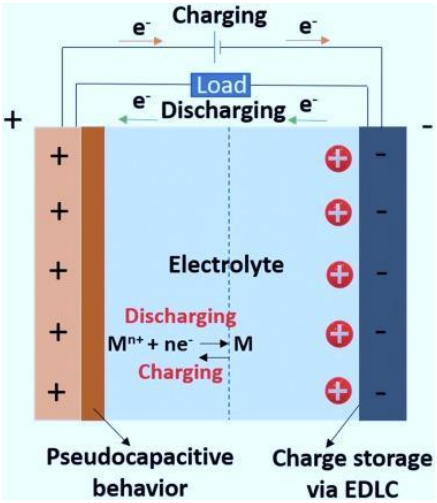

Figure 1.14: Charge storage mechanism in hybrid capacitors (Source: [17])

A hybrid supercapacitor's high energy density serves as one of its advantages, as well as its rapid kinetics and a long life cycle, which is achieved by constructing with suitable electrodes [18]. The challenging aspect for hybrid supercapacitors is to develop material that exhibits high E_d near to battery without altering high power density and long cycle [19]. The development of highly porous structured material is the key to achieving enhanced capacitance. The improvement of C_P is linked with EDLC and pseudocapacitive electrode, while increasing cell voltage is linked with hybrid supercapacitors, resulting in notable advancements in electrochemical performance and application. The development of nano-sized materials with shortened diffusion paths is also considered to be another aspect of improving electrochemical performance. This technique is mainly relevant to supercapacitors and rechargeable batteries. Furthermore, combining battery-type and supercapacitor-type electrodes to develop hybrid supercapacitors has led to higher energy densities and voltages. A key advantage of these hybrid supercapacitors is their faster recharging times compared to traditional lead-acid batteries and other rechargeable batteries. The primary goal is to achieve energy densities for hybrid supercapacitors within the range of 20–30 Wh/kg.

1.6 Major components of a supercapacitor

All the components have important roles in the supercapacitor's electrochemical performance. Supercapacitors, popularly known as ultracapacitors, are distinct categories of energy storage devices that fill the void left by batteries and traditional capacitors. They contain some noteworthy parts that work in combination to release the energy stored into the track. The important parts of supercapacitors include:

Electrode: These are the main parts that are used for storing the electrical charges. An example of materials that are mostly used during the preparation of electrodes includes those having very high surface areas, such as metal oxides for Pseudocapacitors, graphene, carbon nanotubes, or activated carbon. Nonetheless, the electrode material plays a crucial role in controlling the supercapacitor's overall performance, which includes many elements including capacitance, E_d, and P_d, among others. The following section describes the materials that are currently employed in supercapacitors, including PPy, rGO, and ferrite-based materials.

Electrolyte: The charging and discharging process uses this as the medium for ion transfer between electrodes. It may be aqueous, organic, or ionic liquid, each with a different range of operating voltage and temperature stabilities. The ionic conductivity of the electrolyte and the compatibility with the electrode material are important requisites for the supercapacitor to have a great lifetime and efficiency.

Separator: A porous membrane positioned in between the electrodes serves as the separator, enabling ionic movement while securing the electrical insulation of the electrodes from each other to avoid short-circuiting. It should be both chemically indifferent and ion-conductive to allow efficient charge transfer.

Current Collectors: Conductive materials that ensure good contact of the electrode with the external circuit, in addition to allowing free flow of electrons during supercapacitor operation. Most of the current collectors are constructed from nickel foam aluminum or copper metals, as they reveal good conductance and corrosion resistance qualities.

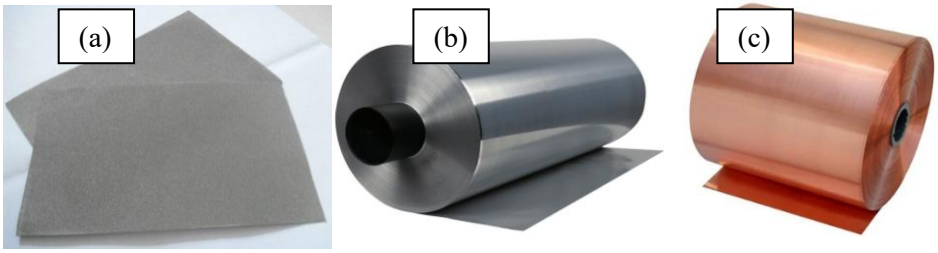

Figure 1.15: Current collectors used in supercapacitor: (a) Nickel foam, (b) Aluminum foil, and (c) Copper foil

Casing and sealing material: This is the material that combines all internal parts to provide mechanical strength and protection from chemicals. The sealing material seals the supercapacitor from any leakage of electrolyte and also from the ingress of moisture or any other impurity that can lead to poor performance.

Figure 1.16: Casing and sealing material

Terminals: These provide help points linked to the outer circuitry, whereby charging or discharging of the supercapacitor is made. The terminals should be conductive in nature for the least possible resistance. The performance features, therefore, of the supercapacitors include quick charge discharge, long cycle life, and high value of power densities achievable; thus, the superimposition of the components should be in proper configurations.

1.7 Supercapacitor Electrode Materials

Different materials, including conducting polymers, metal oxide, carbonaceous, and ferrite, have been used to construct supercapacitors. Generally, electrode material, which is under experiment, is known as active materials. Material selection is very important to construct a supercapacitor to achieve the desired electrochemical properties. The electrode materials determine the energy density and cycle life. Thermal stability, corrosion resistance, high electrical conductivity, high specific surface area,

and surface wettability are essential properties for electrode material. Besides, the electrode material should have the ability to transfer faradaic charge, which is essential to achieve maximum C_P.

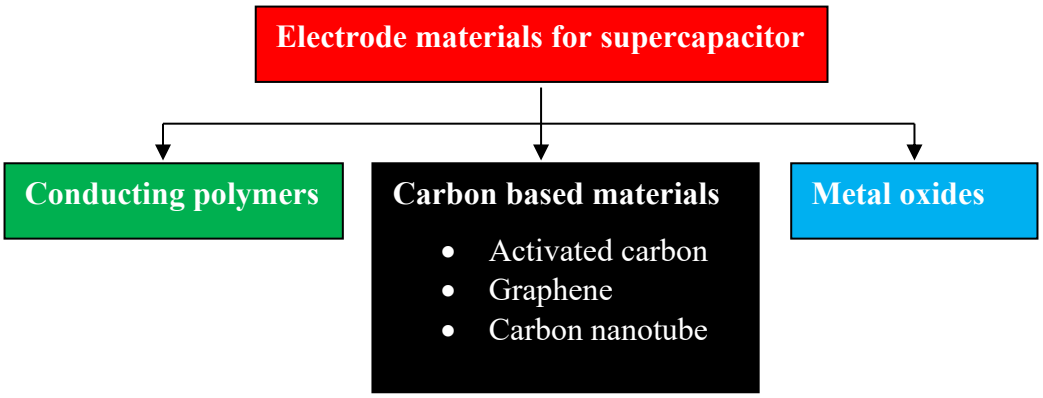

Figure 1.17: Electrode Materials for supercapacitor

Indeed, Optimising the surface area and fine-tuning the surface shape of electrode materials can also increase the C_P. Numerous factors, including the electrolyte's accessibility, the electrodes' geometry, and the size of the pores, affect the capacitance of electrodes. Improving electrochemically active sites and altering pore size and shape are prerequisites for building a supercapacitor. High energy density is also achieved by smaller-sized pores. Subsequently, the choice of electrode mainly depends on the applications.

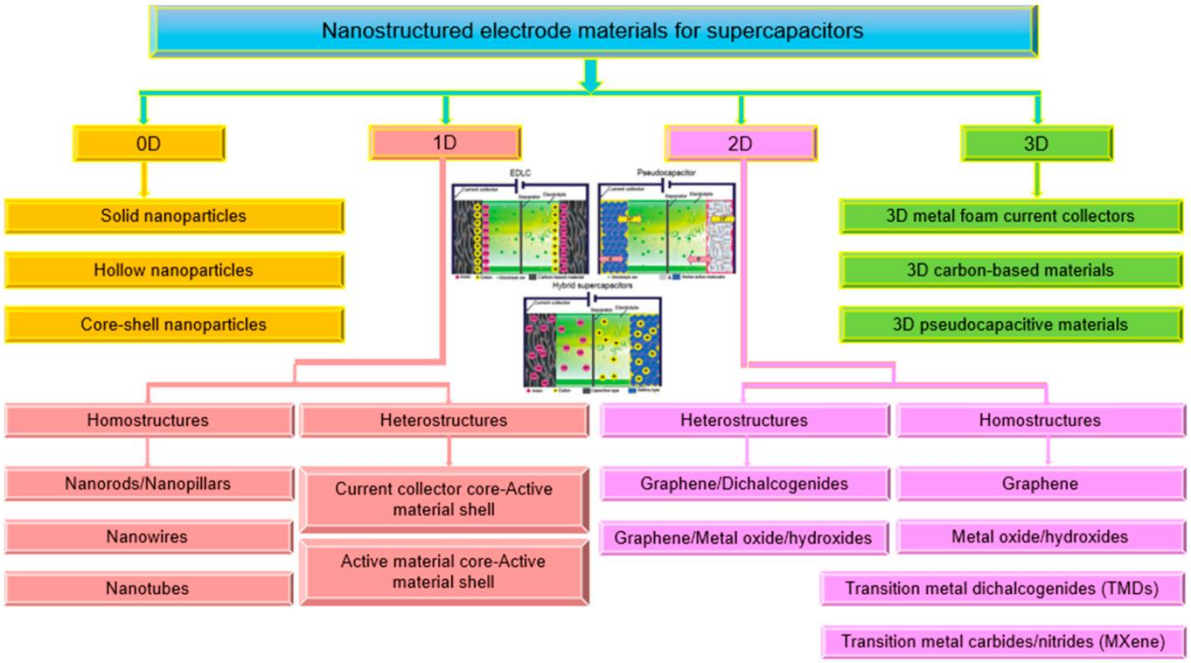

Figure 1.18: Most common electrode materials (0D to 3D) used to construct a supercapacitor (Source: [20])

1.8 Polypyrrole (PPy)

Polypyrrole (PPy) is one of the most extensively studied conducting polymers for supercapacitor applications due to its combination of high electrical conductivity, environmental stability, and simple synthesis routes. Its inherent pseudocapacitive nature enables greater energy storage compared to conventional carbon-based materials, primarily through rapid and reversible Faradaic redox reactions occurring on the polymer surface. Furthermore, PPy can be synthesized chemically or electrochemically on various substrates, allowing precise control over electrode structure and functionality. The ability to modify PPy with different dopant anions also provides a versatile means to tune its electrical properties for optimized supercapacitor performance. [21]–[23].

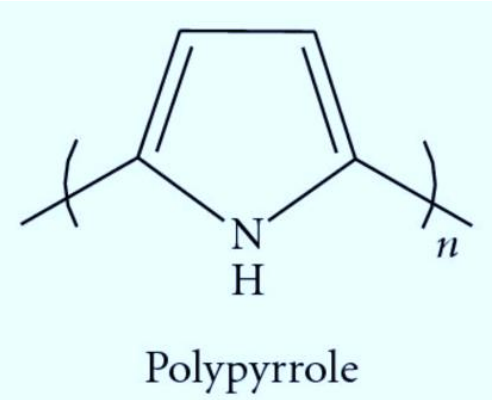

Figure 1.19: Structure of PPy

Besides, it presents good stability in environmental and mechanical properties. All these set up PPy as one of the favorable candidate materials for flexible and wearable energy storage devices. Polypyrrole can also be used as an electrode material compatible with aqueous and organic electrolytes. However, PPy has some shortcomings, such as the material degrading over long time cycling and swells in electrolytes. These drawbacks should be thoroughly investigated for fully exploiting the potential of PPy for supercapacitor applications. Thus, the continual research interest is on composite materials, nano structuring of PPy, and hybrid systems of PPy with other capacitive or pseudocapacitive materials to further increase its performance borders, pursuing larger energetic and power densities, along with cycle stability.

Moreover, polypyrrole (PPy) exhibits higher flexibility and mass density than most conductive polymers; as such, the former ensures better performance within a close, compact volume, hence easily adapted to a myriad of shapes [24]. In addition, further combination of PPy with other nanostructured materials, such as graphene and carbon nanotubes (CNTs), would contribute substantially toward enhancing the charge storage capability of the resultant PPy nanocomposite, besides enhancing the ion diffusion rates along with expanded contact surface area [25], [26]. These features make PPy an ideal material for the manufacture of supercapacitors, which are flexible, light in weight, and at the same time give high performance, so that they provide an appropriate solution for the demands of the developing market for portable and flexible electronic power sources, which at present are one of the issues in the world. Major

limitations linked to the manufacturing of supercapacitors with superior performance based on PPy are the discrepancy between the theoretical capacitance predictions and practical outcomes, along with poor cycling stability of the material during long charge-discharge cycles, as do most conducting polymers. We summarize efficient strategies to meet these challenges: the synthesis of specific morphologies and/or structures of PPy, the fabrication of diverse PPy composites with carbon materials or metal oxides, and the novel design of PPy-based supercapacitor configurations. These strategies aim to optimize PPy's capacitance while substantially improving its cycling stability.

1.9 Reduced graphene oxide

Reduced graphene oxide (rGO) is made from natural graphite using the Hummers' process [27]. rGO has been used for various applications, including for supercapacitor application as an electrode material.

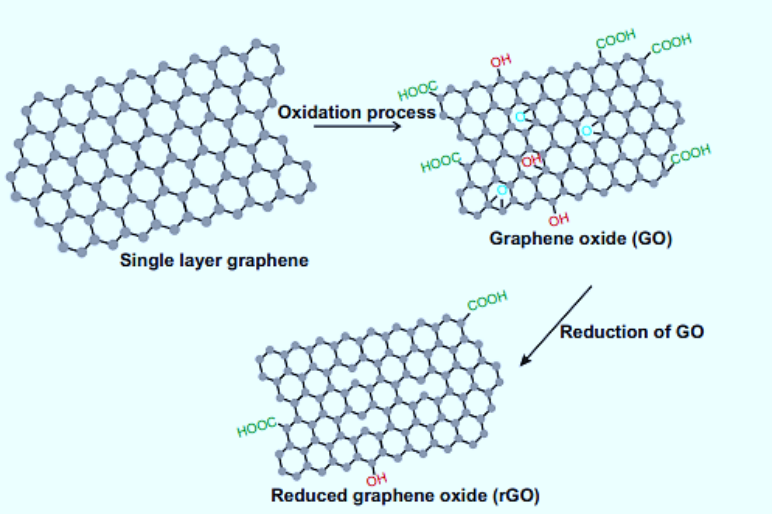

Figure 1.20: rGO from graphite. rGO is obtained after the reduction of GO, another graphene derivative with insulating properties. Source: [28].

The reduction of GO into rGO retains the properties of graphene to some extent. The reduction of graphene oxide is the removal of oxygen-containing groups while maintaining the π-conjugated system of graphene. The physical and chemical properties of rGO are relatively favourable for many applications when compared to raw graphite [29]–[31]. The single layer of rGO obtained through the Hummer's method dominates research and development for various applications. For instance, flexible electrode

material composed of rGO/MWCNT films has been prepared for supercapacitor application [32]. The material has excellent chemical and mechanical stability and is easy to transform into a large-area thin film, making it an ideal candidate for supercapacitor applications. The rGO produced from laser treatment has a surface area of 1520 m^2g^{-1} and a conductivity of 1738 Sm^{-1}. Metal oxides generally have poor electrical conductivity. To improve the performance of metal oxide, it is often mixed with rGO for several applications [33]–[35]. Microwave irradiation helps the rGO to have a conductivity of 200 S m^{-1}; this property is helpful for making an electrode for supercapacitor application.

1.10 Ferrites

Ferrite is a metal oxide with ferromagnetic properties with a lot of potential applications in the field of energy storage devices, solar cells, etc. Ferrite material has distinctive properties, including less eddy current losses and dielectric loss and high electrical resistivity. The ferrite-based composite has fascinating magnetic properties, redox chemistry, and catalytic properties, making them ideal candidates for energy storage application. Due to the intrinsic physicochemical properties, ferrite-based composite has been used for various applications, as shown in the following figure.

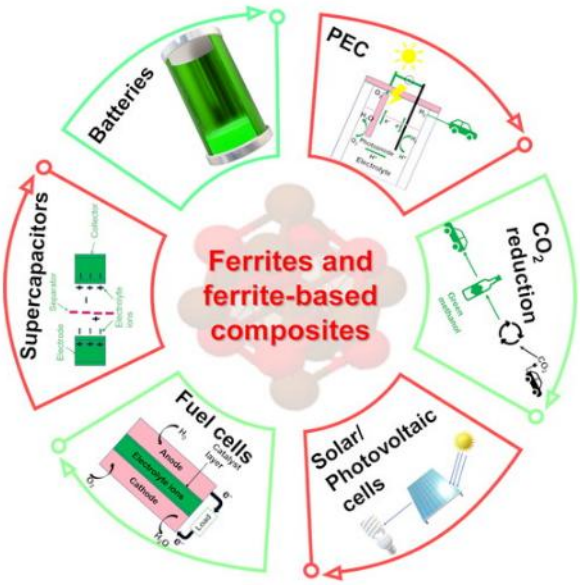

Figure 1.21: Ferrite material based composite for various applications (Source: [36])

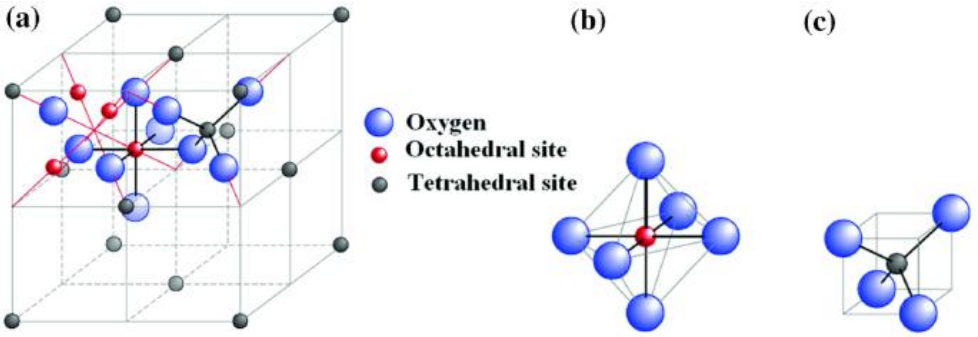

Figure 1.22: Basic ferrite structure (Source: [37])

Ferrite material has poor electrical conductivity and produces C_P that is not economical. The ferrite material has been divided into spinel, garnet, and hexagonal depending on their crystal structure. Among them, the spinel structure of ferrite has gained more attention due to its electrical transport property. The material is often combined with conducting polymers, reduced graphene oxide, or other metal-doped metal oxide to improve the specific capacitance (C_P) [38], [39].

1.11 Scope of the research

The scope of the research is centered on addressing the critical demand for efficient, high-capacity energy storage systems that can bridge the gap between the intermittent nature of renewable energy sources and the continuous energy demand. This requirement emphasizes the significance of supercapacitors, which are distinguished from traditional batteries by their high P_d, quick charge-discharge cycles, and extended lifespan. The research gap identified within the document pertains to the inherent limitations of supercapacitors. Notably, their E_d is rather low. when in contrast to batteries. This limitation restricts the broader application of supercapacitors in energy storage, particularly in applications requiring sustained energy release over longer periods, like large-scale renewable energy storage systems and electric cars. To address this, the document outlines objectives focused on the synthesis and characterization of novel electrode materials, such as polypyrrole (PPy), reduced graphene oxide (rGO), and Ni-Co Ferrite, aiming to enhance the electrochemical properties of supercapacitors. The research aims to investigate these materials' capabilities in boosting

the supercapacitors' energy density and C_P, potentially overcoming the identified gap by enabling supercapacitors to store and release energy more efficiently and over extended periods. The scope of the research is to explore advanced electrode materials for supercapacitors to improve their E_d, making them more viable for broader applications in energy storage. The gap exists in the current energy density limitations of supercapacitors. By using materials that can boost storage capacity without sacrificing the inherent benefits of supercapacitors, namely their quick charging speed and long lifespan, the study seeks to overcome this problem. By offering a more flexible and effective energy storage solution, this development may have a substantial impact on the infrastructure's ability to integrate renewable energy sources, improving the reliability and efficiency of renewable energy systems.

1.12 Objectives

- Synthesis and characterization of polypyrrole, rGO and Ni-Co Ferrite
- Investigation of electrochemical properties of Ppy/rGO electrodes for supercapacitor application
- Study of electrochemical properties of rGO/Ni-Co ferrite electrode for supercapacitor application
- Electrochemical study of Ppy/rGO/Ni-Co ferrite electrode for supercapacitor applications

CHAPTER 2

2.1 Literature review

Supercapacitors have attracted lot of interest lately for their remarkable power density (P_d) and long cycle life [40]. These devices also provide effective energy storage and are widely used in different applications which include renewable energy systems, electric cars and portable electronics, and to improve the efficiency of supercapacitors, researchers are actively developing advanced electrode materials that offer enhanced capacitance and long-term stability. The following section presents an in-depth analysis of electrode materials incorporating polypyrrole, reduced graphene oxide, and ferrites.

2.2 Polypyrrole (PPy) as electrode material for supercapacitor application:

In recent years, addressing energy storage has become crucial for environmental protection and the guarantee of steady and sustainable economic growth. The need for energy storage devices has grown significantly because of rising global warming and the swift exhaustion of non-renewable energy sources. Therefore, Supercapacitors have been developed as novel energy storage solutions and have attracted marked interest because of their remarkable characteristics of fast charge cycles, high P_d, durability, safety, less weight, and efficient reversibility. For supercapacitor applications, a broad range of materials have been employed, from active carbon to graphene and its derivatives, carbon nanotubes, conductive polymers, or transition metal oxides [41]–[44]. Polypyrrole (PPy) is one among them, which is effectively researched and utilized for supercapacitor application because of its unique features, such as conductivity (10–100 Sm^{-1}), flexibility, thermal stability, and environmentally friendly nature. Further, PPy is easy to produce, nontoxic, cheap, and shows appreciable capacitive current. Consequently, it shows a superior redox behavior and thus becomes an ideal EDLC material for such applications [45]–[47]. However, PPy also has some disadvantages, such as poor cycling stability and low rate capability, which limits its use for supercapacitor application [48]–[50]. The drawbacks of PPy could be improved by a combination with carbonaceous materials or transition metal oxides/sulfides. The role

of the metal nanostructure in such hybrids represents a key player in the structure, allowing an increase in the stability of the composite, as discussed by [51]–[53]. Figure 2.1 below provides synthesis process of PPy.

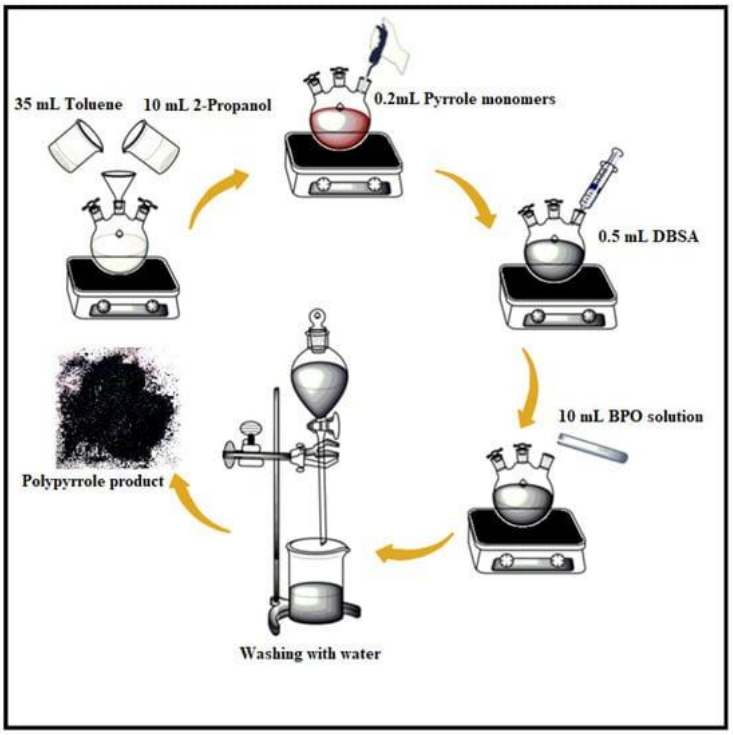

Figure 2.1: Schematic representation of the polypyrrole synthesis method (Source: [54])

Zhu et al. (2016) prepared PPy materials into layered Ti_3C_2 to improve cycling stability. Furthermore, even after 20,000 cycles of charging and discharging, 100% capacitance retention is attained. Strong bonds between the l-Ti_3C_2 surfaces and PPy backbones allowed for the increased capacitance [55]. Notably, the use of polypyrrole (PPy) as an electrode material has shown promising results in enhancing the capacitive performance and stability of supercapacitors. One approach involved the electrodeposition of highly active polypyrrole on titanium foil through CV at a scan rate of 200 mV/s in an oxalic acid solution, followed by characterization in 1 M KCl. A polypyrrole with a highly porous nanostructure was produced using this approach, and it had a C_P of almost 480 ± 50 F/g. The exceptional stability of this electrode material, as shown in cycle life tests, highlights polypyrrole promise in the field of supercapacitors. Using a pulsed polymerization technique, another creative strategy was used to improve the polymer structure's electrical conductivity and hydrophilicity.

By considerably increasing polypyrrole capacitance, operating potential, and stability, this technique supported the viability of this preparation method for supercapacitor applications. At 5 mA/cm^2, it attained a capacitance of 270 F/g during 10,000 cycles of charge and discharge (Thakare et al., 2018).

Furthermore, the investigation into stretchable supercapacitor applications has introduced the use of commonly available nylon-lycra fabric as a base material. By chemically polymerizing PPy onto the fabric, a highly conductive textile was created, exhibiting outstanding flexibility, stretchability, and excellent adhesion between the PPy layer and the fabric. This conductive material showed less than a 10% loss in C_P even after being stretched to 100% strain over 1000 cycles, highlighting its strong mechanical and electrochemical stability. The study also revealed that in situ strain could improve electrochemical properties, with C_P increasing with strain. Despite these advancements, the challenge of cycling stability remains, with ongoing research focusing on forming composites with carbon-based materials to overcome this limitation [56]. The C_P value and corresponding materials' SEM image is shown below for reference.

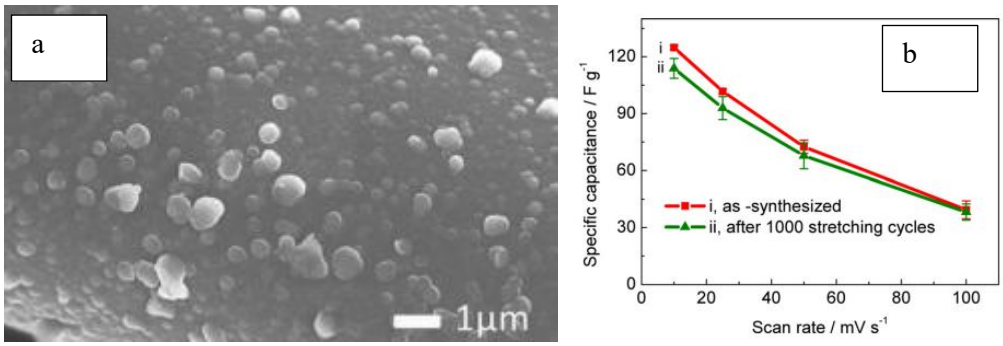

Figure 2.2: The C_P of the as-synthesized PPy-coated fabric (a) the fabric after being stretched to 100% for 1000 times (b) at different scan rates [56]

A notable study introduced a simple and novel chemical synthesis technique for PPy thin films tailored for supercapacitor use [49]. Characterization of these films through XRD, FTIR, and SEM revealed their amorphous nature, a desirable trait for supercapacitors due to its facilitation of ion transport. The FTIR analysis confirmed the formation of PPy, while SEM images showcased a uniform and smooth morphology, indicative of effective electrode coverage. Electrochemical studies employing cyclic

voltammetry showed a high C_P of 329 Fg^{-1} and a low equivalent series resistance (ESR) of 1.08 Ω in a 0.5 M H_2SO_4 electrolyte. 5 mV/s was the scan rate.

Further advancing the field, Yavuz et al. (2020) explored the development of flexible polypyrrole electrodes using a novel approach involving the deposition of graphite on non-conductive tape to serve as a current collector. The subsequent synthesis of PPy on this flexible substrate through potentiation methods in a sulfuric acid medium was thoroughly characterized using AFM, SEM, FTIR, and electrochemical techniques [57].

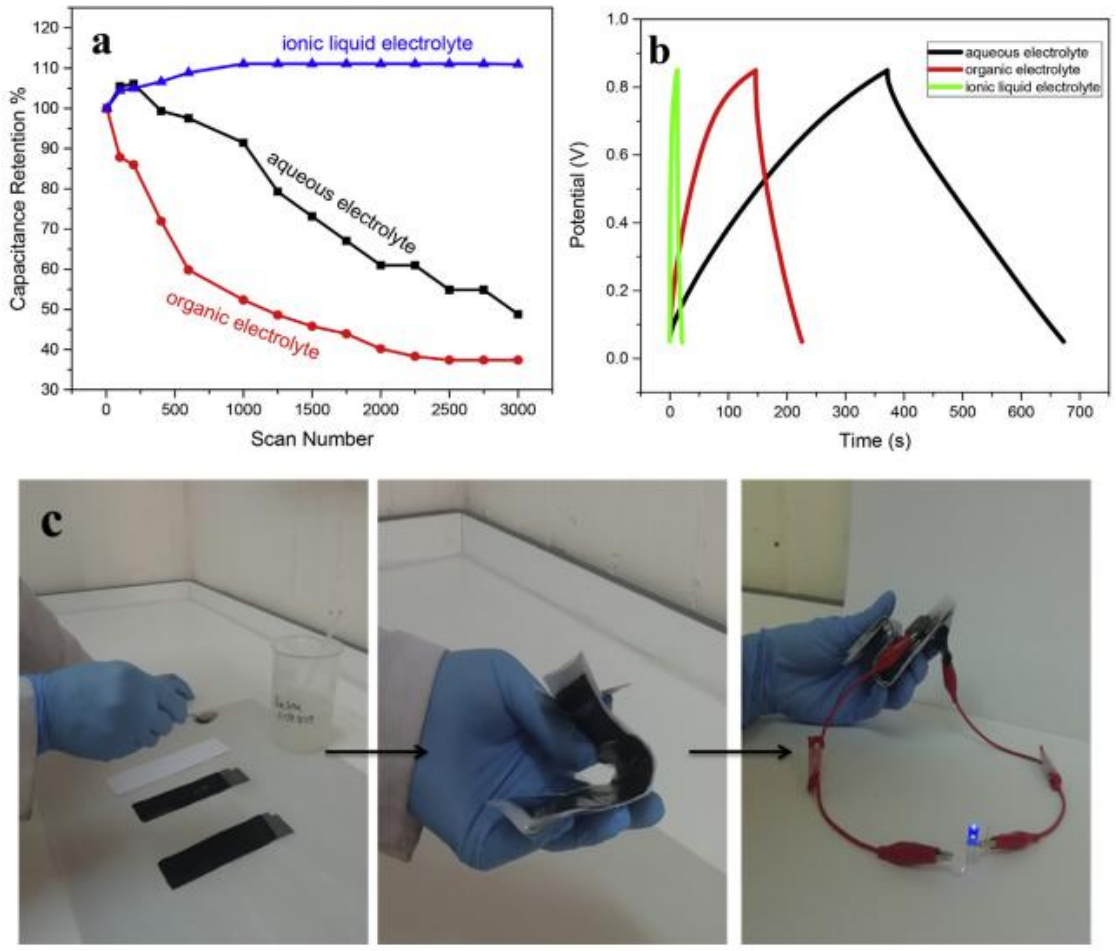

Figure 2.3 (a) Flexible polypyrrole electrodes are tested for cycling at 3000 cycles under different electrolyte conditions (v ¼ 50 mV/s). (b) Polypyrrole film versus bare graphite galvanostatic charge-discharge curves under different electrolyte conditions at a current density of 0.2 mA cm^2. (c) image of symmetric polypyrrole electrodeposited on graphite-based flexible tape electrodes in Reline deep eutectic solvent. Source: [57]

The integration of electronic functionality with the flexibility and comfort of textiles has unlocked new avenues for innovation. Key to the advancement of these wearable technologies is the development of lightweight, stretchable, and wearable power sources that can seamlessly integrate with fabric-based electronics. This review article segment focuses on recent strides in the domain of conductive polymers, specifically polypyrrole (PPy), for use in stretchable supercapacitors, emphasizing their synthesis, characterization, and performance in wearable applications.

Yue et al. (2013) presented a novel approach by synthesizing polypyrrole on daily-used cotton fabric, which had been coated with gold, to create a conductive textile electrode for stretchable supercapacitors. Using doping of p-toluene sulfonic acid (p-TS) in an acetonitrile solution, PPy was electrochemically polymerised during the manufacturing process. This process created a conductive textile with a high C_P of 254.9 F g^{-1} that could endure strains of up to 140% without failing electrically at a scan rate of 10 mV s^{-1}. Remarkably, the electrode maintained its capacitance under applied strains of 30% and 50% while demonstrating enhanced cycling stability. This research underscores the potential of integrating conductive polymers with textiles to make stretchable energy storage devices that do not compromise on performance under mechanical stress [56].

Further advancing the durability of flexible supercapacitors, Huang et al. (2016) reported on supercapacitors fabricated with electropolymerized polypyrrole (e-PPy) electrodes exhibiting unprecedented long-term cycling stability. Impressively, the devices retained over 97%, 91%, and 86% of their initial capacitance after 15,000, 50,000, and 100,000 cycles, respectively. Even after 230,000 continuous cycles, they maintained approximately 50% of their original capacitance, demonstrating exceptional long-term durability. Such durability outperforms previously reported systems and is attributed to the controlled electro-polymerization process, which enhances molecular ordering, promotes the uniform stress distribution, and facilitates efficient charge transfer. Notably, the e-PPy supercapacitors maintained their electrochemical performance even after eight months in ambient conditions, highlighting their potential for commercial utility or applicability in flexible and wearable electronics [9].

The work of Yue et al. and Huang et al. collectively emphasizes the significant potential of polypyrrole and its derivatives in overcoming the challenges of integrating energy storage into wearable devices. By demonstrating the feasibility of fabric-based

electrodes that combine high capacitance with remarkable mechanical and cycling stability, these studies pave the way for the next generation of wearable electronics. The advancements in conductive polymer synthesis and application in supercapacitors not only enhance the performance of wearable devices but also broaden the scope for their practical application, marking a significant leap forward in the realization of fully integrated wearable electronic systems.

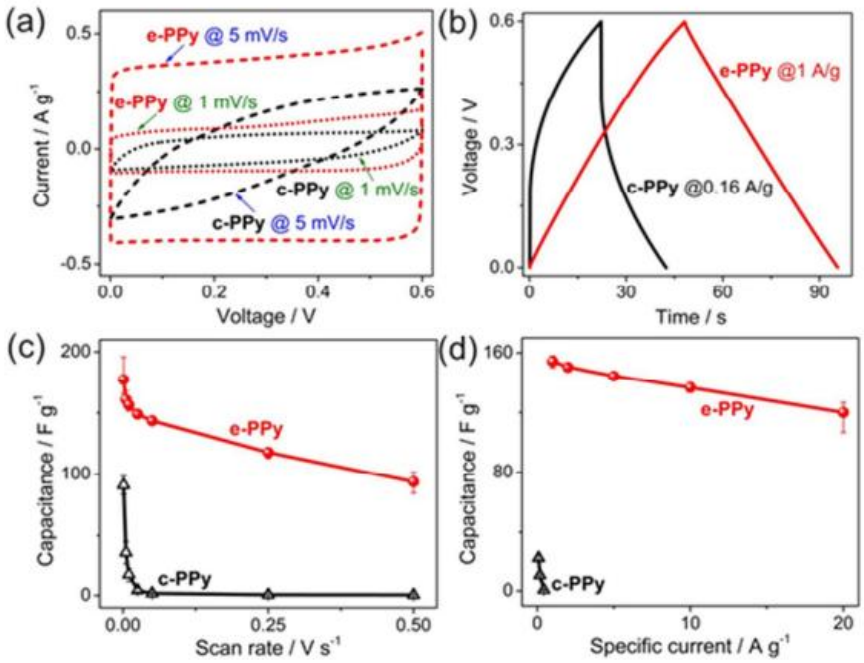

Figure 2.4. Performance of e-PPy and c-PPy supercapacitors electrochemically. (a) CV graphs at scan rates of 1 mV/s and 5 mV/s (b) profiles of GCD charging and discharging with different currents of 0.16 A/g and 1 A/g. (c) Capacitances as functions of scan rates. (d) Capacitors are used for particular charging and discharging currents [58].

Lee et al.. demonstrated PPy thin film for supercapacitor application and evaluated their electrochemical performance by means of impedance spectroscopy. The synthesized PPy nano/microsphere displayed 568 F/g, which is 20–100% more than that of previous PPy electrodes that have been seen and near the theoretical value of 620 F/g. Even after 10,000 charging and discharging cycles, 77% of the PPy electrode's capacitance value was still there. The large surface area and porous architecture were responsible for the improved electrochemical properties. Additionally, these characteristics allow for high ion mobility inside the polymer and favor electrolyte penetration, preventing the

physical structure from mechanically failing during volume variation related to ion insertion and deinsertion during cycling. [59].

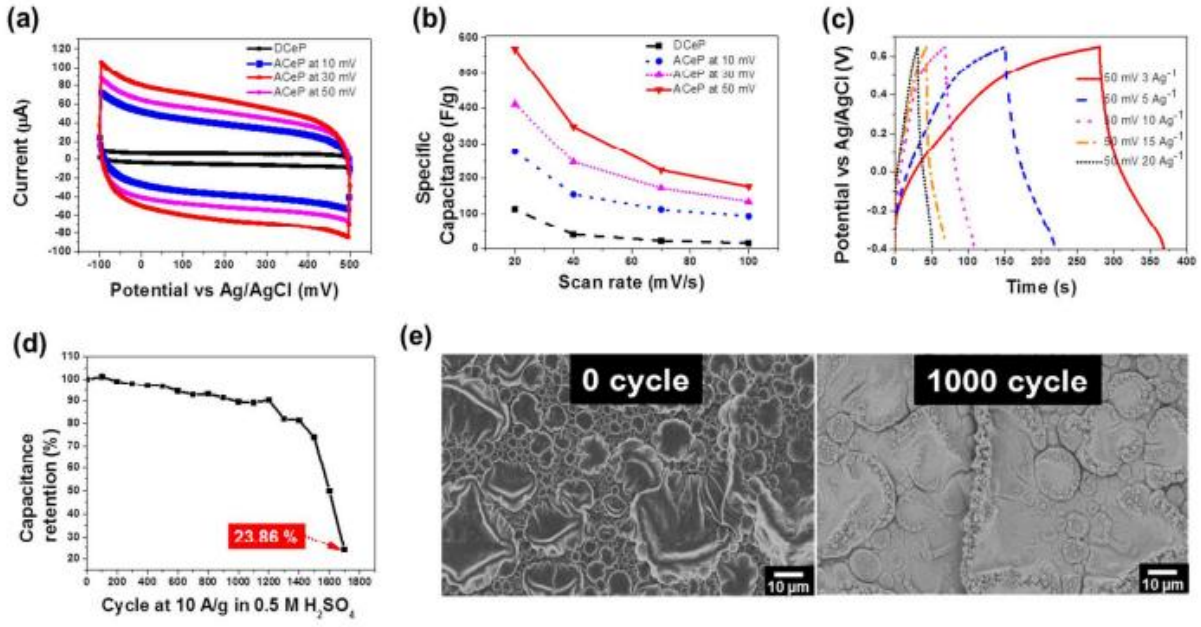

Figure 2.5. (a) A scan rate of 100 mV/s is used to create cyclic voltametric curves (b) grams of active material's specific capacitance (c) GCD curves for PPy-AC 50 mV at different current densities. (d) Using galvanostatic charge/discharge, the cycle stability of PPy-AC 50 mV was evaluated at a current density of 10 A/g. (e) Before and after testing 1000 cycles, SEM pictures of PPy-AC 50 mV were taken. A 3-electrode setup in 0.5 M H_2SO_4 aqueous electrolyte was used for all measurements. Source: [59].

D. P. Dubal et al. prepared 20 nm-sized spherical polypyrrole, It demonstrated an 83% capacitive retention, a 93% discharge/charge efficiency, and a 533 F/g C_P at a current density of 10 mA/cm². The results show that PPy materials have strong electrochemical reversibility and rate capability when used as an electrode in supercapacitors [60].

2.3 Graphene/polypyrrole-based electrodes:

Significant advancements in energy storage technology have been made with the addition of graphene to supercapacitor electrodes. The two-dimensional honeycomb structure of graphene, which is made up of sp2-bonded carbon atoms, gives it exceptional physicochemical and structural qualities [61], making it an ideal candidate for enhancing the performance of supercapacitors. Since its first isolation in 2004 [62],

graphene has been extensively studied for its potential in electrochemical applications, particularly due to its chemical stability, excellent electrical conductivity, vast surface area, high flexibility, and mechanical strength [62], [63]. When compared to single-layered GO/PPy, which has a capacitance of 215 F/g, the C_P of the electrode made of GO/PPy can reach 332 F/g at 10 mV/s [64]. These achievements underscore the potential of graphene-PPy composites in supercapacitor applications. Binder-free, multilayered composite structures have been made using a unique manufacturing technique that combines the van der Waals attraction between the π-conjugated conductive polymer chains and the aromatic graphene basal plane with capillary force-driven Self-arrangement. This approach facilitates the construction of electrodes with enhanced electrochemical performance. Additionally, GCD, EIS, and CV studies were used to examine the electrochemical act of composites. The findings showed that PPy/rGO-CTAB composites outperformed both PPy/rGO composites deprived of CTAB and rGO in terms of thermal stability, C_P, resistance, cyclic properties, and responsiveness to oxidation/reduction [65]. These developments highlight the ongoing effort to optimize the synthesis and application of graphene-PPy composites for supercapacitor electrodes, aiming for environmentally friendly processes that do not compromise on performance. The superior electrochemical characteristics of these composites, including higher capacitance, lower resistance, and improved cyclic stability, position them as promising materials for energy storage devices.

These findings collectively contribute to the body of knowledge on supercapacitor electrode materials, analysing the design and optimization of supercapacitors with enhanced stability, performance, and mechanical flexibility.

2.4 Graphene oxide/polypyrrole

The creation of novel electrode materials in conjunction with other materials is necessary to create a supercapacitor with a high energy density and power. Nonetheless, in the case of graphene, attaining high C_P and E_d is contingent upon performing charge/discharge cycles at low current densities or conducting cyclic voltammetry at slow scan rates. This requirement undermines the fundamental advantage of supercapacitors, which is their capability for rapid charging and discharging. A significant challenge with graphene is its tendency to restack, which

hinders the achievement of a large surface area with the requisite electronic properties for optimal Electric double-layer capacitor (EDLC) performance [66].

Graphene oxide (GO), which is derived from a single layer of graphite oxide, is typically produced by subjecting graphite to a combination of strong acids and oxidising agents. It has a large number of functional groups that contain oxygen around its edges and along its basal planes[67]. The many oxygen-containing groups improve porous carbon's wettability under electrolytes, which is advantageous. As a result, GO's strong solvent solubility opens up a wide range of possibilities for the creation of GO-based hybrid composites and their possible uses. The development of GO-based nanomaterials and research into their possible uses in biosensors and supercapacitors have needed a substantial amount of work. The development of supercapacitor technologies, especially those that employ graphene oxide (GO) and polypyrrole (PPy) composites, has been greatly expedited by the creation of novel electrode materials. In terms of supercapacitor energy density, cycle stability, and C_P, these materials have shown encouraging outcomes. Based on the results of several important studies, this review paper summarizes the latest developments in the synthesis, characterisation, and use of GO/PPy composite electrodes in supercapacitors.

Cao et al. (2015) produced GO/PPy composite electrodes with a high C_P and mass loading for an electrochemical co-deposition process. Composite demonstrated a high-rate capability and maintained more than 80% capacitance. The composite's 3D-connected structure, which promoted the quick diffusion of electrolyte ions, highlighted their uses for energy storage. When Suranshe et al. (2023) investigated the electrochemical deposition of GO-PPy composites, they found that the capacitance rose with the GO content and peaked at 20% GO. This rise highlighted the composite's ideal electrochemical performance and was ascribed to the synergistic effect of the pseudocapacitive PPy and the EDLC-type GO [79].

A polypyrrole–reduced graphite oxide core–shell composite was created by Qian et al. (2013). It demonstrated remarkable cycling stability after 1000 charge–discharge cycles and a C_P of 557 F g^{-1}. The composite's superior performance was mainly ascribed to its higher conductivity and more crumpled surface [80].

In their 2020 study, G. Liu et al. showed that the PPy ornamentation on reduced graphene oxide (rGO) sheets had better electrochemical qualities than the pure

constituents. The optimized rGO/PPy compound demonstrated excellent capacitance and cycling stability in asymmetric supercapacitor devices, emphasizing the composite's effectiveness in enhancing specific surface area and conductivity.

Moyseowicz et al. (2020) proposed a hydrothermal treatment for synthesizing polypyrrole/reduced graphene oxide hybrids. These hybrid materials demonstrated high C_P and sustained considerable capacitance retention even after 3000 charge–discharge cycles, highlighting the critical role of morphology and chemical composition in influencing electrochemical performance. [81].

Guo et al. (2018) demonstrated that flexiblility of all-solid-state supercapacitors, fabricated using free-standing reduced graphene oxide/polypyrrole sheets with a high specific surface area and three-dimensional porous structure, delivered outstanding volumetric C_P and energy density even after prolonged cycling. The improved performance was attributed to the synergistic effects of polypyrene and reduced graphene oxide [68].

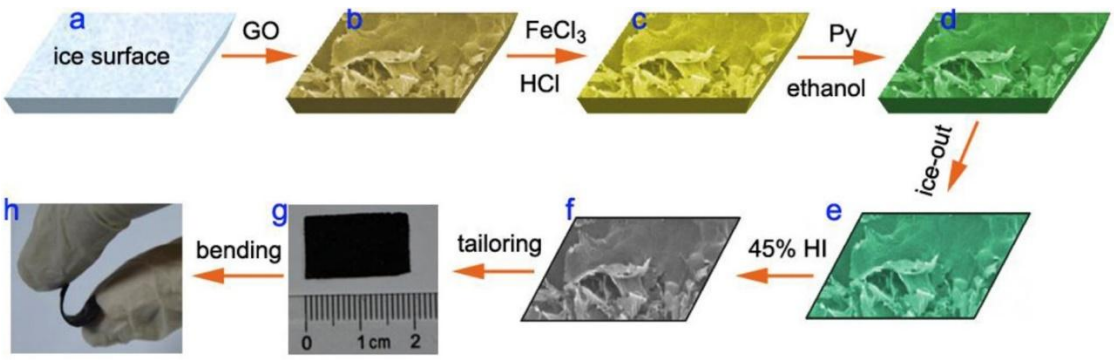

Figure 2.6: Preparation steps for Flexible all-solid-state supercapacitors composed of reduced graphene oxide/polypyrrole films [68].

In the rapidly evolving field of supercapacitors, because of their exceptional structural properties and electrochemical performance, GO/PPy composites have become a promising material for electrode applications. With a focus on their improved capacitance, rate capability, and cycle durability, this review paper summarizes the most recent research on the creation, characterization, and use of GO/PPy composites in supercapacitors.

In situ oxidation polymerization was used by L.-Q. Fan et al. (2014) created GO/PPy

composites with a high C_P of 332.6 F g^{-1}. The homogeneous production of PPy nanoparticles on GO sheets, which in turn increases the specific surface area and electrical conductivity, is responsible for the composite's remarkable performance. An asymmetric supercapacitor using this composite like a the positive electrode showed remarkable E_d and cycling stability, highlighting the material's potential for energy storage applications.

De la Fuente Salas et al. (2014) focused on depositing multilayer films of PPy on GO layers using various dopants. Their study found that multilayer GO/PPy films exhibited greater capacitance compared to single-layer configurations, with C_P reaching up to 332 F g^{-1}. This enhancement is linked to the optimized deposition process, which improves the composite's morphology and electrochemical properties [64].

J. Li & Xie (2012) reported the successful growth of PPy nanowires on GO nanosheets, significantly increasing the C_P to 633 F/g. This remarkable performance, coupled with less than 6% capacitance attenuation after 1000 charge/discharge cycles, underscores the composites' excellent electrochemical rate capability and cycle stability.

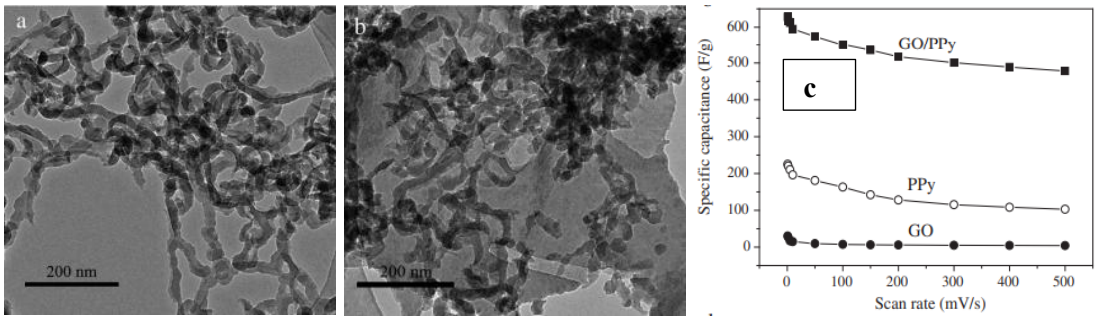

Figure 2.7: TEM images of (a) PPy nanowires and (b) GO/PPy composites, (c) The precise capacitances of GO, PPy and GO/PPy composites at different scan rates Source: [69].

Cao et al. (2015) fabricated 3D GO/PPy composite electrodes via electrochemical co-deposition, achieving a notable capacitance of 481 Fg^{-1}. The 3D interconnected structure of these composites ensures fast electrolyte ion diffusion, contributing to their high capacitance and good rate capability. This study demonstrates the composite's effectiveness in both aqueous and solid-state supercapacitors, highlighting its broad applicability in energy storage technologies [79].

Biswas & Drzal (2010) and Y. Liu et al.. (2013) explored the development of nanostructured PPy with graphene nanosheets and decreased graphene oxide

(rGO)/PPy composites, respectively. The latter study emphasized the use of green solvents like ethylene glycol as a reducing agent for rGO, which not only preserves the composite's structure but also significantly enhances its electrochemical performance. After 200 charge-discharge cycles, the EG-rGO/PPy composite retained 93% of its initial capacitance and demonstrated a C_P of 420 F g^{-1}[78, 70].

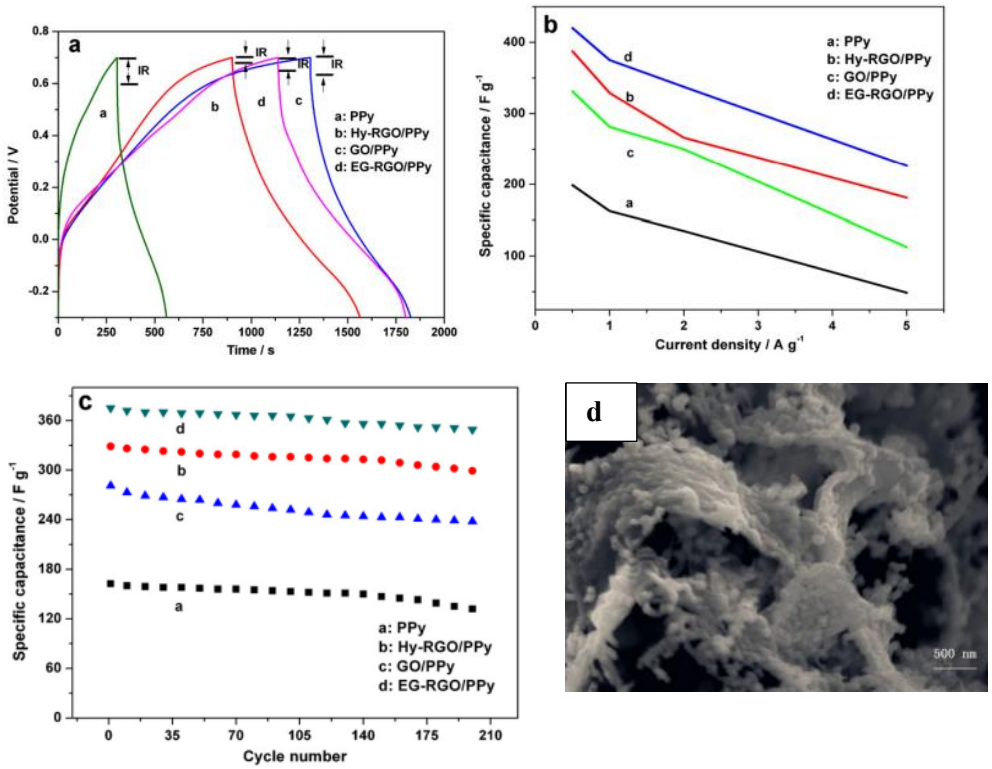

Figure 2.8: (a) At 0.5Ag^{-1}, representative galvanostatic charge-discharge curves, (b) rate performance with current density difference from 0.5 to 5Ag−1, and (c) At a current density of 1.0Ag−1, the charge–discharge cycling performance of the PPy, Hy-RGO/PPy, GO/PPy, and EG-rGO/PPy electrodes was assessed. (d)) SEM image of EG-rGO/PPy (Source: [70])

2.5 Polypyrrole (PPy)/carbon nanotube (CNT) composite

The low weight, high conductivity, chemical inertness, and huge specific surface area of carbon nanotubes (CNTs) have made them one of the potential electrode materials for electrochemical energy storage devices. It is simple to turn CNT dispersions into conductive "bucky-paper" by vacuum filtering them. Using the electrochemical double layer non-Faradaic approach, Bucky-paper showed that the charge-storage mechanisms

of CNT sheets are extremely effective and produce amazing CP and dimensional changes upon charge injection. At the boundary of CNT and the electrolyte, ions balance the charge on CNTs. All these processes are limited by the effective surface area, where the usual capacitance ranges from 15-40 F/g. It goes further to prove that these values can be improved with the proper electrode materials to achieve higher capacity.

For example, electrically conducting polymers have been introduced to enhance CNT sheet electrodes. Devices using conducting polymers also exhibit Faradic processes and have been observed to have capacitance several times higher. However, to these Faradaic electrodes, a few problems are added within the charge/discharge rates and the other solid-state ion diffusion-dependent polymer conductivity linked with the level of intercalation, and one such is their low cycle life. To overcome these disadvantages, CNTs can be added to a polymer matrix for an improvement in its stability, conductivity, and mechanical strength. For example, work by Frackowiak et al.. was very promising regarding the polypyrrole (PPy)-CNT composite obtained by chemical polymerization of pyrrole, where the value of capacitance reached 170 F/g. Similarly, the PPy-coated SWNT, uniformly prepared by the in-situ chemical polymerization, exhibited very high C_P from both the Faradaic and non-Faradaic processes.

This method delineates a scalable and effective way for preparing supercapacitor-industry-applicable, extremely porous SWNT-PPy nanocomposite electrode materials. It further extends the conventional bucky-paper fabrication method to be the host for multi-component systems. Their study included the investigation of electrochemical properties via CV, GCD, and EIS. The capacitance of the electrode was systematically related to the ratio of PPy/SWNT in the nanocomposite, It was found that the C_P for the 1:1 SWNT: PPy ratio was 131 F/g. All such material, thus, may find potential application in a broad spectrum of potential applications, from supercapacitors to battery electrodes and even electromechanical.

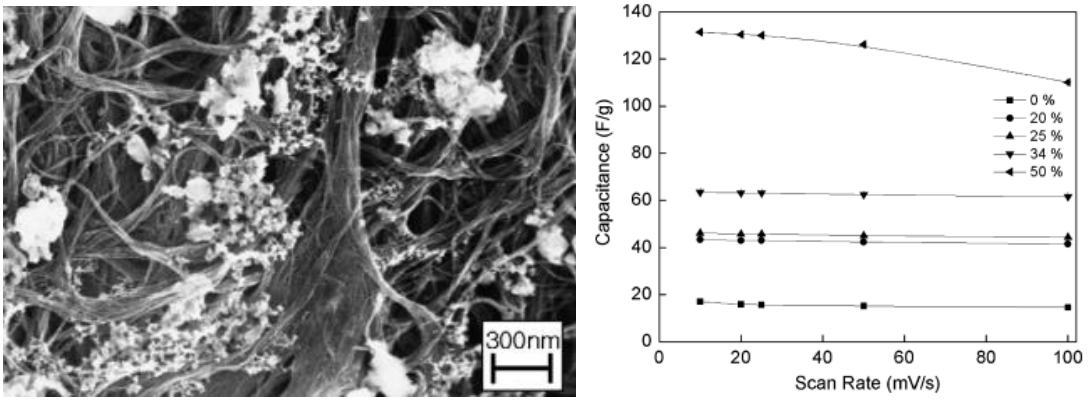

Figure 2.9: (a) SEM pictures of SWNT-PPy nanocomposites with 50 wt. % PPy. (b) capacitances as a function of scan rate for the SWNT sheet and SWNTPPy nanocomposite electrodes in 1M NaCl electrolyte [23].

Amaranth was presented by Y. Zhu et al. (2014) as a new redox-active anionic dopant for the chemical polymerisation of PPy, emphasising how well it works to increase the electrodes' mass loading and PPy to current collector mass ratio. This approach achieved a C_P of 4.2 F cm^{-2} at a scan rate of 2 mV s^{-1}, providing insights into the dopant's role in improving the microstructure, electrochemical properties, and cycling stability of PPy electrodes.

The amalgamation of PPy with MWCNT has significantly improved capacitance retention at high charge-discharge rates and ensured good cycling stability. This is attributed to the fine microstructure of PPy coatings on MWCNTs, facilitated by the dispersant pyrocatechol violet and the amaranth dopant, as detailed by Y. Zhu et al. (2014). Additionally, the introduction of XC-72 has been found to enhance the potential window, reversibility, C_P, and stability of rGO/CNT/PPy composites, making them suitable for use in aqueous asymmetric supercapacitors (ASCs), as Peng et al. (2014) have demonstrated.

In situ polymerization techniques have been employed to create carbon nanotube-reinforced PPy nanowire networks, resulting in electrodes with decreased charge transfer resistance and improved ion/electron diffusion. Fu et al. (2013) reported a C_P of 183.2 F g^{-1} and a capacitance retention of 85% after 1000 cycles, emphasizing the benefits of embedding carbon nanotubes into the polypyrrole nanowire matrix.

The research by Shi & Zhitomirsky (2013) introduced an efficient dispersion technique using malachite green (MG) dye as a co-dispersant for PPy and MWCNTs. This method

facilitated the preparation of composite PPy–MWCNT electrodes with superior electrochemical performance and excellent capacitance retention, highlighting the potential of colloidal processing in supercapacitor electrode fabrication.

The development of flexible supercapacitors, particularly for wearable electronics, has gained attention, with conductive, twistable, and bendable CNT composite fibers coated with PPy showing promising results. Xu et al. (2015) demonstrated that such fibers exhibit high C_P and stability, benefiting from the core-shell structure that facilitates easy charge transfer between PPy and CNTs [17].

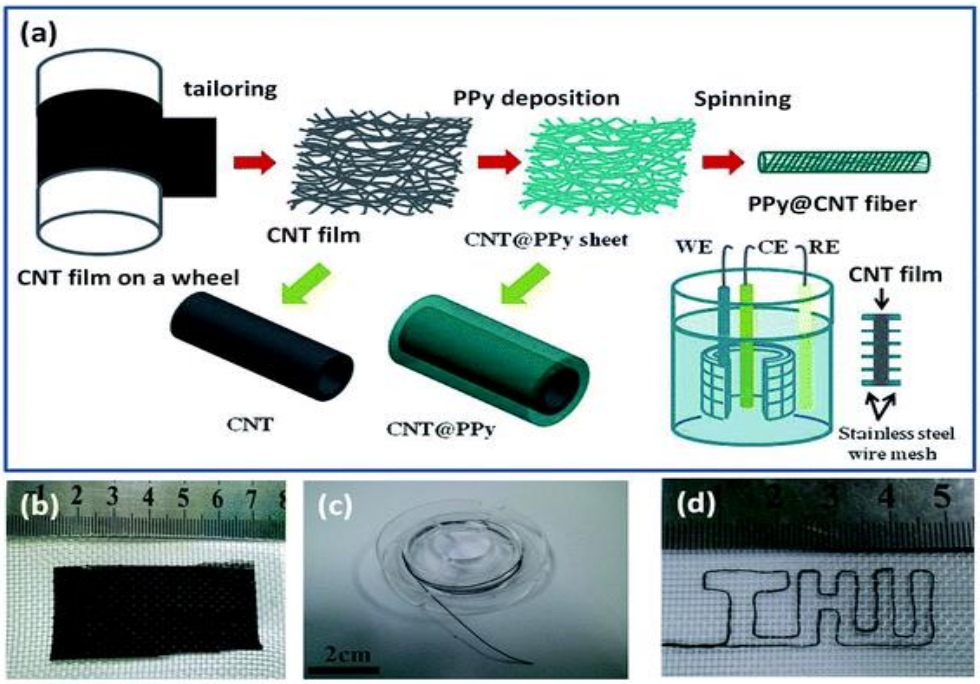

Figure 2.10: 1 (a) PPy@CNT fibre preparation: a schematic diagram. (b) An optical image of a CNT film situated between two stainless steel wire meshes. (c) A PPy@CNT fibre longer than one metre. (d) The letters of THU are fabricated from a lengthy PPy@CNT fibre. Source: [71]

A study by H. Lee et al. (2011) addresses a critical challenge in the field of electrochemical capacitors, specifically the detrimental effects of using insulating binders like PVDF and PTFE in electrode fabrication. These binders, while commonly employed for their binding properties, increase the internal resistance and limit the accessibility and surface area of carbon nanotubes (CNTs), thus negatively impacting the electrochemical performance of capacitors. To overcome these limitations, Lee et al. propose an innovative approach by fabricating a composite electrode that combines CNTs with a conducting polymer, specifically polypyrrole (PPy), which serves as a

conductive binder. This method not only enhances the electrode's electrical conductivity but also preserves the intrinsic high surface area of the CNTs, which is crucial for energy storage applications.

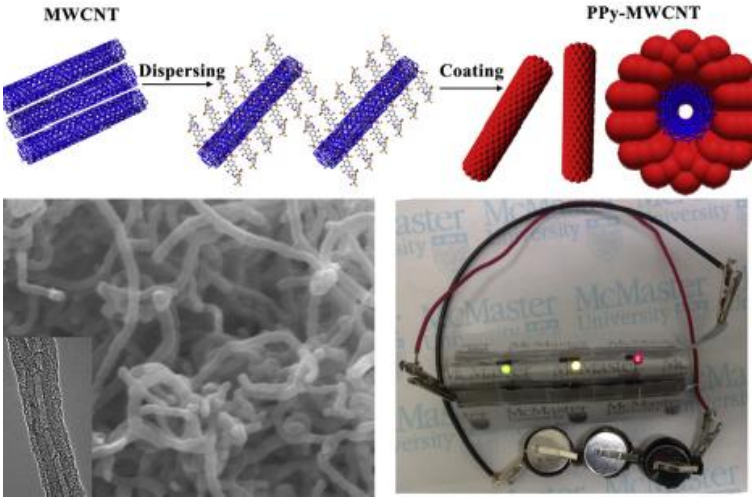

Figure 2.11: Carbon nanotube electrodes covered with polypyrrole are used to produce an asymmetric electrochemical supercapacitor.Source: [72]

The synthesis and application of PPy polymer MWCNT composites in electrochemical supercapacitors (ES) have been extensively explored due to their promising electrochemical properties. These studies demonstrate the potential of PPy/MWCNT composites to address the limitations of each component when used independently, offering a pathway to enhance the performance of supercapacitors through innovative material engineering and design.

Su & Zhitomirsky (2015) introduced doping of sulfanilic acid azochromotrop (SPADNS) and sulfonazo III sodium salt (CHR-BS) for the chemical polymerization of PPy. The employment of CHR-BS notably improved the dispersion of MWCNTs and facilitated the formation of PPy coatings on MWCNTs, resulting in composites with higher capacitance and excellent cyclic stability compared to those prepared with SPADNS. This approach underscores the importance of dopant selection in optimizing the interfacial characteristics and electrochemical performance of composite electrodes [72].

The literature highlights the synthetic challenges in achieving high mass loading of PPy

on CNTs deprived of compromising the accessibility to electrolyte channels. Traditional methods often result in the need for additional binders and conductive additives, which can detract from the supercapacitor's performance. However, freestanding approaches that directly grow PPy on preformed CNT films have shown promise in improving interfacial conductance and supercapacitor performance, despite difficulties in depositing large amounts of PPy.

A groundbreaking study by Parayangattil Jyothibasu et al. (2020) utilized curcumin as a green template for fabricating a composite film of PPy nanoparticles and functionalized CNTs (f-CNTs). This binder-free, freestanding electrode demonstrated exceptional areal and volumetric capacitance, highlighting the potential of plant-derived templates in creating high-performance supercapacitor electrodes with superior energy storage capabilities.

Wang et al. (2015) described a new technique for creating composites of GO, Ppy, MWNCT (PCMG), demonstrating how PPy acts as a bridge between graphene oxide and chlorinated-MWCNTs. This 3-D structured composite exhibited high capacitance and remarkable capacitance retention, emphasizing the synergistic effects of combining graphene oxide with PPy/MWCNT composites for energy storage applications [83].

Lu et al. (2012) developed unique flexible films that incorporate PPy/CNT composites between graphene sheets. This layered structure not only enhances the total capacitance of the electrodes but also provides excellent cycling stability, demonstrating the potential of such flexible electrodes in portable electronic devices.

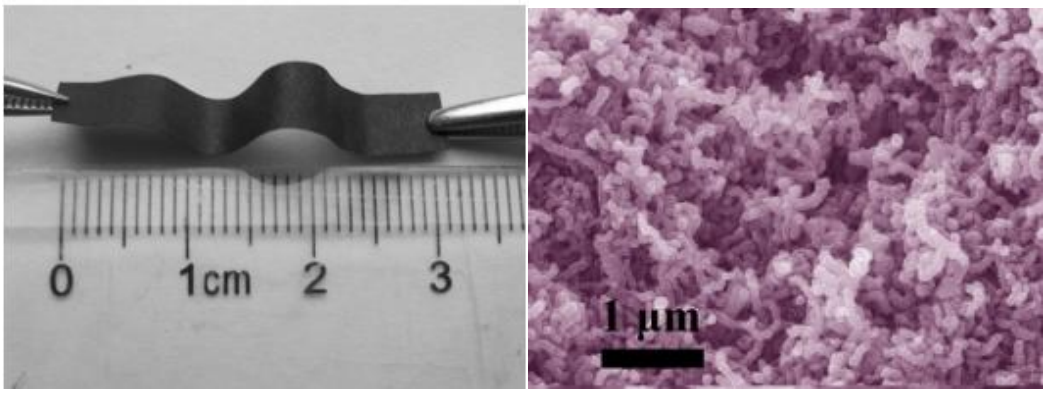

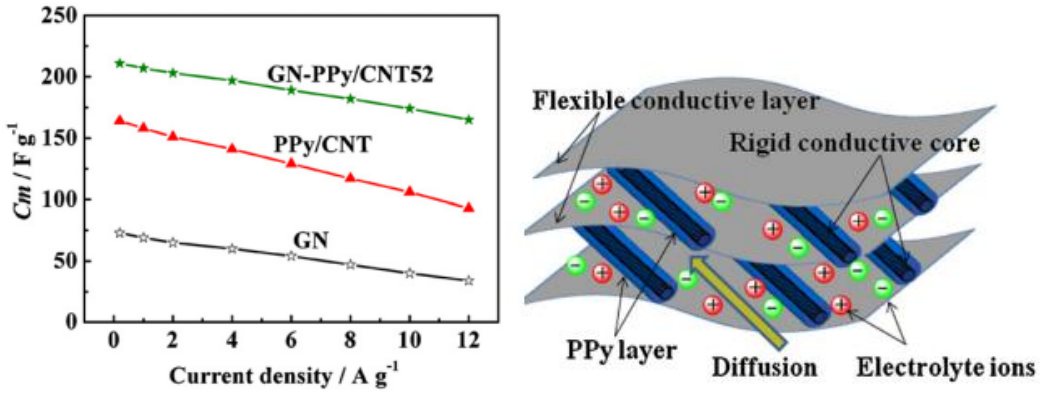

Figure 2.12: (a) Image GN-PPy/CNT film52 (b) SEM image of PPy/CNT. (c) Cm values of GN, PPy/CNT and GN-PPy/CNT52 at different current densities. (d) Diagrammatic illustration of the GN-PPy/CNT52 film's microstructure and energy storage characteristics [73]

X. Li and Zhitomirsky (2013) reported an electrochemical method that uses an anionic dopant made from pyrocatechol violet (PV) to improve the adhesion of PPy coatings to nickel and stainless steel substrates. This method not only promotes strong adhesion via catecholate-type bonding but also supports efficient dispersion and controlled electrophoretic deposition of MWCNTs. The incorporation of PV in the electropolymerization of PPy and the EPD of MWCNTs resulted in composite films with notably higher material loading and improved capacitive performance, especially with nickel-plaque current collectors.

Y. Chen et al. (2017) fabricated PPy/functionalized MWCNT (FM) composites by CV, forming core-shell structures via hydrogen bonding. The electrochemical performance of these composites demonstrated a substantial increase in C_P and capacitance retention, outperforming pure PPy materials. This technique highpoints the importance of molecular interactions and composite architecture in enhancing supercapacitor efficiency [84].

Dhibar et al. (2013) synthesized copper chloride (CuCl2)-doped PPy/MWCNT nanocomposites through in situ oxidative polymerization, revealing that metal cation interaction could significantly enhance the electrochemical properties of conducting polymers. The CuCl2-doped composites exhibited the highest C_P among the variants tested, showcasing the potential of transition-metal-ion doping in boosting the capacitive performance of supercapacitor electrodes [76].

Xiao & Zhou (2003) explored the deposition of conducting polymers like PPy and poly

(3-methylthiophene) on MWCNTs, leading to the growth of various supercapacitor prototypes. These composites demonstrated enhanced pseudo-capacitance effects and specific energy, highlighting the faradaic contributions of conducting polymers to the overall energy storage capacity of supercapacitors [21].

P. Li et al. (2014) introduced a novel CNT@PPy core-shell sponge, leveraging a three-dimensional conductive nanotube network for supercapacitor electrodes. This unique structure offered high performance and elasticity, maintaining stable capacitance under compression cycles. The approach exemplifies the potential of nano-engineered materials in creating flexible and durable energy storage solutions.

In another study by P. Li et al. (2014), a sustainable freeze–thaw technique was employed to fabricate freestanding composite films with a paper-like appearance, which were then subjected to in situ chemical polymerization of polypyrrole (PPy) This methodology resulted in electrodes with high electrical conductivity, excellent areal capacitance, and outstanding cycling stability, indicating a promising direction for green and sustainable electrode materials in flexible supercapacitors.

In recognition of their excellent cycling stability and high C_P, polypyrrole/MnO_2 nanocomposites have been investigated for use in supercapacitors. However, challenges such as capacitance retention over extended cycling and the trade-off between stability and C_P have been noted, underscoring the need for further optimization in electrode formulations. These studies collectively advance the field of supercapacitor development by demonstrating the effectiveness of novel material composites and fabrication techniques. The insights gained from these research efforts pave the way for future innovations in supercapacitor technology, focusing on high performance, durability, and application in advanced energy storage systems.

2.6 Polypyrrole/carbon composite electrode materials

Polypyrrole (PPy), recognized for its highest inherent conductivity among conducting polymers, plays a pivotal role in the progress of advanced electrode materials for supercapacitors. Its attractiveness lies in the easy oxidation of pyrrole, water solubility, high conductivity, strong redox reversibility, and environmental stability. These features position PPy as a promising candidate to improve the performance of supercapacitors, especially when considering the need for materials that exhibit both

high energy storage capacity and stability under operational conditions (Dubal et al., 2012; Haider et al., 2020; N. Li et al., 2016).

The integration of nano-sized materials, recognized for large surface area and porosity, with PPy shows to significant improvement in the electrochemical characteristics of electrodes. Nanostructured materials such as nanoparticles, nanowires, nanosheets, nanotubes, and nanoribbons offer pathways to augment electrical conductivity and, by extension, the performance of supercapacitor electrodes. However, challenges related to the polymeric composition and structural features of PPy, such as stability issues and life cycle degradation during prolonged charge-discharge processes, have been identified as limiting factors in its application.

To overcome these limitations, PPy is often doped with carbon and metal oxide materials, forming composites that leverage the electrochemical activity of PPy while improving stability and lifecycle performance. Various carbon-based materials, including activated carbon, multi-wall CNTs (MWCNTs), single-wall CNTs (SWCNTs), carbon foam, glassy carbon, carbon fiber, and graphite fiber matrix, have been explored as components of PPy/carbon composite electrodes. These composites have demonstrated enhanced electrochemical properties, making them suitable for supercapacitor applications.

Among the novel materials explored, carbon aerogel stands out due to its mesoporous structure, electrically conductive carbon network, and low density. While carbon aerogel has been utilized in photovoltaic materials, its application in conjunction with PPy for supercapacitor electrodes has been less reported. Hongfang An et al.. (2010) prepared a PPy/carbon aerogel (PPy/CA) composite and investigated its electrochemical performance through CV, GCD, and EIS. The PPy/CA composite exhibited an impressive C_P of 433 F g^{-1}, significantly higher than that of carbon aerogel alone. The study highlights the potential of PPy/CA composites as efficient supercapacitor electrode materials, providing a means of achieving high-performance energy storage systems.

2.7 Ferrite nanoparticles as electrode materials

The advancement in supercapacitor technology has been significantly propelled by the exploration and development of novel electrode materials, particularly focusing on

ferrite-based composites. These materials, including nickel ferrite (NiFe2O4), cobalt ferrite (CoFe2O4), and manganese cobalt ferrite (MnCoFeO4), among others, have garnered attention due to their abundant availability, environmental friendliness, and unique electrochemical properties conducive to energy storage applications. The studies reviewed here illustrate a broad spectrum of synthesis methods, structural characterizations, and electrochemical evaluations, underscoring the potential of ferrite-based nanoparticles in enhancing supercapacitor performance.

Mordina et al. (2020) demonstrated the superior performance of binder-free NiFe2O4 positive electrodes paired with activated carbon negative electrodes in a hybrid supercapacitor device. The NiFe2O4 nanoparticles, grown directly on Ni-foam using a surfactant-assisted co-precipitation technique, showcased excellent specific capacity and energy density, alongside remarkable cyclic stability over 6500 cycles. This highlights NiFe2O4's potential as a reliable electrode material for high-performance supercapacitors [86].

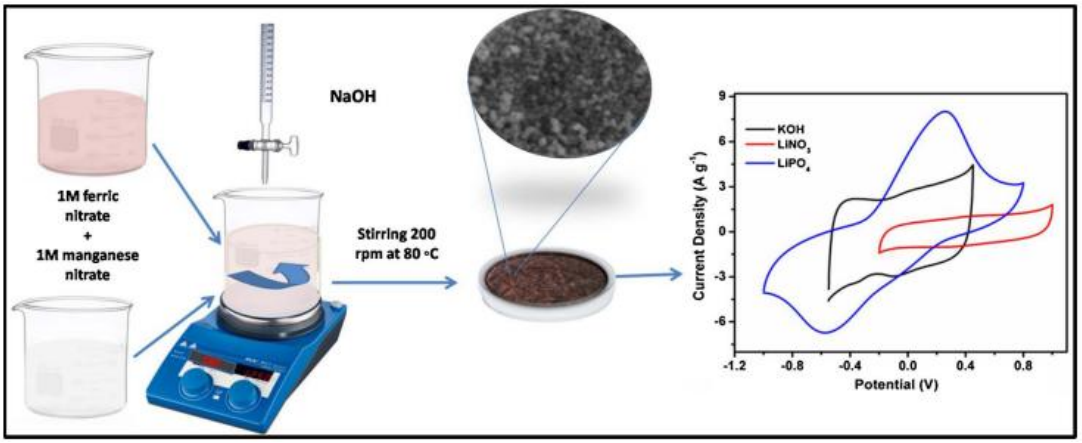

Figure 2.13: (a) The columbic efficiency was used to measure the cyclic performance at 3 A g^{-1}, (b) $MnFe_2O_4$ NS symmetric electrode Ragone plot in 3.5 M KOH electrolyte [74]

The study by Vignesh et al. (2018) represents a significant development in the preparation and use of manganese ferrite ($MnFe_2O_4$) nanoparticles for supercapacitor electrode applications. Using a simple and economical chemical co-precipitation technique, where 1 M NaOH served as the oxidizing agent, the researchers synthesized $MnFe_2O_4$ nanoparticles with a uniform spherical shape, measuring between 20 and 50 nanometers in diameter. This method not only proved to be low-cost but also resulted

in nanoparticles with favorable electrochemical characteristics suitable for energy storage.

Among the various electrolytes evaluated, the 3.5 M KOH solution delivered the best electrochemical outcomes, with the $MnFe_2O_4$ nanoparticles achieving a peak specific capacitance (CP) of 430 F g^{-1}. This high performance is credited to the material's improved surface area, electronic conductivity, and synergistic interactions within the electrode structure. In a symmetric two-electrode configuration using the same electrolyte, the $MnFe_2O_4$-based electrodes demonstrated notable energy storage metrics—245 F g^{-1} for capacitance, 12.6 Wh kg^{-1} for energy density (Ed), and 1207 W kg^{-1} for P_d.

Remarkably, the supercapacitor exhibited excellent cycling durability, maintaining 105% of its original capacitance after 10,000 charge-discharge cycles at a high current density of 1.5 A g^{-1}, and a stable Coulombic efficiency of around 98%. These findings underscore the stability and strong performance potential of $MnFe_2O_4$ nanoparticles as electrode materials in next-generation supercapacitors. The work highlights the importance of using affordable synthesis routes like co-precipitation to create high-performance materials for energy storage, encouraging further research into ferrite-based systems to improve both efficiency and device lifespan [74].

Kennaz et al. (2018) and Martinez-Vargas et al. (2020) explored the electrochemical capabilities of $CoFe_2O_4$ nanoparticles synthesized via hydrothermal and co-precipitation methods. These nanoparticles exhibited significant C_P and stability improvements in supercapacitors, with enhanced performance observed in flexible supercapacitor configurations. The research indicates the effectiveness of $CoFe_2O_4$ in developing supercapacitors with high capacitance and extended discharge times, which are beneficial for flexible electronics applications.

Soam et al. (2019) and Alshehri et al. (2017) investigated the electrochemical performance of nickel ferrite/graphene and nitrogen-doped $CoFe_2O_4$/C nanocomposites, respectively. These studies revealed that the incorporation of graphene and nitrogen doping could significantly enhance the C_P and cycling stability of ferrite-based supercapacitors. The synergistic effect between the ferrite nanoparticles and the

conductive matrix underscores the importance of composite strategies in achieving superior electrochemical properties [88, 990].

Research by Raza et al. (2021), Al Kiey et al. (2022), and Vignesh et al. (2018) introduced innovative ferrite compositions, such as lanthanum cerium ferrite and manganese ferrite nanoparticles, synthesized through various methods. These materials demonstrated exceptional C_P and E_d, showcasing the impact of material composition and synthesis technique on the electrochemical performance of supercapacitors.

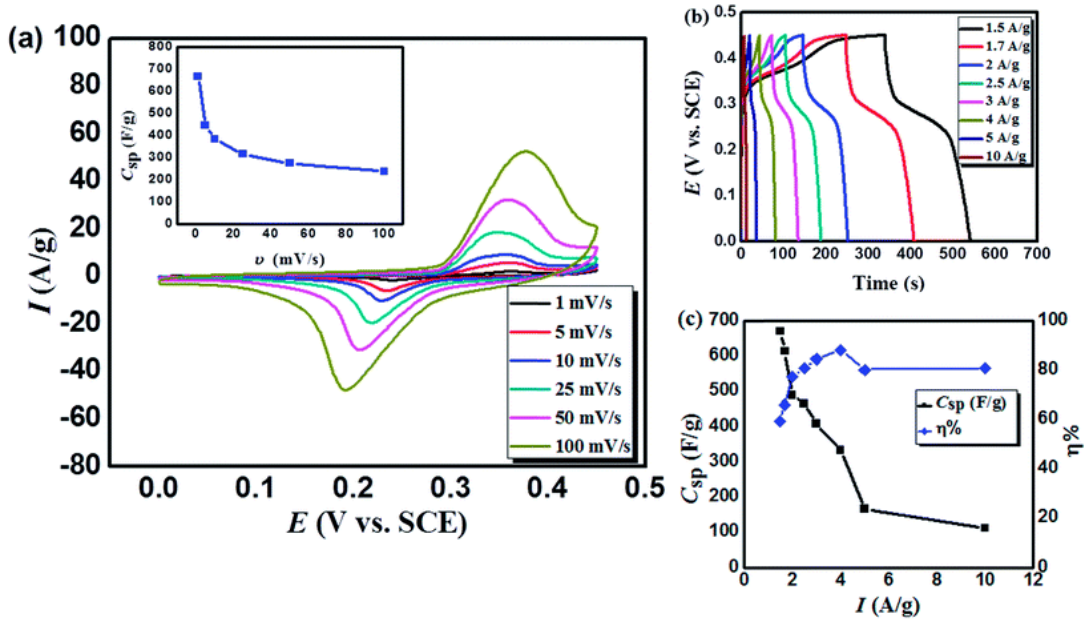

Figure 2.14 (a) CV curves for as-prepared MnCoFeO4 at various scan speeds in the 6 M KOH electrolyte potential range of 0–0.45 V_{SCE}, with the inset illustrating how the specific capacitance varies with scan rate. In the 6 M KOH electrolyte, (b) galvanostatic charge/discharge curves for $MnCoFeO_4$ and (c) the computed Csp and η% at various current densities in the potential range of 0–0.45 V_{SCE} Source: [75].

Elkholy et al. (2017) have conducted research that produces significant new data on the synthesis of manganese cobalt ferrite ($MnCoFe_2O_4$) nanoparticles for high-performance supercapacitors. Method used is effective one-pot co-precipitation technique. This study underscores the potential of $MnCoFe_2O_4$ as a promising electrode material for supercapacitor applications, considering its exceptional cycle stability and electrochemical performance, which includes high C_P, E_d, and P_d. Compared to many other ferrite-based materials reported in the literature, the $MnCoFe_2O_4$ supercapacitor's electrochemical evaluation showed a maximum C_P of 675 F g^{-1} at a scan rate of 1 mV

s^{-1}. Additionally, the E_d and P_d of 18.85 W h kg^{-1} and 337.50 W kg^{-1}, respectively, at a current density of 1.5 A g^{-1}, highlight the efficient energy storage and rapid charge-discharge capabilities of the $MnCoFeO_4$ supercapacitor. These metrics are critical for the application of supercapacitors in various fields, including renewable energy systems, portable electronics, and electric vehicles, where both high energy storage and quick energy release are desirable. The long-term cyclic stability of the $MnCoFeO_4$ supercapacitor, with only a 7.14% degradation in supercapacitive performance after 1000 GCD cycles, speaks volumes about the durability and reliability of this electrode material. Moreover, the nearly constant equivalent series resistance (ESR) throughout the cyclic testing further underscores the robustness of the MnCoFeO4 nanoparticles, ensuring minimal energy loss during operation and enhancing the overall efficiency of the supercapacitor.

Aparna et al. (2018) reported on the synthesis of mesoporous metal ferrite nanoassemblies, highlighting the role of pore structure and crystallinity in determining the supercapacitive performance. CoFe2O4, among other ferrites, exhibited the highest C_P, emphasizing the potential of mesoporous structures in enhancing electrochemical activity and energy storage efficiency.

2.8 Ppy/rGO/Ferrite based electrodes

One viable method to overcome the drawbacks of conducting polymers (CPs) is their combination with carbon-based materials and transition metal oxides, particularly their poor stability, which adversely affects their capacitive performance over long cycles. This approach aims to enhance the lifecycle and overall performance of supercapacitor materials by leveraging the synergistic effects of these composite materials.

Conducting polymers, despite their attractive electrochemical properties, suffer from significant drawbacks such as poor stability and a notable capacity drop during prolonged cycling. These issues stem from the inherent material properties of CPs, This may eventually cause capacitive performance to decline.

To address the stability challenges associated with conducting polymers (CPs), researchers have integrated various carbon-based materials—such as graphene,

activated carbon, and carbon nanotubes—into CP-based supercapacitor systems. These carbon materials offer excellent electrical conductivity, high surface area, and robust mechanical properties, which collectively enhance the electrochemical stability and overall performance of the composite electrodes.

Transition metal oxides like RuO_2, Co_3O_4, TiO_2, NiO, MnO_2, CeO_2, Co_2O_3, and V_2O_5 have also been widely explored in supercapacitor research due to their high pseudocapacitance and charge storage capabilities. Iron oxides, in particular, are attractive for energy storage because of their reversible Fe^{3+}/Fe^{2+} redox activity, abundance, low cost, environmental friendliness, and non-toxicity. However, the practical application of Fe_2O_3 is hindered by its poor electrical conductivity and limited cycling stability.

One effective strategy to overcome these drawbacks is to combine Fe_2O_3 with conductive polymers and carbon materials. This synergistic approach enhances both the electrical conductivity and cycling durability of the composite, leading to improved specific capacitance (CP). Hybrid materials that incorporate conducting polymers, metal oxides, and two-dimensional reduced graphene oxide (rGO) have demonstrated notable improvements in capacitance and stability.

For example, Shu et al. used electrochemical polymerization to fabricate free-standing rGO/polypyrrole (PPy) hybrid nanocomposites, achieving an impressive areal capacitance of 440 mF cm^{-2} at a current density of 0.5 mA cm^{-2}. Similarly, Bashid et al. developed a two-step electrodeposition method to grow PPy and rGO on carbon bundle fibers, resulting in a symmetric solid-state supercapacitor that retained 71% of its capacitance after 500 cycles and delivered a CP of 96 F g^{-1} at 1 A g^{-1}.

These studies highlight the potential of combining CPs with carbon-based structures and transition metal oxides to engineer advanced supercapacitor electrodes with enhanced performance, stability, and lifespan. This integrated approach paves the way for the development of next-generation, high-efficiency energy storage devices.

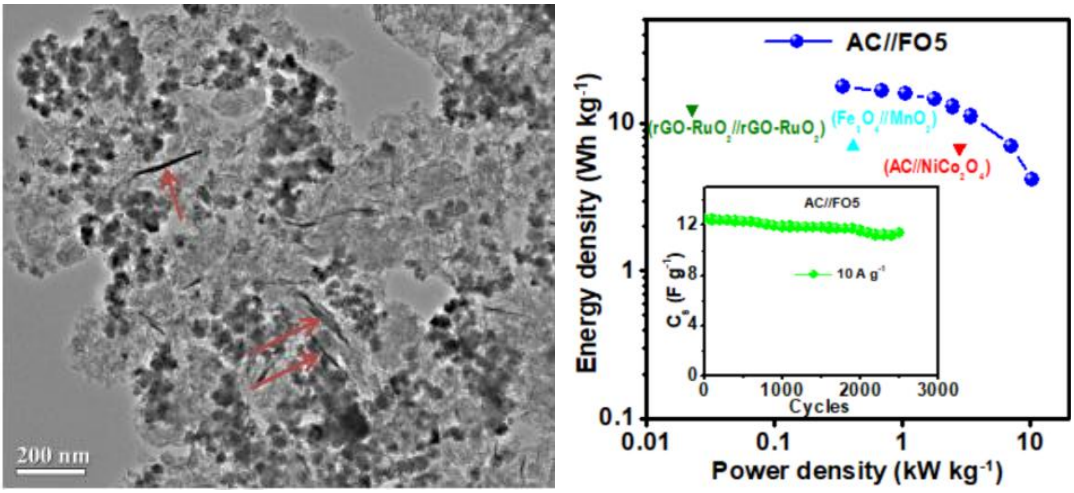

Figure 2.15: TEM imaje of rGO/Ppy/Fe_3O_4 and power/energy density profile. Source: [38]

Mariappan et al. successfully synthesized rGO/PPy/metal oxide ternary hybrids, revealing their structure and morphology through comprehensive analyses, including FTIR, Raman spectroscopy, XRD, and TEM. These characterizations confirmed the formation of spinel-type metal oxide nanoparticles embedded in branched PPy chains on rGO sheets. The electrochemical performance of these nanocomposites, assessed in 1 M $LiNO_3$ electrolyte, demonstrated significant variations in C_P based on the content and type of metal oxide used. The FO5 composite, containing Fe3O4, exhibited the highest C_P and rate performance among the tested samples, underscoring the impact of the composition on the supercapacitive properties.

Thu et al.. explored the capacitive performance enhancement through the chemical growth of PPy on graphene-supported manganese ferrite microspheres to create PPy/MG hybrids. The comprehensive characterization of these materials provided insights into their structural and morphological properties, correlating these attributes to their improved electrochemical performances. The incorporation of PPy significantly enhanced the C_P of the hybrids compared to individual components, demonstrating the synergistic effects of combining conductive polymers with metal oxide-supported graphene.

Table 2.1: PPy, Graphene/PPy, Graphene/PPy/Ferrite based electrodes and their electrochemical properties

S. No	Electrode materials	Size/Morphology/Structure	Specific capacitance (C_P) (Fg^{-1})	Energy density Wh/Kg at 10 mV/s	Capacitance retention at a current density of 10 mA cm^{-2}	Ref
1	Polypyrrole	20nm, spherical	533(10 mV/s)	-	83%	[60]
2	Graphene polypyrrole	Nano fiber	466(10 mV/s)	165.7	-	[76]
3	Graphene/Polypyrrole	Nanotube	400(10 mV/s)	-	-	[77]
4	Graphene/ppy	nanowire	165(10 mV/s)	-	92 %	[78]
5	GO/PPy composite	3D interconnected structure	481.1(10 mV/s)	-	80%	[79]
6	graphene oxide-polypyrrole	core–shell composite	557(10 mV/s)	49.5		[80]
7	polypyrrole/reduced graphene oxide	Spherical, cauliflower like structure	198(10 mV/s)	-	92%	[81]
8	GO/PPy	multlilayer films	332(10 mV/s)	78	-	[64]
9	EG-RGO/PPy	quazi-2D ordered structures	420(10 mV/s)	-	93%	[70]
10	PPy coated multiwalled carbon nanotubes (MWCNT)	Nanotube	183.2 current density of 8 A g^{-1}	15.1	85%	[82]
11	PPy@CNT	Nanotube	350(10 mV/s)	-	-	[71]

12	graphene oxide/polypyrrole/multi-walled carbon nanotubes	Nanotube	406.7 0.5 A g^{-1}	-	92%	[83]
13	polypyrrole(PPy)/functionalized-multiwalled carbon nanotubes (FM) composites	nanotubes	1269(10 mV/s)	-	88.1	[84]
14	CNT@PPy	nanotubes	300(10 mV/s)	-	90%	[85]
15	$NiFe_2O_4$	Spherical	398(10 mV/s)	27.71	98%	[86]
16	Lanthanum cerium ferrite	Spherical clustered	1195(10 mV/s)	59 Wh/kg	92.3%	[87]
17	nickel ferrite/graphene	, flakes and particles type	207(10 mV/s)	-	95	[88]
18	Ni0.2Co0.8Fe2O4	clustered molecule grouped together	561(10 mV/s)	-	-	[89]
19	CoFe2- O4	clustered molecule grouped together	517(10 mV/s)	-	-	[89]
20	Nitrogen-doped $CoFe_2O_4$/C	average size of ~ 10 nm	474 (10 mV/s)	116	-	[90]
21	$CoFe_2O_4$	average size of ~ 10 nm	94(10 mV/s)	23	-	[90]
22	$ZrCoFe_2O_4$/nitrogen-doped reduced graphene oxide	Spherical	307 at 1 A g^{-1}	42.7	-	[91]
23	Co–Cu ferrite	spherical shape with	893 (10	-	90	[92]

		a size ranging from 30 to 50 nm.	mV/s)			
24	$MnFe_2O_4$	nanosphere	245 (10 mV/s)	12.6	105	
25	$MnCoFeO_4$	spherical shape	670(10 mV/s)	3.15	-	
26	$CoMnFeO_4$	spherical shape	770 (10 mV/s)	-	88	[93]
27	PPy/MnFe2O4/ rGO	globular form and often aggregates with granular components into bigger entities.	∼147 F/g (10 mV/s)	66.1	-	[94]

Both studies illustrate the potential of hybrid nanocomposites in supercapacitor applications, showcasing improved C_p, rate capability, and cycling performance. The research emphasizes the role of material hybridization in overcoming the limitations of individual components, such as poor conductivity and cycle stability, by exploiting the synergistic properties of conducting polymers, carbon materials, and metal oxides. These findings contribute to the ongoing efforts to develop high-performance, durable, and efficient supercapacitors, highlighting the importance of material design and composition optimization. Future research in this area may focus on further enhancing the electrochemical properties of hybrid nanocomposites, exploring new material combinations, and scaling up the synthesis processes for practical applications in energy storage systems.

CHAPTER 3

Materials, methodology and characterizations

This section describes the materials and methods of the research work carried out on the investigation of the electrochemical properties of polypyrrole/reduced graphene oxide/nickel cobalt ferrite as an electrode material for supercapacitor application. The method of preparation of electrode material, characterization of electrode materials, construction of electrodes, and electrochemical measurement of electrodes are discussed in detail.

3.1 Materials and methods

Analytical grade chemicals, reagents, and solvents were used for all experiments. The received chemicals were pure (>98%) and used without further purification. Nickel nitrate, Cobalt nitrate, Iron nitrate, Sodium nitrate, $FeCl_3$, Pyrrole, CTAB, NH_3 graphite powder, polyvinylidine fluoride (PVDF), and acetylene black, citric acid, potassium permanganate. N-methylpyrrolydone (NMP), H_2SO_4, and HCl were received from Sigma Aldrich Chemical Company. Distilled water was prepared in the laboratory and used for the preparation of the solution.

3.1.1 Synthesis of reduced graphene oxide (Hummer's method)

The modified Hummers' method was used to prepare reduced graphene oxide. Briefly, 2g of graphite powder and 2g of $NaNO_3$ were slowly added to 100 mL of concentrated H_2SO_4. The entire mixture was slowly stirred in an ice bath. Then, 6g of $KMnO_4$ was added slowly to the resulting mixture, and the temperature was gradually raised to 45 °C while stirring for 2h. After that, distilled water (300 ml) and H_2O_2 (15 ml, 35%) were added to the above mixture, and then the obtained precipitate was washed with concentrated HCl to obtain graphene oxide (Kim et al., 2013). The graphene oxide (GO) obtained was dried in a hot air oven for 3 hours to convert reduced graphene oxide (rGO)

3.1.2 Synthesis of NiCoFerrite nanoparticles

Stoichiometric amounts of Nickel nitrate (3M), cobalt nitrate (3M), Ferric Nitrate (12M), and citric acid were added to 150ml of DI. The mixture was stirred at 250 rpm in a magnetic stirrer for 20 minutes to obtain a homogenous solution. After that, the solution pH was gradually raised to 8 by a drop addition of NH_3. The resulting mixture was stirred at 250 rpm for 30 minutes. Then, the temperature of the above mixture was raised to 100 °C to evaporate water molecules and convert into gel. The obtained gel was further dried in a hot air oven at 80 °C for 6 hours to get powder. The powder sample was named NiCoFerrite and stored in a glass vial for further experiment and characterization.

3.1.3 Synthesis of rGO/NiCoFerrite nanoparticles

To prepare the rGO/NiCoFerrite composite, the NiCoFerrite mixture preparation procedure was followed with little modification. Briefly, stoichiometric amounts of cobalt nitrate (3M), Nickel nitrate (3M), Ferric Nitrate (12M), and citric acid were added to 150 mL of deionized water. To this mixture, 0.92 grams of rGO sonicated in 75 mL of water was added. The mixture was stirred at 250 rpm in a magnetic stirrer for 20 minutes to obtain a homogenous solution. After that, the solution pH was gradually raised to 8-9 by dropwise addition of NH_3. The resulting mixture was stirred at 250 rpm for 30 minutes. Then, the temperature of the above mixture was raised to 100 °C to evaporate water molecules and convert it into a gel. The obtained gel was further dried in a hot air oven at 80 °C for 6 hours to get powder. The powder sample was designated as rGO/NiCoFerrite and stored in a glass vial for further experiments and characterization.

3.1.4 Synthesis of PPy/rGO/NiCoFerrite nanoparticles

The same binary mixture preparation procedure was followed for the preparation of ternary composite materials with little modification. Briefly, stoichiometric amounts of cobalt nitrate (3M), Nickel nitrate (3M), Ferric Nitrate (12M), and citric acid were added to 150 mL of deionized water. The surfactant CTAB 0.025M was added to the above mixture. The entire mixture was stirred at 250 rpm in a magnetic stirrer for 20 minutes to obtain a homogenous solution. To this mixture, pyrrole (0.6 mL) in ethanol

3ml was added with constant stirring. After that, the solution pH was gradually raised to 8-9 by drop wise addition of NH_3. The resulting mixture was stirred at 250 rpm for 30 minutes. Then, the temperature of the above mixture was raised to 100 °C to evaporate water molecules and convert into gel. The obtained gel was further dried in a hot air oven at 80 °C for 6 hours to get powder. The powder sample was named NiCoFerrite and stored in a glass vial for further experiment and characterization.

3.2 Characterization

3.2.1 X-ray diffraction analysis

XRD was performed on an X-ray diffractometer (Model – Bruker D8, Cu Kα – radiation and λ – 1.5406 Å) for the prepared samples to elucidate crystal lattice, phase composition, and crystalline properties of the samples. The XRD instrument is composed of a source, primary and secondary optics, goniometers, and a detector, depending on the applications. The working principles of the XRD are given in the following figure 3.1.

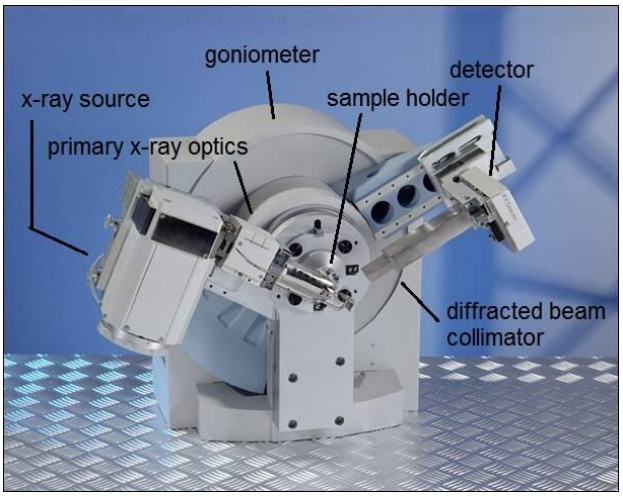

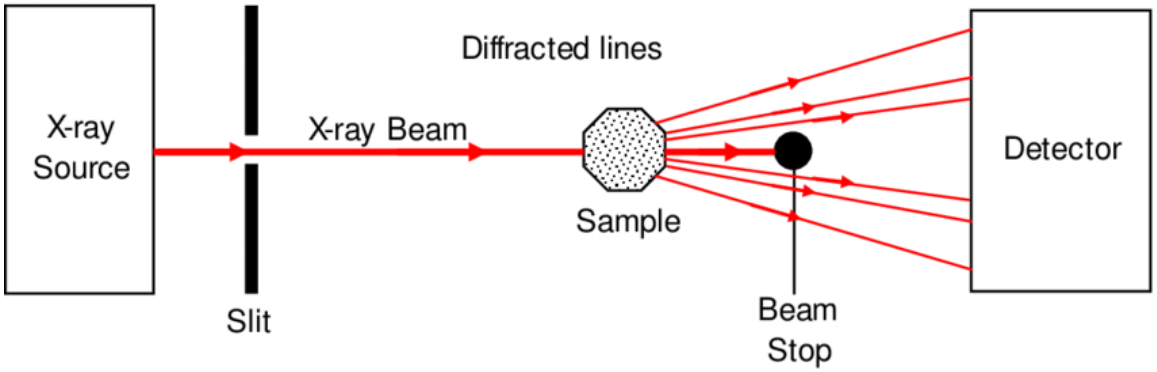

Figure 3.1: XRD instrumentation – schematic representation

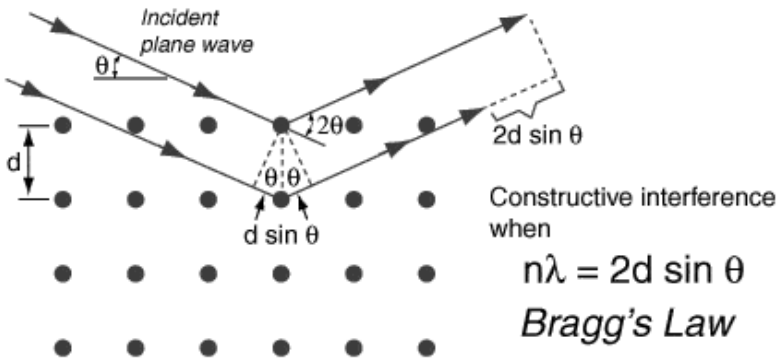

Figure 3.2: Bragg's law in XRD – schematic representation

The diffracted rays undergo constructive and destructive interference depending on whether they obey Bragg's law or not. The constructive interference of rays yields diffraction patterns that are characteristic of crystals. XRD demonstrated peaks due to beams of x-ray scattered at specific angles in each lattice of the samples. The distribution of atoms in the lattice is denoted by the intensities of the peak. The plot arrived from peak intensity versus the function of 2 theta.

The XRD data were collected within the 2θ range of 10° to 80° with a scan rate of 1°/min. These parameters were selected to obtain noise-free data. The obtained data was analyzed with standard JCPDS crystallographic data card to identify the sample phase composition. Debye Scherer's formula Eq (3.1) was used to calculate the crystallite size of the materials.

$$D = \frac{K\lambda}{\beta cos\theta} \qquad \text{----- (3.1)}$$

Where D- crystallite size of the particles

λ – Wavelength of the X-ray

β - Full width half maxima (FWHM)

θ – Bragg angle

The results of XRD analysis were used to elucidate structural properties of the sample and further supported the materials' properties and performance in the context of the study.

3.2.2 Photoluminescence analysis

Photoluminescence (PL) is a non-destructive method of investigating the luminescence properties of the materials. PL study for the samples was conducted on an instrument Agilent spectrophotometer. In photoluminescence, the material absorbs photons from electromagnetic radiation and reemits the photons. Quantum mechanically, the excited atoms come to the ground state accompanied by emitting the photon. The radiative process of the materials is determined by the amount of photons emitted from the light. The principle of photoluminescence spectroscopy is described in Figure 3.3.

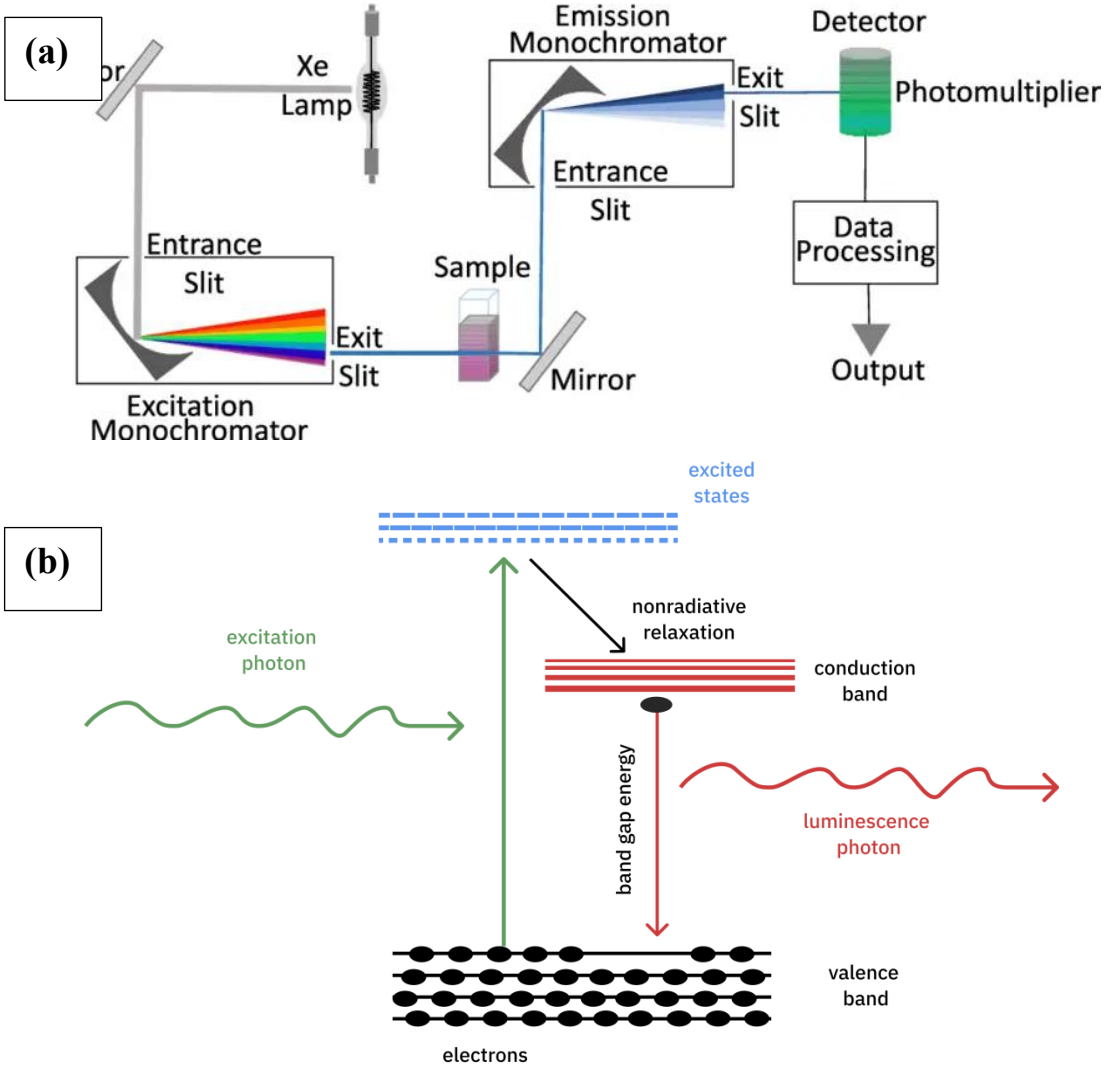

Figure 3.3: (a) Instrumentation of PL spectroscopy and (b) Principles of photoluminescence spectroscopy

3.2.3 Fourier transform infrared analysis

Fourier transform infrared (FTIR) analysis is an important analytical technique to

analyze the functional groups of the materials. FTIR for all the samples was carried out on an instrument of Perkin Elmer spectrum II, in attenuated total reflection (ATR) mode, IR range 4000 – 400 cm^{-1}. The sample was placed on a diamond crystal of the instrument, exposed to IR beam ranging from 4000 – 400 cm^{-1} passes through the crystal forming an evanescent wave that penetrates and reflects off the surface off the sample.

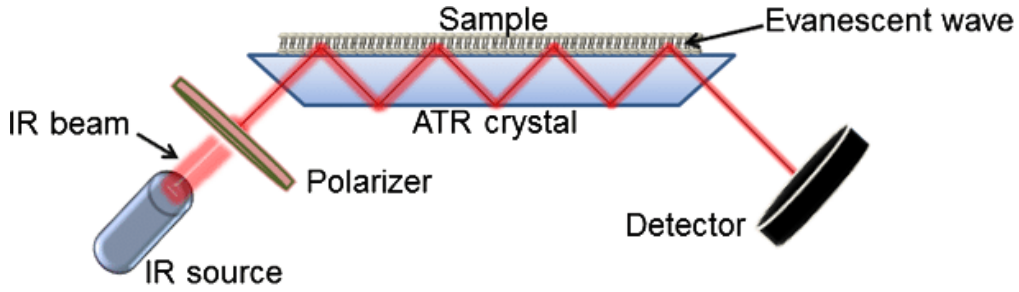

Figure 3.4: Working principles of FTIR-ATR mode

FTIR-ATR was used to analyze the chemical functional groups present on the prepared samples that have vibrational characteristics in the mid-range of the IR region (4000 – 400 cm^{-1}).

3.2.4 Scanning electron microscope analysis

The SEM analytical method is a versatile tool to determine the surface morphology, topography, and size of the materials. The surface profile of the samples is essential to optimize the composite materials ratio for supercapacitor applications. The surface morphology of the prepared samples, rGO, NiCoFerrite, rGO/NiCoFerrite, and PPy/rGO/NiCoFerrite, was analyzed on an HRSEM instrument, Hitachi, Japan. The instrument also included the energy dispersive X-ray analysis (EDAX) accessories. An EDAX profile is necessary to identify the purity of prepared samples. The working principle of SEM is illustrated in the following Figure 3.5.

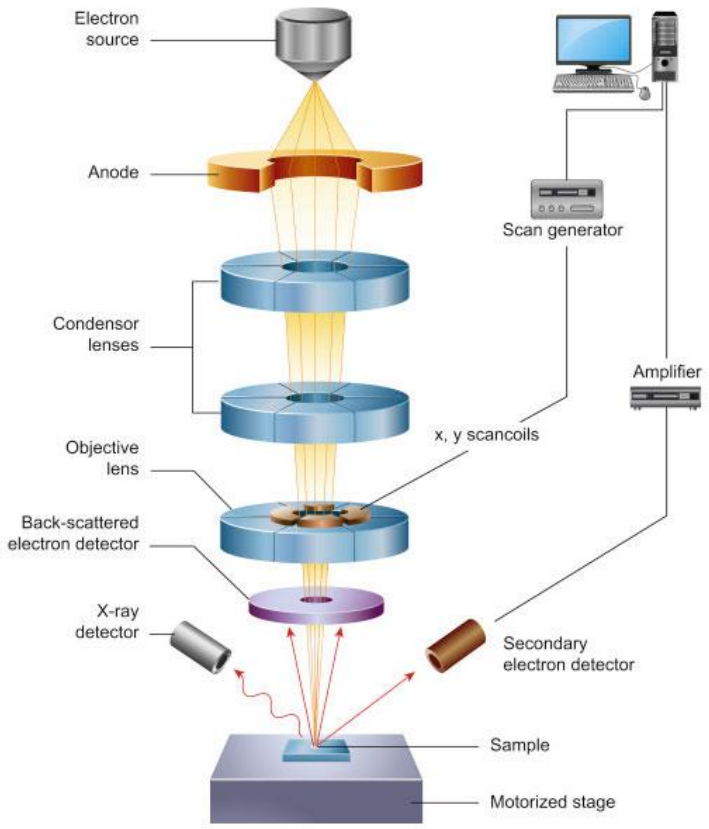

Figure 3.5: Scanning electron microscopy - Instrumentation (Source: https://www.nanoscience.com/techniques/scanning-electron-microscopy/)

SEM was employed to investigate the surface morphology and microstructural features of the samples. The samples were securely mounted on a specialized stage within the SEM chamber, and the entire system was evacuated to achieve a high vacuum environment, essential for maintaining electron beam stability and sample integrity. The electron gun at the top of the SEM column emitted a beam of electrons, which was accelerated between 1 keV and 30 keV, depending on the desired resolution and depth of field. The beam was subsequently narrowed and directed through a series of condenser lenses and apertures, optimizing the beam's focus and intensity. At the heart of the imaging process, the objective lens focused the electron beam onto a minute area of the sample, achieving a beam diameter ranging from less than 1 nanometer to 20 nanometers. The precise manipulation of the beam over the sample's surface was controlled by scan coils located above the objective lens, facilitating detailed scanning in the X-Y plane.

As the electron beam interacted with the sample, it elicited various signals, including secondary electrons, backscattered electrons, and characteristic X-rays, which were captured by dedicated detectors. The intensity of these signals was correlated with the beam's position by a scan generator integrated with an external computer system equipped with specialized software. This setup allowed for the real-time rendering of a grayscale image, pixel by pixel. The magnification of the images was determined by the size of the area scanned, with higher magnifications achieved by scanning smaller areas. The resolution was further refined by adjusting the number of pixels within the scan area and the dwell time of the electron beam at each coordinate, which also allowed for modulation of the signal-to-noise ratio. This meticulous adjustment enabled detailed visualization of the sample's topography at various magnifications and depths.

This SEM methodology provided critical insights into the structural and compositional properties of the materials under study, facilitating a deeper understanding of their fundamental characteristics.

3.2.5 X-ray photoelectron spectroscopy

X-ray photoelectron spectroscopy (XPS) is an excellent analytical tool used to determine the chemical composition of prepared samples. The chemical oxidation state of the samples can be studied using the shift in binding energy peaks of the elements. The XPS analysis of all the samples was done on an instrument ULVAC-PHI Model: PHI5000. The working principle of XPS is schematically illustrated in the following figure 3.6.

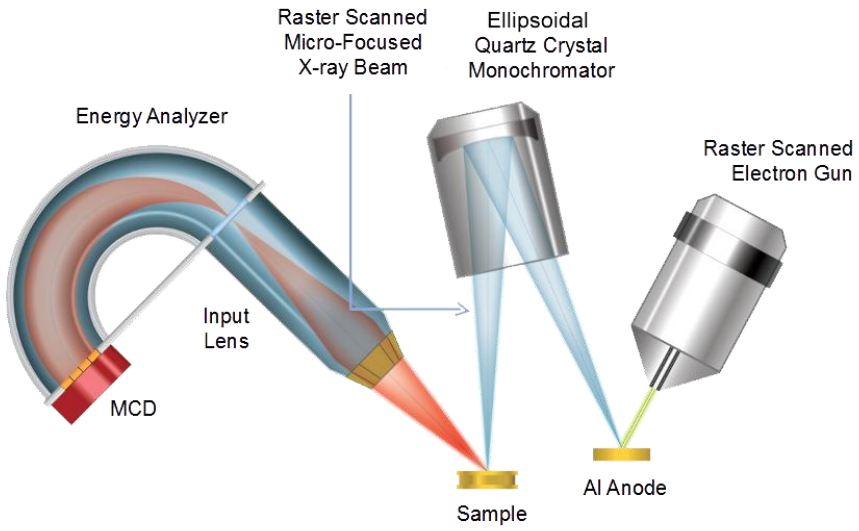

Figure 3.6: Instrumentation – XPS surface profile analysis (Source: https://www.phi.com/surface-analysis-techniques/xps-esca.html)

Characterization of surface composition and chemical states of the material under investigation was performed by X-ray Photoelectron Spectroscopy (XPS) or Electron Spectroscopy for Chemical Analysis (ESCA). A critical technique is indispensable for the assessment of surfaces and films because it delivers data of an elemental character in both quantitative and qualitative ways. Mono-energetic aluminum Kα X-rays were used to excite the photoelectrons from the material surface. The photoelectrons were then studied for their energy through an electron energy analyzer. From the spectrum, the full-width half-maximum of these peaks was used to calculate the binding energy and intensity to acquire the information of the elemental composition, chemical state, and concentration of the elements in the material to a depth from approximately 5 nm. This analysis was performed using an XPS instrument; the micro-focused X-ray beam allows for spatial resolution down to 7.5 µm. Even with such a high resolution, the sample could be scanned to obtain more information about spatial distribution.

Apart from performing better in-depth profiling of thin-film structures, XPS, in combination with ion milling, performs sequential layer-by-layer analysis. This is an especially well-suited analytical technique for the characterization of critical ultra-thin films and surface layers' performance in those advanced materials, which find applications in nanotechnology, photovoltaics, and electronic device fabrication. As compared with SEM/EDS, which analyzes sample features, typically to 1-3 µm, the

XPS has the ability to probe and acquire important information on the elemental and chemical composition of such surface features of a sample at a nanometer scale. This is especially true in the case of the surface features from which the most knowledge is investigated by disciplines such as materials science or other various types of scales.

3.2.6 Electrochemical studies

Electrochemical analyses such as cyclic voltammetry, galvanostatic charging and discharging, and electrochemical impedance spectroscopy for the prepared samples were analyzed on an instrument Metrohum. It is a multichannel potentiostat/galvanostat based on compact Autolab PGSTAT204. The electrochemical measurement was carried out in ambient conditions.

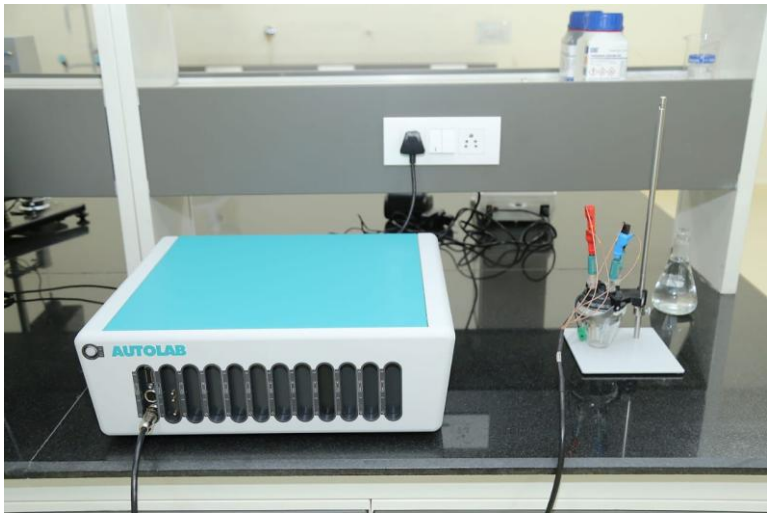

Figure 3.7: Metrohum

Construction of electrodes for electrochemical measurement –

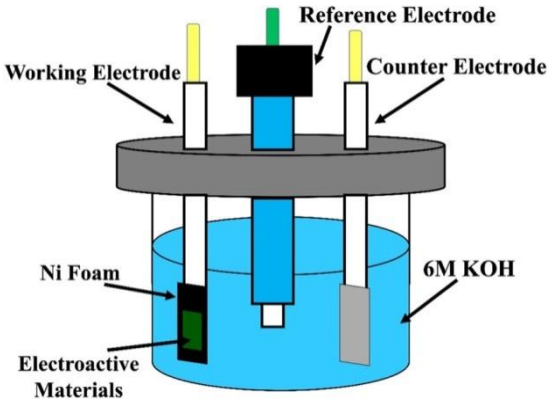

Figure 3.8: Typical three electrode system for electrochemical measurement of composite materials

A typical three-electrode system consists of a working electrode (Prepared samples), reference electrode (saturated calomel electrode and counter electrode (platinum electrode) immersed in 3M potassium hydroxide aqueous electrolyte. The platinum counter electrode surface was served as 1x1 cm^2. The prepared samples such as NiCoFerrite, rGO/NiCoFerrite, PPy/rGO/NiCoFerrite were used as active materials. Different ratios of the active materials electrochemical performance were analyzed. The detailed electrochemical studies and results are discussed in chapter 4. The working electrode was fabricated via mixing of active materials (85%), carbon black (10%) and polyvinylidene fluoride (5%) in N-methylpyrrolidone to make it as fine slurry. The slurry was applied on nickel foam (1x1 cm^2) current collector and subsequently dried at 80 °C for 12 hours for subsequent electrochemical study.

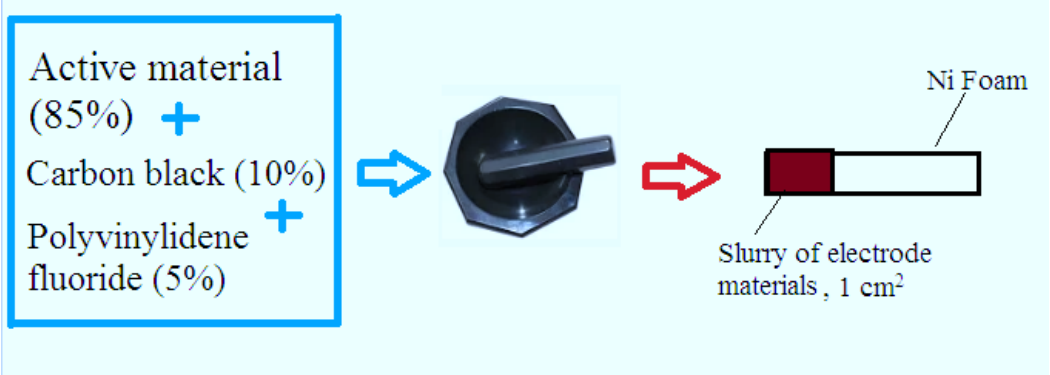

Figure 3.9: Construction of electrode from prepared materials for electrochemical measurement

The active electrode mass loading was adjusted to 2mg/cm^2 for all the electrodes during electrochemical analysis.

(a) Cyclic voltammetry:

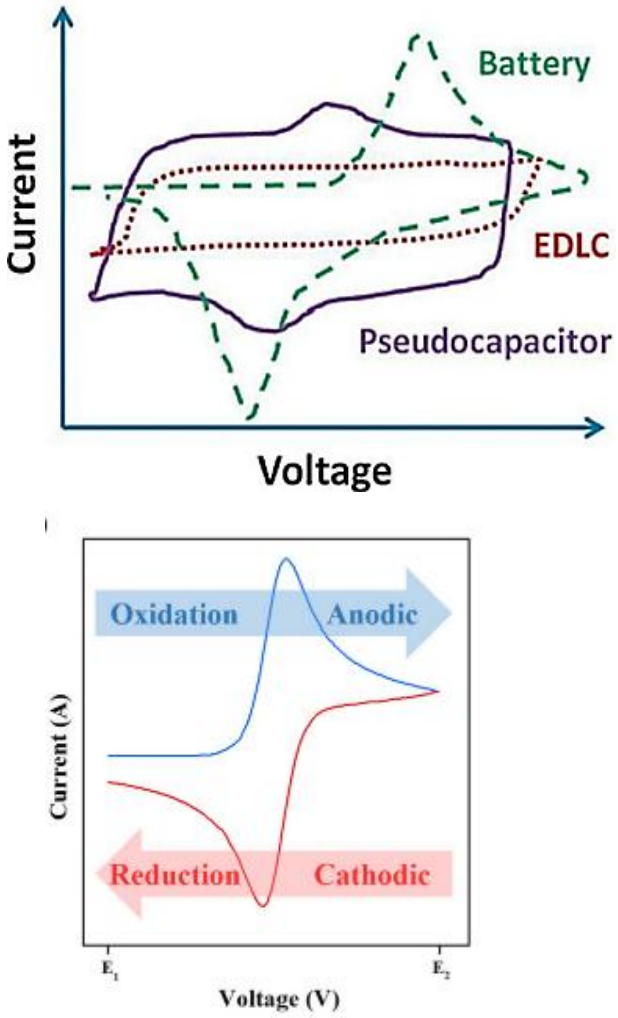

Figure 3.10: Typical cyclic voltammogram for EDLC, battery and pseudocapacitor

Cyclic voltammetry is an excellent technique for determination of electrode materials electrochemical properties. Different scan rate was 5, 10, 20, 30, 40 and 50 mV/s were applied for cyclic voltammetry measurement. The applied potential range between 0 to + 0.8V and 0 to 0.7 V was applied. The electrodes loss and acceptance of electron during the reaction is determined by applying different potential between the electrodes. Current value was measured between working and counter electrode from the graph of applied potential versus current.

The current density in a cell is measured based on applied voltage to electrode material greater that standard electrode potential (SEP) of electrode. The working electrode's potential is cyclic by measuring the current density, which redox behavior is analyzed. The current-voltage curve in redox reactions with peaks is called cyclic

voltammograms, where the redox reaction is reversible or not. It offers a rapid screening process to find possible capacitor materials. In an ideal case, an EDLC would exhibit a rectangle-shaped CV curve, indicating the current density remains independent of the potential. However, the above rectangular shape holds good only for such non-ideal EDLCs and Pseudocapacitors. It is now an apex means of evaluating the SC performance because it is very convenient to establish cycle life. Voltammogram shapes as a function of time may also provide insight into the impacts of internal resistance and the resulting dissipative losses. Faradaic capacitors should have a curved shape with anodic and cathodic peaks for a reversible electrochemical process, whereas EDLCs should have a shape that is similar to a rectangle for a reversible electrochemical process.

The following formula was used to determine the electrode material's specific capacitance:

$$Csp = [\int IdV / (s \times \Delta V \times m)]$$

$\int IdV$ is the integral area under CV curve

ΔV is potential window (V)

m is Mass of the electrode material (g)

s is the scan rate (mVs^{-1})

(b) Galvanostatic charging discharging studies of electrode:

GCD profile of an electrode material is essential for supercapacitor applications, which is an energy storage device, known for its high charging and discharging capabilities. In this study, the constant current was applied to electrode to charge and discharge, which helps in obtaining various parameters including, capacitance, E_d, P_d, and efficiency and life cycle, internal resistance. The capacitance of electrode was obtained from GCD studies and the results were calculated based on following formula.

$$C = \frac{I \times \Delta t}{\Delta V}$$

where C is the capacitance, I is the current, Δt is the time interval of the discharge, and ΔV is the change in voltage during the discharge.

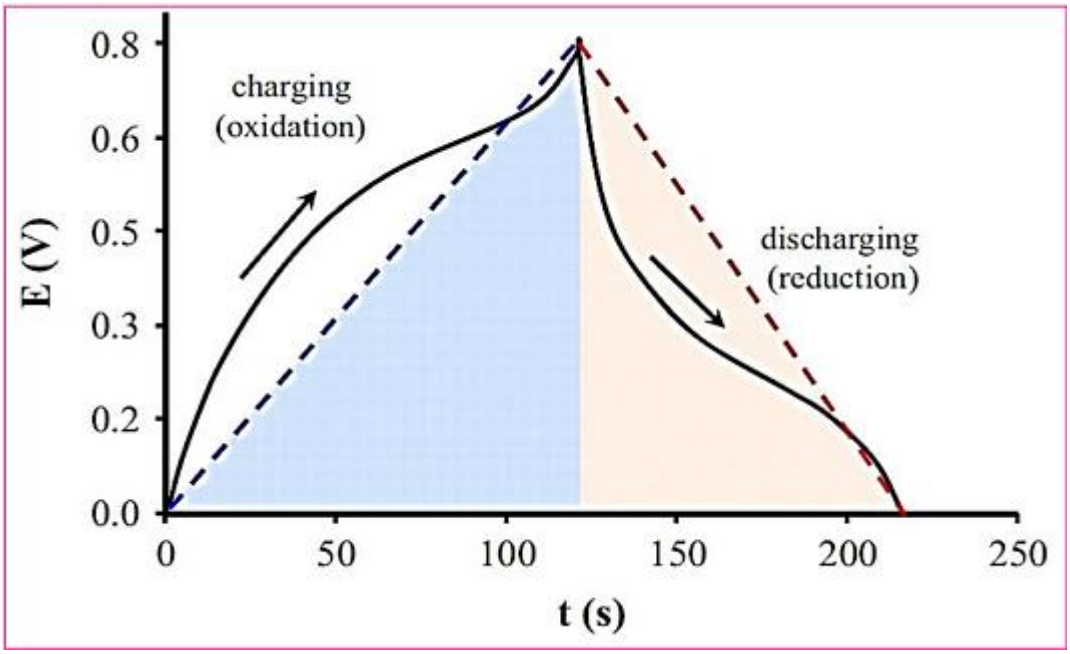

Figure 3.11: Typical galvanostatic charging and discharging profile of an electrode

Energy density is also an important parameter which helps to determine how much the electrode store energy per unit volume area. The energy density was calculated using formula.

$$E = \frac{1}{2} \times C \times (\Delta V)^2$$

Power density is yet another important parameter for determining electrode efficiency. Power density of a supercapacitor is known for its quick energy delivery, which was calculated using following formula.

$$P = \frac{E}{\Delta t}$$

Power density of an electrode is key advantage over other energy storage devices.

Efficiency and Cycle Life: GCD tests can also provide information on the efficiency of charge and discharge processes and the cycle life of the supercapacitor.

The efficiency is often derived from the ratio of the discharge energy to the charge energy, and the cycle life is determined by repeating the GCD tests until a significant drop in performance is observed.

Internal Resistance: The internal resistance can be estimated from the voltage drop at the beginning of the discharge phase, often known as the equivalent series resistance (ESR). A lower ESR is typically better, as it means less energy is lost as heat, and the supercapacitor can operate more efficiently.

(c) Electrochemical impedance spectroscopy

EIS is an excellent non-destructive technique used to measure complex electrical resistance and bulk material changes. EIS provides information about an electrode's conductance, charge transfer properties, electric co-efficiency, and dynamic change to adsorption. EIS data contains different circuit element values such as R, L, and C constructing an equivalent circuit will provide complete information about the electrode, suitable for the construction of a supercapacitor.

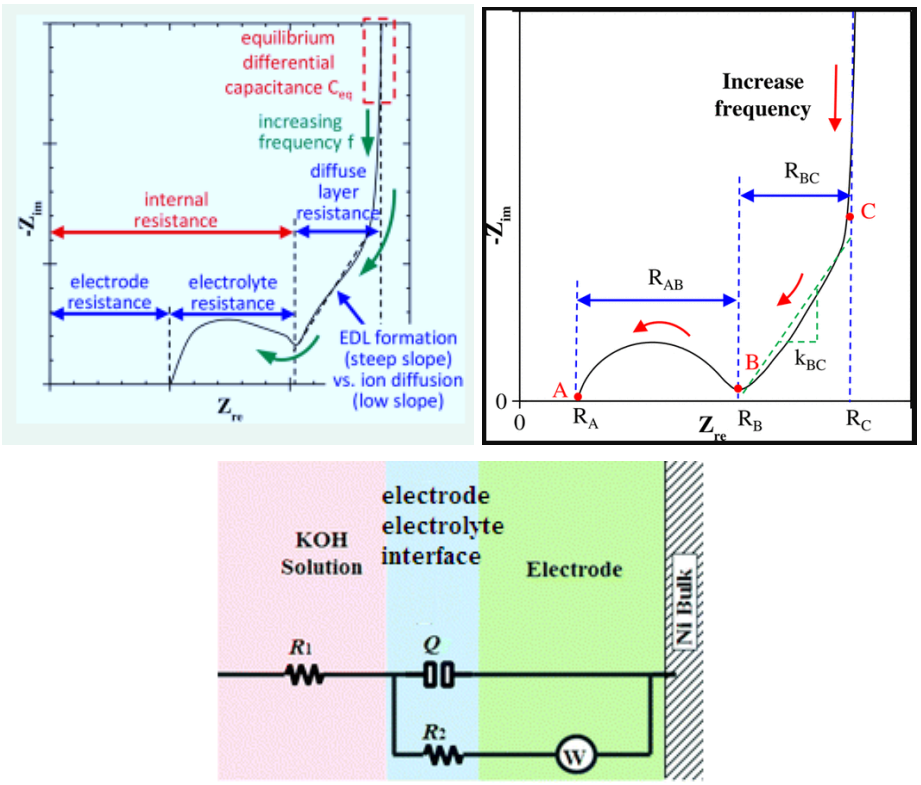

Figure 3.12: Typical Nyquist plot and equivalent circuit representation for an electrode in supercapacitor application [75]

Typical Nyquist plot of an electrode for supercapacitor applications is presented

in figure 1. From the figure (3.12), the diameter of the semicircle RAB = RB − RA (Figure 1) has been assigned to (i) the electrolyte resistance in the pores of the electrodes, (ii) the electrode-current collector contact resistance,38 (iii) the sum of the electrode resistance and contact resistance between the electrode and the current collector, or (iv) the so-called charge transfer resistance.

In EDLC devices, charge transfer resistance arises from the electrode resistance, the electrode–current collector contact resistance, and the electrolyte resistance within the porous electrode. Based on this, and interpreting R_A as the bulk electrolyte resistance, R_B (Figure 3.12), where $R_B = R_A = R_{AB}$, represents the internal resistance combining bulk and charge transfer resistances.
The non-vertical BC segment (Figure 3.12) at intermediate frequencies is attributed to ion transport limitations within the porous electrode, in the bulk electrolyte, or due to irregular ion pathways caused by surface roughness and pore size variations. Accordingly, R_{BC} (Figure 1) is termed the "equivalent distribution resistance". At low frequencies, beyond point C (Figure 1), the vertical line reflects the dominant capacitive behavior of the electric double layer. The intersection at Z_{re} , labeled R_C, corresponds to the internal resistance, equivalent series resistance (ESR), or total device resistance.

For real-time applications, stability is essential for synthesized electrode materials. The electrode materials get charged and discharged in one cycle by applying at a specific current density. Similarly, a n number cycle was performed to assess the electrochemical stability of a prepared material. EDLC stores energy at the surface of the electrode, whereas the Pseudocapacitors possess irreversible redox behavior. Due to these phenomena, the EDLC has a longer life cycle, and pseudocapacitive based electrode possess the shorter life cycle.

The following flow chart represents the summary of electrochemical measurement of electrode materials.

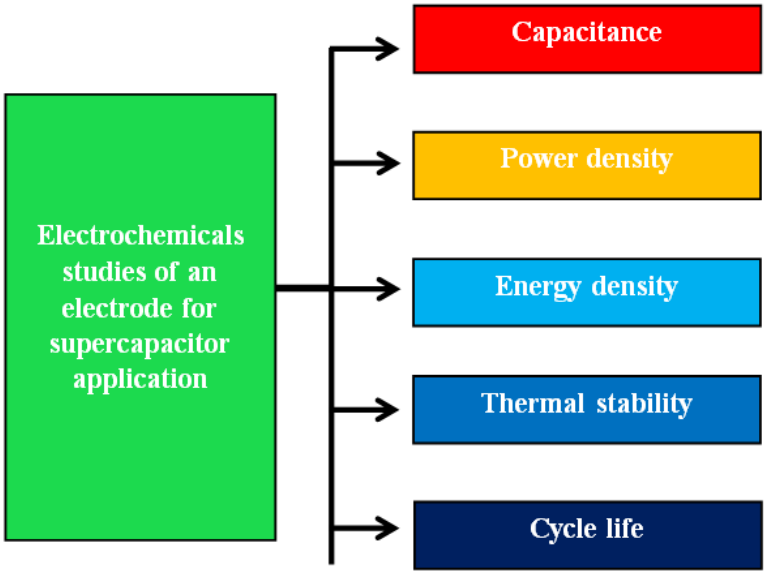

Figure 3.13: Flow chart representing the summary of electrochemical measurement

Several analytical methods were used to thoroughly characterize the produced electrode materials. Electrochemical studies were employed for all the prepared samples. The results obtained above are discussed in detail in the coming chapter.

Chapter 4

Synthesis of binary nanocomposite conductive Polypyrrole and reduced graphene oxide as electrode materials for high-performance supercapacitor

4.1 Introduction

Energy demand has been rising rapidly on a worldwide scale, and this growing consumption presents significant challenges as current energy resources are insufficient to meet future needs [95]. This trajectory could lead to potential energy crises, further compounded by the depletion of fossil fuels, environmental concerns related to greenhouse gas emissions, and rising energy needs across various sectors[96], [97]. To address this challenge, the development of safe and effective power sources is of vital importance.

Supercapacitors, with their unique characteristics, stand out as promising solutions for energy storage. Their advantages include long life cycles, capability for quick charging and discharging, high P_d, and notable energy density E_d, making them vital additions to conventional energy storage technologies like batteries and fuel cells [98], [99]. Since their introduction by Nippon Electric Company (NEC), supercapacitors have found wide-ranging applications in industries like electronics, transportation, aerospace, military, and sensor technologies [100]. Their continued development holds great potential for addressing global energy challenges.

Among materials explored for supercapacitor applications, graphene has attracted significant attention due to its exceptional properties, including high electrical conductivity, low density, large surface area (2670 m^2/g), mechanical strength, and chemical stability [101], [78]. Studies have shown that graphene can achieve gravimetric capacitance values of up to 135 F/g in aqueous electrolytes and 99 F/g in organic electrolytes [102]. For instance, Wang et al. utilized hydrazine to reduce graphene oxide (GO) and achieved a gravimetric capacitance of 205 F/g. However,

variations in reported capacitance values, ranging from 59 F/g to 169.3 F/g, often stem from factors such as graphene purity and the composition of the electrolyte.

Conducting polymers like polypyrrole (PPy) have also emerged as promising materials for pseudo-capacitors due to their ability to deliver high specific capacitance (C_P) through reversible redox reactions. Among these, polypyrrole has gained prominence due to its excellent conductivity, environmental stability, and mechanical flexibility. Despite these advantages, the challenge lies in effectively integrating polypyrrole with graphene to create a composite material that maintains the high conductivity of graphene while leveraging the electrochemical properties of polypyrrole. This has led to increased interest in developing composite materials that can overcome these limitations. The combination of PPy with carbon-based nanomaterials has been shown to enhance supercapacitor performance. Biswas et al. synthesized a graphene/polypyrrole composite material that achieved a gravimetric capacitance of 165 F/g at a current density of 1 A/g [103], while Parl et al. demonstrated a C_P of 400 F/g with a graphite/PPy composite in a three-electrode system.

In response to challenges, this study aims to build on previous research by synthesizing and characterizing PPy/rGO composite electrodes for supercapacitor applications. By integrating reduced graphene oxide with polypyrrole, the unique properties of both materials are harnessed to create a composite with enhanced electrochemical performance. Compared to previous methods such as electrochemical polymerization and in situ chemical reduction, the chemical oxidative method used in this study is both simpler and more environmentally friendly, as it eliminates the need for hazardous chemicals and complex equipment. Additionally, it offers scalability for industrial applications, making it more cost-effective while still achieving comparable or improved electrochemical performance. Reduced graphene oxide was incorporated during the polymerization process of PPy, resulting in a composite material with high conductivity and superior energy storage capabilities.

The central focus of this research is to investigate the electrochemical properties of the PPy/rGO composite, evaluating its synergistic effects and potential for use in

efficient supercapacitors. Polypyrrole was chosen due to its widespread use and high specific capacitance (136 F/g, as determined using a three-electrode system) [104]. Additionally, this study presents an environmentally friendly and cost-effective synthesis method for the composite, with an optimal oxidant-to-pyrrole (O/py) ratio of 4, ensuring the highest conductivity [104][105].

Our results demonstrate that the PPy/rGO composite exhibits an impressive C_P of 365.1 F/g at a scan rate of 10 mV/s, as determined by cyclic voltammetry (CV). Furthermore, galvanostatic charge- discharge (GCD) measurements revealed a C_P of 375 F/g at a current density of 2 A/g, significantly surpassing 165 F/g. These findings highlight the superior performance of the PPy/rGO composite and its potential for large-scale energy storage applications.

4.2 Characterization Techniques

We conducted XRD and surface morphology analysis to study the crystallographic structure of a synthesized PPy/rGO composite. Surface morphology was examined using a JEOL SEM and EDS system, while FTIR spectra were obtained using a Perkin-Elmer infrared spectrophotometer. Electrochemical experiments were conducted using METHROM NOVA software.

4.3 Result and Discussion

4.3.1 Structural and surface characterizations

Figure 4.1 shows XRD patterns that represent the distinctive features of rGO, PPy, and the composite of PPy/rGO. In Fig 3, the discernible diffraction peak at 2 Theta = 26.33^0 is attributed to rGO. The interlayer spacing of rGO is measured at 3.38 Å. XRD of Polypyrrole shows the broad peak in the region 20^0-30^0 showing the amorphous nature of Polypyrrole. The XRD pattern for PPy/rGO reveals a distinct diffraction peak within the 20^0-30^0 range [106]. This observation suggests the

complete deposition of Polypyrrole onto the carbon matrix. However, the peak lacks sharpness, indicating the

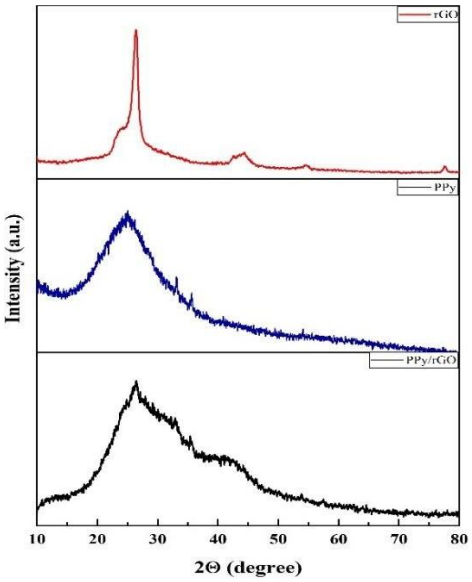

Figure 4.1: XRD of PPy/rGO composite

disruption of the regular stacking of graphene sheets. The characteristic broadness of this peak suggests that PPy exists in an amorphous form. The XRD analysis highlights the presence of rGO and the successful deposition of Polypyrrole on the carbon matrix in the PPy/rGO composite. The observed characteristics of the diffraction peaks provide insights into the structural features of these materials, with the amorphous nature of PPy being particularly notable in the XRD pattern[107] [108].

4.3.2 Morphological characterization

The morphologies of the prepared composite PPy/rGO are summarized in Field Emission Scanning

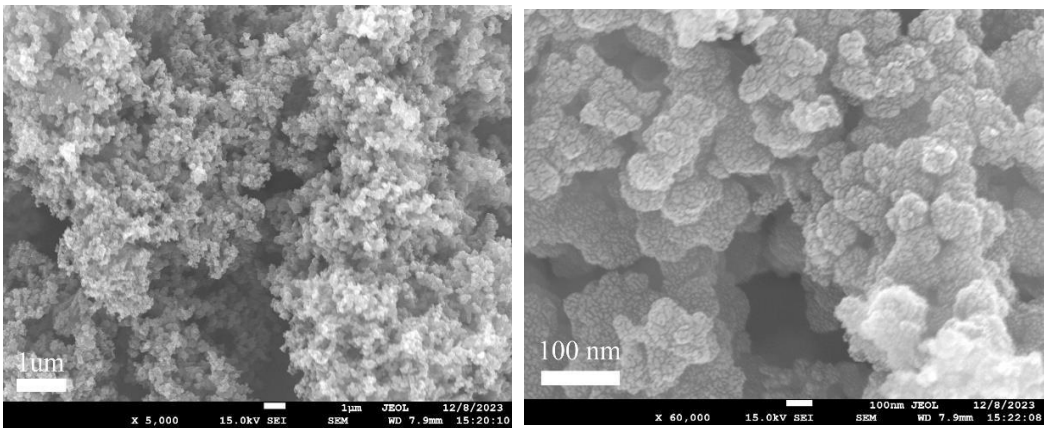

Figure 4.2: FESEM images of (PPy/rGO) Polypyrrole and reduced graphene oxide composite

Electron Microscopy (FESEM) Figure 4.2. FESEM images reveal the sponge-like porous structure of the composite. Due to strong interactions between PPy and rGO, including stacking, hydrogen bonding, van der Waals force, and physical force, rGO appears to be encircled by PPy[106], [109]. An abundance of pores on the electrode surface can improve the PPy/rGO electrode's capacitance and charge-discharge rate. The PPy/rGO electrode's specific capacitance should increase as a result of more active materials coming into contact with the electrolyte.

4.3.3 Spectroscopic characterization

Figure 4.3 illustrates the FTIR spectrum of the synthesized PPy/rGO composite, with transmittance (%) plotted against wavenumber (cm^{-1}). The spectrum reveals several prominent peaks characteristic of polypyrrole (PPy), accompanied by subtle shifts that suggest potential π-π interactions between the reduced graphene oxide (rGO) layers and the polypyrrole rings. A peak observed at 1040 cm^{-1} is associated with C–H in-plane bending vibrations, which are indicative of the polypyrrole framework. Another distinct peak at 1166 cm^{-1} corresponds to C–N stretching vibrations, confirming the successful polymerization of pyrrole. The band near 1293 cm^{-1} is attributed to C–H deformation within the polymer backbone, highlighting

the structural integrity of the polypyrrole. Additional peaks at 1466 cm^{-1} and 1543 cm^{-1} represent the C=C stretching vibrations within the pyrrole rings, further validating the presence of the conjugated backbone typical of polypyrrole. These vibrational modes are reflective of the inherent electronic properties of the polymer, which contribute to its potential for energy storage applications. The FTIR spectrum also shows characteristic peaks at 789 cm^{-1} and 888 cm^{-1}, which are associated with bipolaron ring deformations and polaron symmetric C–H in-plane bending vibrations. These features provide evidence of charge carriers within the polymer matrix, underscoring the conductive nature of polypyrrole in the composite. In the case of rGO, the spectrum reveals a broad band around 1620 cm^{-1}, which is attributed to C=O stretching vibrations originating from residual oxygen groups within the rGO. This indicates that some oxygenated functionalities remain after the reduction process, likely enhancing the interaction between rGO and polypyrrole and contributing to the composite's structural stability. Additionally, a peak near 1050 cm^{-1} corresponds to C–O stretching vibrations, further indicating the presence of oxygen-containing groups in the rGO[98]. These vibrational modes confirm the successful integration of polypyrrole and reduced graphene oxide in the composite, highlighting their strong interactions and the unique structural characteristics of the PPy/rGO material. This detailed FTIR analysis provides valuable insight into the chemical composition and bonding interactions within the composite, further supporting its potential for applications requiring enhanced electronic and structural properties[110], [111], [112].

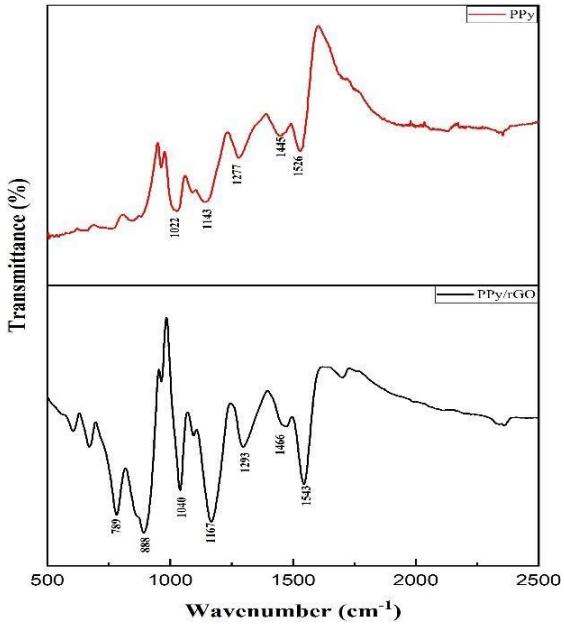

Figure 4.3: FTIR of composite PPy/rGO

4.3.4 Electrochemical characteristics

4.3.4.1 CV Analysis

The specific capacitance was obtained through the application of Equation (1).

$$C_P = \frac{dQ}{mdV} = \frac{idt}{mdV} = \frac{\bar{\imath}}{mv} = \frac{1}{2mv(V_1 - V_2)} \int_{V_1}^{V_2} i(V)dV \qquad (1)$$

Cyclic voltammograms of PPy/rGO were recorded over a potential range of 0 V to 0.5 V at various scan rates (10, 20, 30, 40, 50, 60, 80, and 100 mV/s), as illustrated in Figure 4.4. The findings unveiled unique redox peaks, which are indicative of the electrochemical characteristics of the PPy/rGO composite. The CV curves exhibited well-defined and separated oxidation and reduction peaks at lower scan rates, indicating efficient charge storage and redox processes within the composite material. As the scan rate increased, the peak currents exhibited a corresponding rise, suggesting good electrochemical reversibility. The composite's C_P at a scan rate of 10 mV/s is 365.1 F/g. Specific capacitance for scan rates 20, 30, 40, 50, 60, 80, and 100 mV/s are 340.15, 306.6, 275, 240, 233.3, 225, and 210 F/g respectively. In summary, the outcomes from cyclic voltammetry underscore the appropriateness of PPy/rGO composites for electrochemical energy storage applications, showcasing their robust

electrochemical performance and potential for use in supercapacitors and related devices. Further analysis and optimization can be pursued for tailored applications in energy storage systems[110], [111].

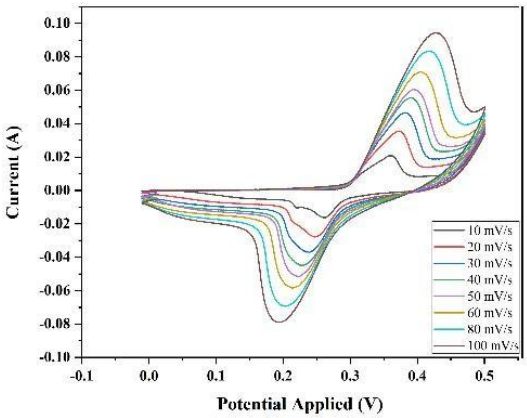

(a)

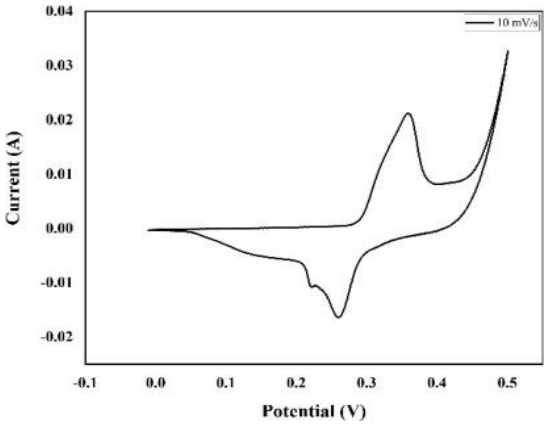

(b)

Figure 4.4: CV of PPy/rGO composite at various scan rates (b) CV of PPy/rGO composite at a scan rate of 10 mVs^{-1}

4.3.4.2 GCD Analysis

The specific capacitance is derived from the GCD curve using Equation (2).

$$C_P = \frac{I\Delta t}{m.V} \qquad (2)$$

The GCD curves for the Polypyrrole-reduced graphene oxide composite at various current densities are displayed in Figure 4.5. Figure 4.5(a) demonstrates the similarities among the curves of different current densities, indicating the excellent capacitive performance of the electrode material. The values of specific capacitance corresponding to the current densities of 1, 2, 4, and 6 A/g are 367.5 F/g, 375 F/g, 370 F/g, and 345 F/g, respectively. Figure 4.5 (b) shows the nearly stable result of C_P for different current densities.

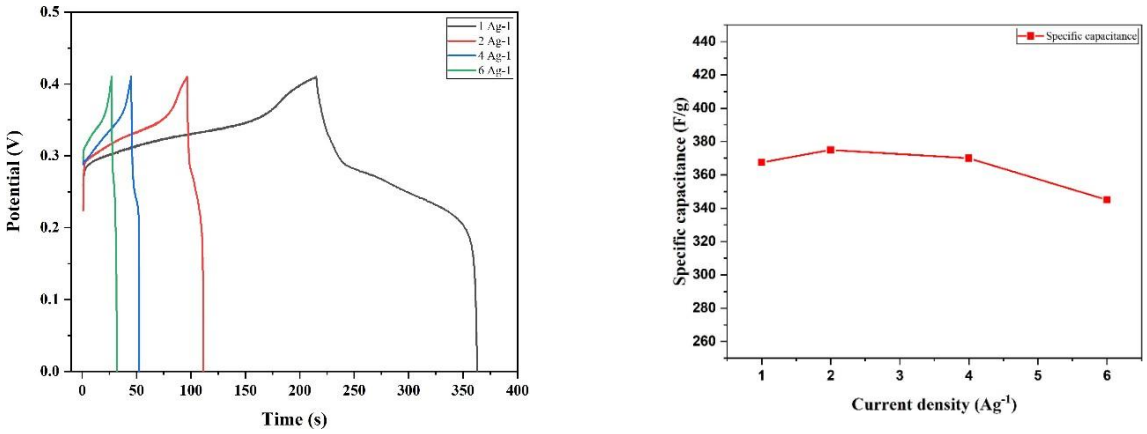

Figure 4.5. (a) GCD curve of PPy/rGO composites at various current densities (b) Plot illustrating specific capacitance as a function of current densities

The E_d and P_d of the material were determined by equations 3, and 4 respectively.

The E_d and P_d values were determined based on the C_P 375 F/g are 46.875 Wh/kg and 1140.20 W/kg respectively.

4.3.4.3 EIS Analysis

An effective experimental way for determining a material's impedance characteristics is electrochemical impedance spectroscopy (EIS), which uses a low-amplitude alternating current (AC) signal. Using a range of frequencies to measure the system's impedance, this method creates an impedance spectrum for the electrochemical material being investigated[112] The equivalent circuit was formed by using ZSimp software.

Table 4.1: Parameters values from fitted impedance equivalent circuit

Sample	R	Q	R	C	R
PPy/rGO	0.9013	0.003564	7.371	$2.85E^{-06}$	$1.13E^{+04}$
% error	6.931	12.52	$5.45E^{+04}$	$2.04E^{+04}$	598.4

PPy/rGO was subjected to EIS (Electro Impedance Spectroscopy) in the frequency

range 10^5 to 10^{-1} in 3M KOH solution. The Nyquist plot illustrated in Figure 4.6(a) displays a minor semicircle in the high- frequency range, indicating the presence of solution resistance and charge transfer resistance. Furthermore, a linear line observed in the high-frequency region indicates the presence of Warburg resistance [113]. Essentially, the behavior seen in Figure 4.6(b), the impedance spectrum reflects the material's response to varying frequencies. Figure 4.6(c) represents Bode Phase plot, in low frequency region impedance is relatively high representing capacitive behavior of material. In higher frequency region impedance is relatively low, showing the good conductivity of material at higher frequency. The material presents a higher resistance to the passage of electrical current at lower frequencies. This could be due to factors such as internal resistances, surface effects, or slower charge transfer processes within the material. Conversely, as the frequency of the applied signal rises, the impedance steadily decreases. This phenomenon often indicates an improved ability of the material to conduct electricity efficiently. The material becomes more responsive to the alternating current at these higher frequencies, allowing for easier movement of charges and a lower overall impedance [114]. Table 4.1 represents parameter values from fitted impedance equivalent circuits. Table 1 has the symbols "Q", C, and "R" to stand for certain elements. R stands for the electrochemical system's resistive elements, which may consist of Resistance to solutions (Rs). the electrolyte's resistance between the reference and working electrodes. The resistance connected to the transfer of charge across the electrode/electrolyte interface during a redox reaction is known as charge transfer resistance or Rct. Q (CPE, or constant phase element), This helps to explain why capacitive behavior isn't perfect. C represents the Capacitive element. The second peak observed in the Bode plot's phase angle curve at higher frequencies signifies the capacitive behavior of the PPy/rGO composite. As the phase angle approaches 45°, the material transitions into a capacitive- dominant state, indicating efficient charge storage and release. This peak highlights the material's ability to maintain capacitive properties over a wide frequency range, crucial for supercapacitor applications. Additionally, the impedance behavior at higher frequencies suggests the influence of resistive components, such as internal and contact resistance, as the capacitive response diminishes at very high frequencies. EIS results indicate that the

series resistance (Rs) of the PPy/rGO composite is 15 Ω, representing the combined resistance of the electrolyte, electrodes, and contact points. Additionally, the charge transfer resistance (Rct), corresponding to the Faradaic processes at the electrode/electrolyte interface, was found to be 130 Ω, indicating good charge transfer kinetics within the system.

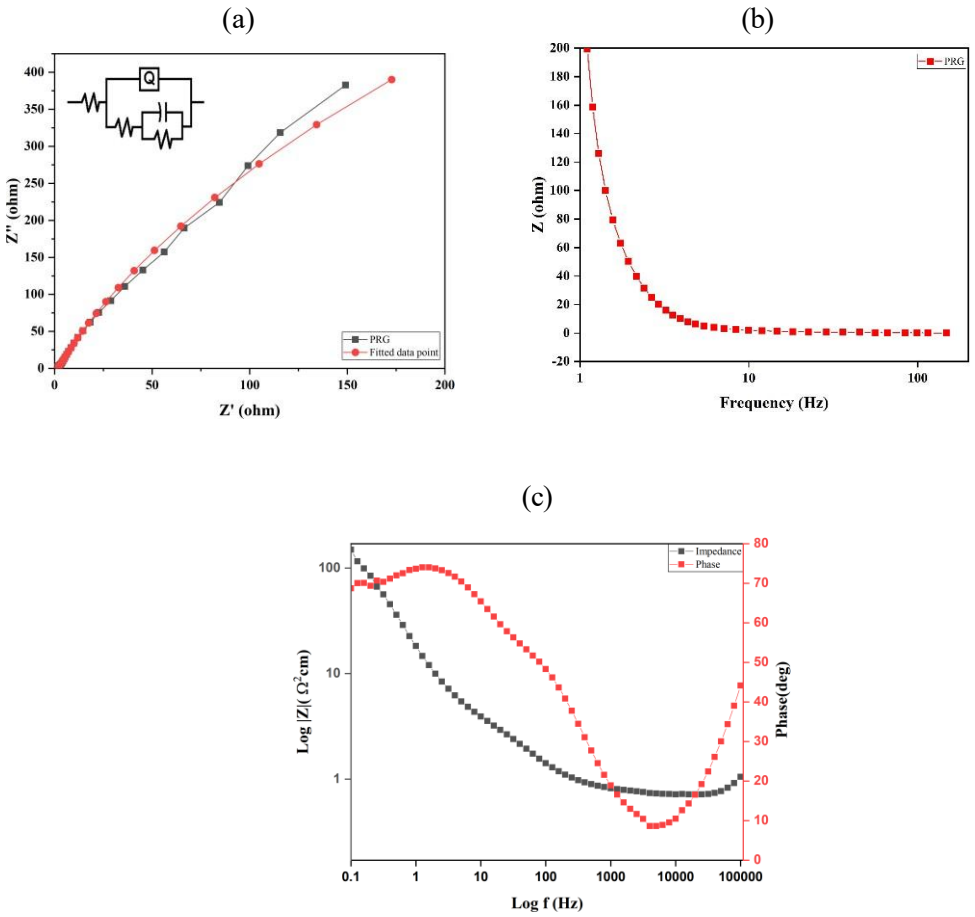

Figure 4.6 (a) Nyquist plot of Polypyrrole-reduced graphene oxide composite (b) Real impedance vs Frequency (c) Bode phase plot

Table 4.2: Comparison of PPy/rGO with previously reported

Electrode material	Galvanic charge-discharge/scan rate	Electrolyte	Specific capacitance (Fg^{-1})	References
Ppy/GO/ZnO	$1Ag^{-1}$	1M Na_2SO_4	94.6	[115]
CNT/PPy/MnO_2	20 mVs^{-1}	1 M Na_2SO_4	281	[116]
PEDOT-GO/CNTs	10 mVs^{-1}	1 M KCl	104	[117]
Ppy-GO/CNTs	10 mVs^{-1}	1 M KCl	143.6	[117]
PPy/rGO	10 mVs^{-1}	3 M KOH	365.1	Present work

4.4 Conclusion

In conclusion, we introduce a straightforward, scalable, and environmentally friendly approach for fabricating binary composite electrodes composed of conductive PPy and rGO, tailored for supercapacitor applications. Formation of the composite was done by using the Chemical Oxidative method, the synthesis process allows for the uniform distribution of PPy within the rGO matrix, leading to a highly porous structure that improves the accessibility of electrolytes and enhances charge storage capacity. The controlled synthesis parameters can be adjusted to tailor the composite's morphology, resulting in optimized electrochemical performance. Electrochemical characterizations showed binary PPy/rGO composite electrode delivers 365.1 F/g C_P at the scan rate of 10 mV/s in Cyclic voltammetry measurement, while in Galvanic Charge Discharge analysis specific capacitance was 375 Fg^{-1} for 2 Ag^{-1}. These findings validate the potential of employing this straightforward synthesis approach to create composite electrode materials featuring a blend of reduced graphene and conductive polymers. This approach holds promise for designing and customizing the characteristics of advanced supercapacitors.

Chapter 5

Electrochemical and Structural Analysis of rGO/$NiCoFe_2O_4$ Composites for Energy Storage Applications

5.1 Introduction

The synthesis of complex supercapacitor electrode materials has been the subject of extensive research due to the need for high-performance energy storage devices. Of the ferrites and oxides of transition metals, nickel cobalt ferrite ($NiCoFe_2O_4$) has attracted the most interest because of its remarkable electrochemical stability, high electrical conductivity, and profusion of redox-active sites. Because of its remarkable electron transmission speed and remarkable specific capacitance (C_P), $NiCoFe_2O_4$, a spinel ferrite, is a great option for next-generation energy storage applications[118]. However, limited electrical conductivity, slow ion transit, and particle aggregation typically limit its practical use and charge storage efficiency. Because of its remarkable electrical conductivity, large surface area, and ability to inhibit the aggregation of metal oxide nanoparticles, reduced graphene oxide (rGO) has become the best support material for overcoming these limitations. By adding rGO to $NiCoFe_2O_4$ matrices, the electroactive site efficacy, electrode stability, and charge transfer are all markedly improved. Because of their synergistic interaction, rGO-based nanocomposites have been shown in numerous investigations to have better electrochemical kinetics and faster electron mobility than ferrites[119]. Isara Kotutha used one-pot hydrothermal synthesis to obtain a C_P of 190.3 F/g of rGO/$MnFe_2O_4$[120]. The electrochemical performance of nanocomposites is heavily impacted by the method of synthesis. In order to guarantee that the nanoparticles were evenly dispersed throughout the rGO matrix, the auto-combustion sol-gel approach was used in this investigation. This method is economical, scalable, and energy-efficient. This process creates uniformly distributed $NiCoFe_2O_4$ nanoparticles with improved electrochemical characteristics and regulated morphologies by using an exothermic redox reaction between metal nitrates and fuel (citric acid). The total conductivity and charge storage capacity are greatly enhanced by adding rGO to the ferrite matrix during the synthesis process. Using GCD, EIS, and CV, the electrochemical characteristics of the synthesized rGO/$NiCoFe_2O_4$ composites

were methodically examined. Certain capacitance values derived from GCD and CV tests demonstrate how rGO considerably improves the charge storage capabilities. Because of its enhanced charge transfer properties and suitable Ni-to-Co ratio, the RNC80 composite demonstrated the highest C_P of 250 F/g (CV) and 275 F/g (GCD) among the composites that were synthesized. RNC80 demonstrated previously unheard-of electrical conductivity and quick ion transport, according to the Nyquist plot analysis. The charge transfer resistance (Rct) was 72.5 ohms, and the series resistance (Rs) was the lowest at 1.62 ohms. Consequently, it was through structural, morphological, and electrochemical investigations, this study seeks to evaluate the potential of rGO/$NiCoFe_2O_4$ composites as high-performance supercapacitor electrode materials. The auto-combustion sol-gel process was used to synthesize these composites. It is expected that adding rGO to the $NiCoFe_2O_4$ matrix will improve electrode stability, increase charge storage efficiency, and provide a scalable and affordable way to make energy storage materials. The results of this work open the door for the practical use of high-energy-density, eco-friendly supercapacitor electrodes in energy storage technologies by providing important insights into their design.

5.2 Characterization Techniques

XRD analysis of the powdered samples of the synthesized PPy/rGO composite was performed using a BRUKER diffractometer. This method lets us probe the composite's crystallographic configuration. The surface morphology of the composites was examined using a JEOL FESEM, which was equipped with an electron dispersive X-ray spectroscopy (EDS) system featuring a BRUKER Nano detector. This setup facilitated the analysis of the morphological features and elemental composition of the materials. FTIR`` spectra were obtained with a Perkin-Elmer infrared spectrophotometer, providing insights into the functional groups present in the composite. For electrochemical experiments, the METHROM NOVA software was utilized, enabling precise control and analysis of the electrochemical measurements conducted in our study.

5.3. Results and discussions

5.3.1 Structural and surface characterizations

XRD patterns of the RNC composites, shown in Figure 5.1, show that the materials were successfully synthesized and are crystalline. The diffraction peaks at about 30.08°, 35.45°, 42.91°, 57.00°, and 62.69°, respectively, reflect the (220), (311), (400), (511), and (440) planes[116], [117], [121]. The alignment of these peaks with the distinctive spinel structure validates the creation of $NiCoFe_2O_4$. The accuracy and strength of these peaks indicate a high degree of crystallinity in the materials. All samples have a peak at 26.41°, which is caused by the (002) plane of reduced graphene oxide (rGO). The persistence of this peak demonstrates that the structural integrity of rGO remains unaffected during the synthesis process, signifying a strong interaction between rGO and the ferrite nanoparticles. Using the Debye-Scherrer equation, the crystallite size was determined for the (311) plane. The results reveal a decreasing trend in crystallite size with increasing nickel content. For example, the crystallite size of RNC 40 was approximately 458.25 nm, while RNC 100 exhibited a smaller size of 310.04 nm. This reduction in crystallite size suggests that the incorporation of nickel affects the nucleation and growth of the ferrite crystallites, which could influence the material's electrochemical properties. The d-spacing values calculated from Bragg's law remain consistent at around 2.53 Å for the (311) plane across all samples, indicating negligible variations in the interplanar spacing due to compositional changes. Similarly, the lattice constants, derived from the d-spacing, were found to be approximately 8.39 Å, with slight variations reflecting minimal distortions in the spinel structure. The structural insights are further supported by the analysis of the diffraction peaks' Full Width at Half Maximum (FWHM). The FWHM of 0.182° for RNC 40 indicates that when the peaks are smaller, the crystallite size is larger and the crystallinity is higher. The larger peak for RNC 100, on the other hand, with an FWHM of 0.269°, suggests a smaller crystallite size and maybe more structural flaws. In conclusion, the constant existence of spinel ferrite diffraction peaks throughout the samples, irrespective of the concentrations of nickel and cobalt, highlights the stability of the $NiCoFe_2O_4$ structure. The crystal structure appears to be fairly flexible, as indicated by variations in crystallite size and lattice characteristics. This could be important for improving the performance of these composites in energy-related applications.

Table 5.1: X-ray Diffraction (XRD) Parameters for rGO/$NiCoFe_2O_4$ Composites

Composites	2θ (Degree)	FWHM (Degree)	Crystallite Size (nm)	d-Spacing (Å)	Lattice Constant (a_0) (Å)
RNC 0	35.45	0.25	5.05	2.13	8.353
RNC 20	35.45	0.24	7.86	2.21	8.370
RNC 40	35.45	0.182	8.19	2.11	8.368
RNC 60	35.45	0.21	7.14	2.13	8.361
RNC 80	35.45	0.26	4.74	2.15	8.367
RNC 100	35.45	0.269	3.58	2.12	8.358

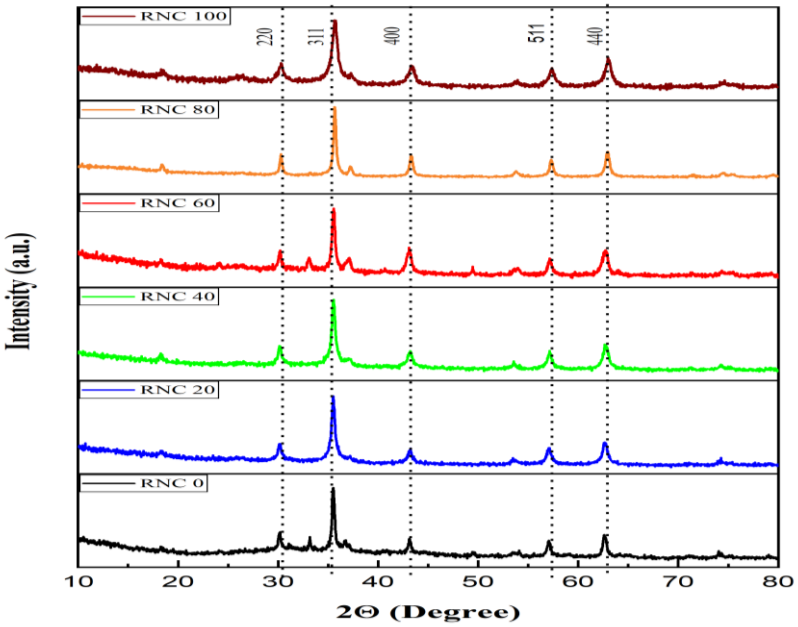

Fig. 5.1: XRD of rGO/$NiCoFe_2O_4$ composites

5.3.2 Morphological characterization

The morphological features of rGO/$NiCoFe_2O_4$ composites with various nickel concentrations were examined using FESEM, as depicted in Figure 5.2. The images show the composites' microstructure as the nickel content changes, giving details on their surface shape, porosity, and particle dispersion, all crucial for electrochemical

performance. The porous and networked structure shown in the FESEM pictures is advantageous for ion diffusion and charge storage in supercapacitor applications. rGO sheets are clearly visible and integrate with the $NiCoFe_2O_4$ nanoparticles to form a conductive network. The loosely packed and irregularly linked rGO sheets with the metal oxide phase result in a more disordered microstructure with lower nickel concentrations. The density of $NiCoFe_2O_4$ particles rises with increasing nickel concentration, giving the particles a more distinct granular look. The composite's porosity and uniformly distributed structure at intermediate compositions (such as RNC40–RNC80) is intriguing since it shows that $NiCoFe_2O_4$ nanoparticles are successfully attached to the rGO sheets[116], [122]. The uniform dispersion of particles improves the electrochemical contact and facilitates improved charge transfer. Furthermore, an ideal shape for ion transport and electrolyte penetration—two essential components of high-performance supercapacitors—is suggested by the structure's mesopore and micropore development. At the maximum nickel content (RNC100), the microstructure seems more compact, with bigger aggregated $NiCoFe_2O_4$ clusters dominating the surface. This implies that particle agglomeration brought on by excessive metal oxide loading may decrease the total surface area and active sites accessible for electrochemical reactions. The observed morphological changes, which need an ideal balance between conductivity, porosity, and particle distribution to achieve an enhanced capacitance, provide strong support for the trends in electrochemical performance. Improved charge storage properties are the outcome of the synergistic interaction between rGO and $NiCoFe_2O_4$.

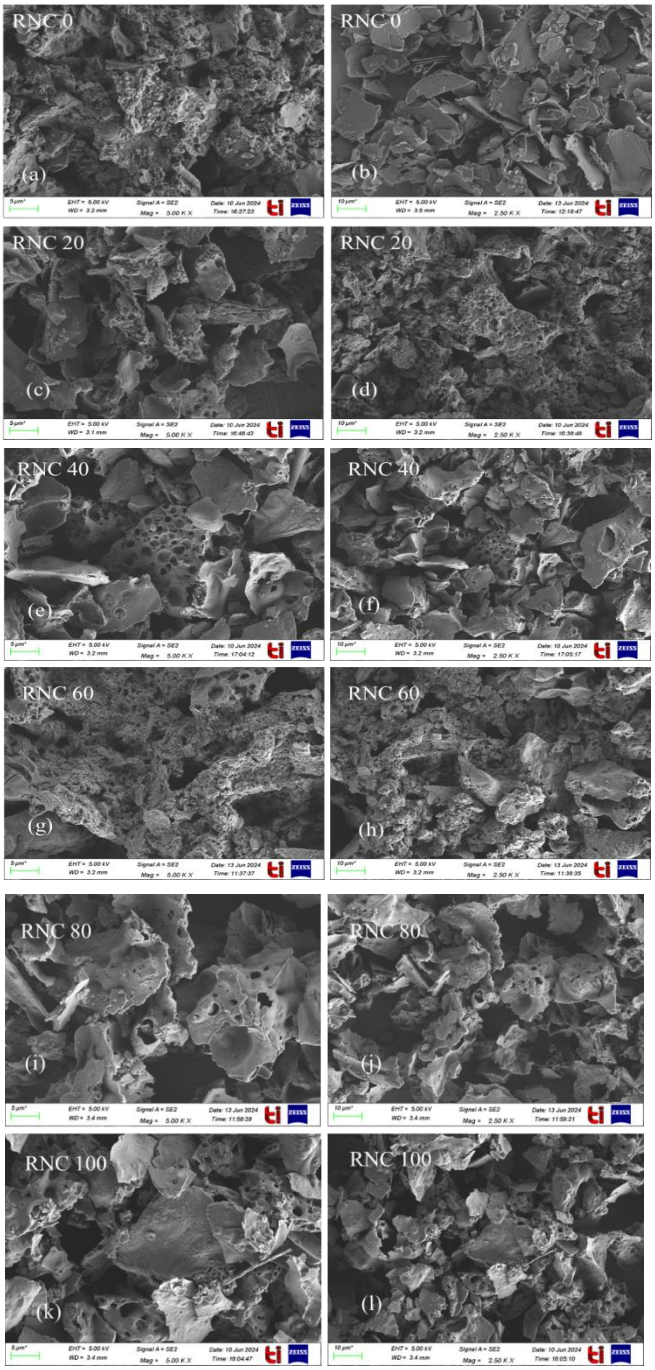

Fig.5.2: FESEM images of rGO/$NiCoFe_2O_4$ composites

5.3.3 Spectroscopic characterization

The functional groups and chemical interactions in the rGO/$NiCoFe_2O_4$ composites that were synthesized with different Ni concentrations (0%, 20%, 40%, 60%, 80%, and 100%) were analyzed using Fourier Transform Infrared Spectroscopy (FTIR), as shown

in Figure 5.3. The FTIR spectra show distinctive vibrational bands that match the functional groups in $NiCoFe_2O_4$ and rGO), demonstrating the effective synthesis of the composites. By limiting the characteristic absorption bands seen in the 500–700 cm^{-1} range to the metal-oxygen (M–O) stretching vibrations of Ni–O, Co–O, and Fe–O bonds, the spinel $NiCoFe_2O_4$ phase is verified. These peaks, which show that the ferrite structure contains octahedral and tetrahedral coordination environments, are a basic feature of oxides of the

spinel type. The broad band at about 3400 cm^{-1} reflects the stretching vibrations of hydroxyl (-OH) groups, which are created by surface-adsorbed water molecules or residual moisture. This band's existence suggests a particular level of surface hydroxylation, which could have an impact on electrochemical performance via ion transport. A noticeable peak at about 1600 cm^{-1} indicates the C=C stretching vibration for the sp^2-hybridized carbon domains in rGO. This illustrates how much the decrease in graphene oxide has revitalized the graphitic structures. An interaction between rGO and $NiCoFe_2O_4$ is suggested by the fact that the signal's intensity varies with nickel content. The peak at about 1380 cm^{-1} is linked to C–O stretching vibrations, which are probably sourced from the remaining oxygen-containing functional groups of rGO. This implies that the persistence of particular oxygen functions after the reduction process may be the cause of the composite's pseudocapacitive qualities. The presence of partially reduced graphene oxide is further supported by the allocation of C–O–C stretching vibrations to the weak absorption band about 1100 cm^{-1}[123], [124]. A stronger interaction between $NiCoFe_2O_4$ and rGO is shown by the peak's decreased intensity in composites with a higher Ni content. The addition of metal oxides to the graphene matrix is probably what caused this behavior. By showing the presence of spinel ferrite connections and the distinct functional groups of rGO, the FTIR data generally support the effective synthesis of rGO/$NiCoFe_2O_4$ composites. The spectrum variations highlight the composite's potential for electrochemical applications and clearly show the interaction between rGO and $NiCoFe_2O_4$.

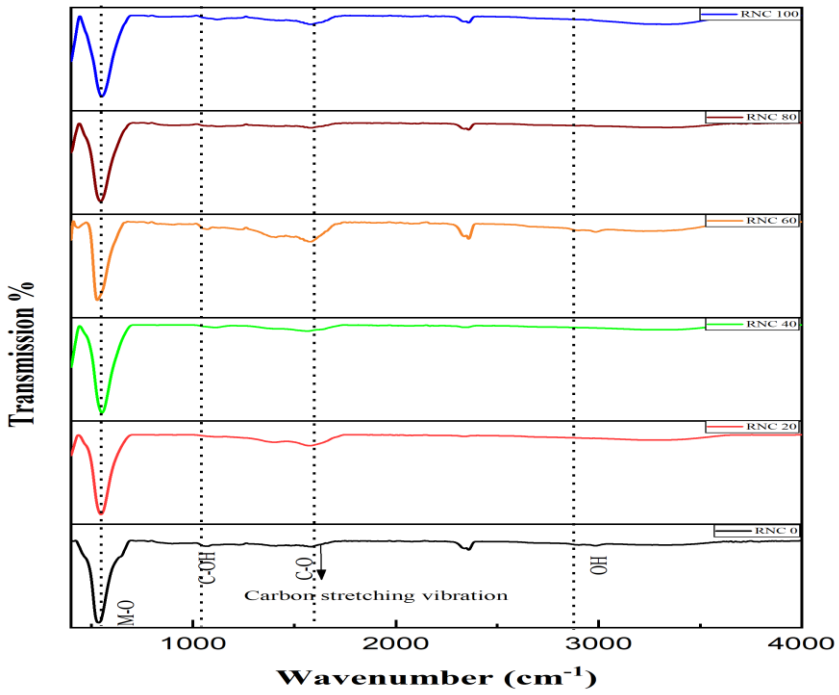

Fig. 5.3: FTIR of rGO/$NiCoFe_2O_4$ composites

5.3.4 Electrochemical characteristics

5.3.4.1 CV Analysis

The electrochemical performance of the rGO/$NiCoFe_2O_4$ composites was assessed under CV at various scan rates (10–100 mV/s) using a 3M KOH electrolyte. Figure 4 presents the CV curves of the composites with different Ni content (RNC0 to RNC100). The curves show redox peaks and quasi-rectangular forms, suggesting a combination of Faradaic redox processes and double-layer capacitance, characteristic of pseudocapacitive behavior. As the nickel content increases, the CV curves show noticeable variations in current response and peak separation. The increased peak intensity at higher nickel compositions suggests enhanced charge storage capability due to improved redox activity of $NiCoFe_2O_4$. Among all compositions, the RNC80 composite exhibits the highest current response, indicating superior charge storage performance, likely due to the optimized interaction between rGO and $NiCoFe_2O_4$. The trend in specific capacitance values suggests that the major influence on the

electrochemical performance is on the $NiCoFe_2O_4$ content. At lower Ni concentrations, the capacitance is lower due to the limited contribution of redox-active sites. As the nickel content increases, the synergistic effect between rGO and $NiCoFe_2O_4$ enhances the capacitance, reaching a maximum at RNC80. Beyond this composition, a slight decrease is observed in RNC100, likely due to excessive $NiCoFe_2O_4$ aggregation, which may hinder ion diffusion and reduce active surface area. The CV analysis confirms that the optimized composite (RNC80) demonstrates the best electrochemical performance, attributed to its well-balanced conductivity, redox activity, and porous architecture, making it a viable option for applications requiring high-performance supercapacitors.

Table 5.2 The specific capacitance of rGO/$NiCoFe_2O_4$ Composites by CV

Composites	**Specific capacitance F/g**
RNC 0	193
RNC 20	180
RNC 40	220
RNC 60	220
RNC 80	250
RNC 100	230

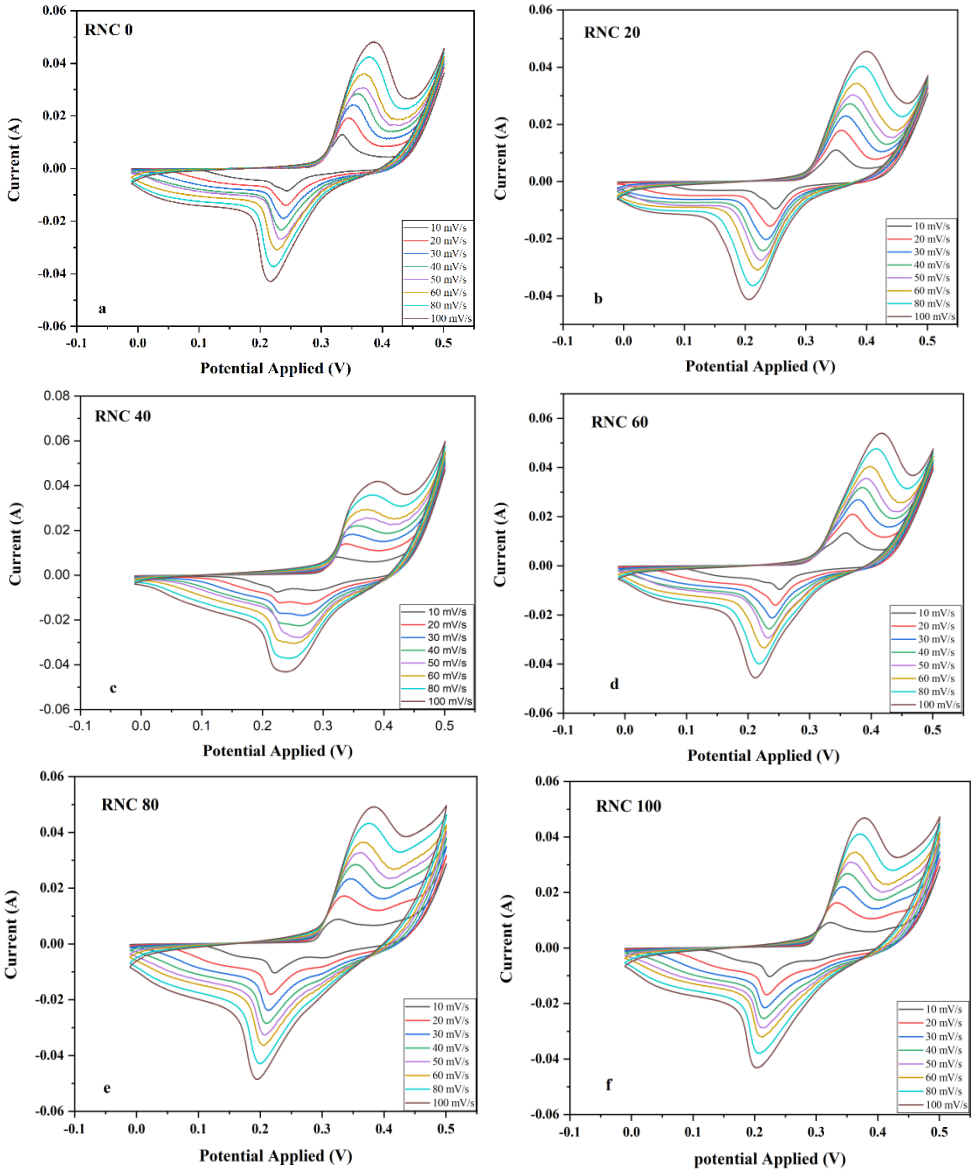

Fig.5.4: CV of rGO/$NiCoFe_2O_4$ composites

5.3.4.2 GCD Analysis

The electrochemical charge storage behavior of the rGO/$NiCoFe_2O_4$ composites was further evaluated using GCD measurements at different current densities. The GCD curves, presented in Figure 5.5, reveal the potential time profiles of the composites, providing insights into their charge storage mechanism and rate capability. The charge-discharge curves exhibit a nearly symmetric profile, indicating a highly reversible charge storage process, characteristic of an efficient pseudocapacitive material. The

non-linear character of the discharge curves implies the participation of Faradaic redox reactions, which contribute to the overall capacitance. This behavior aligns the cyclic voltammetry results, confirming the hybrid capacitive nature of the composites.

Table 5.3: The specific capacitance of rGO/$NiCoFe_2O_4$ Composites by GCD

Composites	Specific capacitance F/g
RNC 0	187.5
RNC 20	217.5
RNC 40	237.5
RNC 60	242.5
RNC 80	275
RNC 100	230

These values demonstrate a significant enhancement in capacitance with increasing $NiCoFe_2O_4$ content, reaching a maximum at RNC80. This enhanced capacitance is ascribed to the synergistic interaction between rGO and $NiCoFe_2O_4$, where rGO provides a conductive network for electron transfer while $NiCoFe_2O_4$ contributes to redox-active sites for charge storage. At higher Ni content (RNC100), a slight decrease in capacitance is observed, likely due to the agglomeration of metal oxide particles, which can reduce the available electroactive surface area and hinder ion diffusion. The longer charge-discharge duration observed for RNC80 suggests superior energy storage capability, making it the most promising composition for supercapacitor applications. At lower current densities, the almost linear discharge profile shows excellent charge retention; at higher current densities, a slight deviation indicates negligible resistance losses. This behaviour demonstrates the outstanding stability and performance of the ideal composite. The rGO/$NiCoFe_2O_4$ composites, especially RNC80, have better electrochemical performance because of their balanced composition, improved ion transport, and elevated redox activity, according to the GCD study. The findings highlight the need to modify the metal oxide-to-rGO ratio to maximize supercapacitor performance.

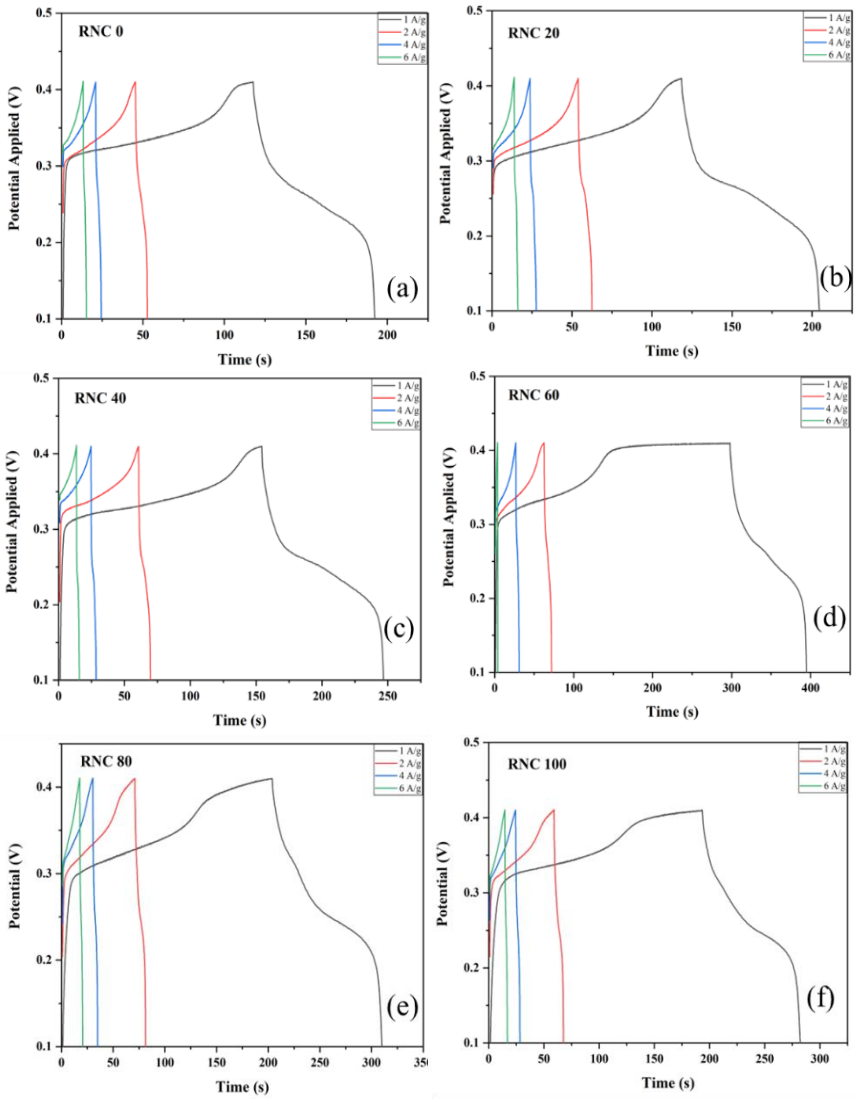

Fig.5.5: GCD of rGO/$NiCoFe_2O_4$ composites

5.3.4.3 EIS Analysis

The rGO/$NiCoFe_2O_4$ (RNC) composites were analyzed by electrochemical impedance spectroscopy (EIS) in the frequency range of 10^5 to 10^{-1} Hz using a 3 M KOH electrolyte. The Nyquist plots shown in Figure 5.6 are crucial for understanding the electrochemical behavior of the electrode materials, as they reveal the solution resistance (Rs) and charge transfer resistance (Rct), which represent the intrinsic resistive and capacitive characteristics of the system. A lower Rct value signifies enhanced charge transfer kinetics and higher electrical conductivity, both of which contribute to improved electrochemical performance.

As the $NiCoFe_2O_4$ content increased, the EIS spectra exhibited a noticeable reduction in Rct, indicating improved electron transport and stronger electrode–electrolyte interactions. Among all samples, RNC0 exhibited the highest resistances (Rs = 2.50 Ω and Rct = 160.2 Ω), implying limited electrical conductivity and sluggish charge kinetics. RNC20 showed moderate resistance values (Rs = 2.10 Ω, Rct = 142.8 Ω),

correlating with its lower specific capacitance observed in CV and GCD analyses. A substantial decrease in impedance was observed for RNC40 (Rs = 1.75 Ω, Rct = 81.7 Ω) and RNC60 (Rs = 1.85 Ω, Rct = 95.4 Ω), suggesting that $NiCoFe_2O_4$ became more uniformly incorporated into the rGO matrix, leading to better interfacial contact and electron mobility.

The most significant improvement was observed for RNC80, which showed the lowest Rs (1.62 Ω) and Rct (72.5 Ω), confirming excellent electrode–electrolyte interaction and rapid charge transfer kinetics. The nearly vertical slope in the low-frequency region of the Nyquist plot indicates superior ion diffusion behavior, a key requirement for high-rate charge storage. These characteristics demonstrate that RNC80 provides the most efficient electron/ion transport network, which directly aligns with its highest specific capacitance values obtained in electrochemical measurements. The synergistic effect of rGO's high conductivity and the optimized $NiCoFe_2O_4$ content results in a balanced structure that Favors both double-layer and faradaic charge storage, making RNC80 a promising electrode material for advanced supercapacitor applications.

Table 5.4: R_s and R_{ct} values of rGO/$NiCoFe_2O_4$ composites

Composites	R_s (Ohm)	R_{ct} (Ohm)
RNC0	2.5	160.2
RNC20	2.1	142.8
RNC40	1.85	95.4
RNC60	1.75	81.7
RNC80	1.62	72.5
RNC100	1.95	115.6

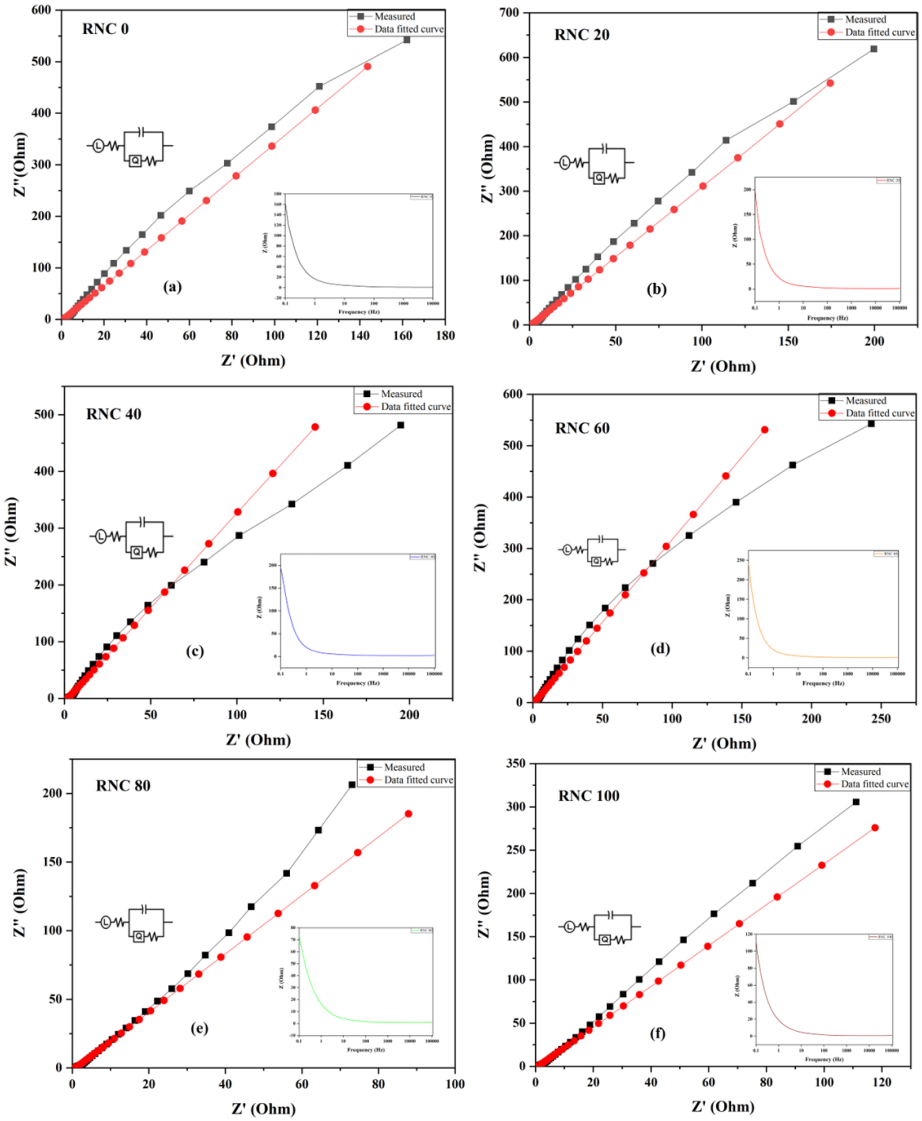

Fig.5.6: EIS of rGO/$NiCoFe_2O_4$ composites

5.3.5 Energy Density (E_d) and Power Density (P_d) measurements

The E_d and P_d of the rGO/$NiCoFe_2O_4$ composites were calculated to evaluate their suitability for supercapacitor applications. Energy density represents the total charge storage capacity of the electrode, while P_d indicates how quickly the stored energy can be delivered. The energy density ranges from 6.51 Wh/kg (RNC0) to 9.55 Wh/kg (RNC80), with RNC80 exhibiting the highest energy storage capability. This trend aligns with the specific capacitance results, where the optimized Ni-Co ratio in RNC80 enhances charge storage through a combination of electric double-layer capacitance

(from rGO) and pseudo capacitance (from Ni and Co redox reactions). The gradual increase in energy density with Ni incorporation suggests that Ni-rich compositions contribute more efficiently to charge storage, with the maximum observed at RNC80. However, a slight decrease in RNC100 (8.42 Wh/kg) indicates that excessive Ni content may lead to reduced electroactive sites due to particle agglomeration or increased internal resistance. Power densities range from 202.08 W/kg (RNC60) to 234.38 W/kg (RNC0). Interestingly, while RNC80 has the highest energy density, its power density (202.2 W/kg) is slightly lower than that of lower Ni compositions, such as RNC0 (234.38 W/kg) and RNC20 (226.56 W/kg). This is likely due to longer discharge times in RNC80, which extend energy delivery but slightly reduce power output.

The specific capacitance was determined through cyclic voltammetry using Equation (1).

$$C_p = \frac{dQ}{mdV} = \frac{idt}{mdV} = \frac{\bar{\imath}}{mv} = \frac{1}{2mv(V_1 - V_2)} \int_{V_1}^{V_2} i(V)dV \quad (1)$$

$$S = \int_{V1}^{V2} i(V)dV \quad (2)$$

The specific capacitance was determined using GCD as outlined in Equation (3).

$$C_m = \frac{I\Delta t}{m.V} \quad (3)$$

Eq. The material's E_d and P_d were determined, respectively, from 4 and 5.

$$E_d = \frac{C_p(\Delta V)^2}{2} \quad (4)$$

$$P = \frac{E}{\Delta t} \quad (5)$$

5.4 Conclusion

This study synthesized rGO/$NiCoFe_2O_4$ (RNC) composites using the sol-gel auto-combustion technique for $NiCoFe_2O_4$ and the modified Hummers' method for rGO. Structural and morphological characterizations confirmed the successful synthesis of a well-integrated hybrid composite, in which $NiCoFe_2O_4$ nanoparticles were evenly dispersed throughout the rGO matrix. As a result, electrochemical activity and charge

transfer were greatly enhanced. Electrochemical studies using CV, GCD, and EIS showed that the nickel-to-cobalt ratio had a substantial impact on the composites' charge storage effectiveness. RNC80 was the most efficient electrode composition among the materials that were created; it had the best ion diffusion properties, the lowest charge transfer resistance (Rct=72.5 Ohm), and the largest C_P (250 F/g (CV). The enhancement in electrochemical performance is the result of rGO and $NiCoFe_2O_4$ working together. This action increases the speed of electron transport, the accessibility of electrolytes, and the effectiveness of redox-active sites. The findings support the need for the $NiCoFe_2O_4$ to rGO ratio in order to maximize the electrode materials' conductivity, capacitance, and electrochemical stability. The remarkable performance of RNC80 highlights its promise for scalable, low-cost, and high-performance supercapacitor applications. Both symmetric and asymmetric supercapacitor devices, as well as the continued optimization of the synthesis parameters, including dopants, may benefit from this enhanced composite. Future studies might concentrate on these topics.

Chapter 6

Electrochemical Optimization of PPy/rGO/$NiCoFe_2O_4$ Composites for Supercapacitor Applications

6.1 Introduction

Supercapacitors have gained substantial recognition as a pivotal technology in energy storage due to their ability to deliver high power density, rapid charge-discharge cycles, long lifespan, and superior energy efficiency. These attributes make supercapacitors essential components for future energy storage systems, particularly in critical applications such as renewable energy integration, electric vehicles, and portable electronics. Alongside continuous developments in this field, a number of electrode materials have been studied, such as conducting polymers, transition metal oxides, and carbon-based materials [125].

Due to its high conductivity and pseudocapacitive properties, PPy is one of the conducting polymers that is most frequently studied, which allows for effective energy storage through quick and reversible redox processes. Despite these advantages, PPy exhibits poor mechanical stability and limited cycle life when used in isolation. To mitigate these limitations, PPy is frequently mixed with additional materials to improve its overall durability and electrochemical performance [126],[127].

Among carbon-based materials, rGO stands out for its high surface area, remarkable mechanical durability, and electrical conductivity. These properties make rGO an ideal support material in composite electrodes, aiding in the enhancement of electron transport while improving the stability and overall performance of the electrode system. Incorporating rGO into composite systems also significantly enhances the mechanical stability and cycling lifespan of the electrode material[128].

Nickel cobalt ferrite ($NiCoFe_2O_4$), a spinel ferrite, has emerged as another promising material due to its excellent redox activity and chemical stability. $NiCoFe_2O_4$ contributes significantly to the overall capacitance of the composite through faradaic reactions, providing a high energy storage capacity. Its multiple oxidation states allow for more extensive redox reactions, further boosting the C_P of the electrode material[116],[129].

The novelty of this research lies in the development of a straightforward, scalable synthesis method to fabricate a ternary composite of PPy, rGO, and $NiCoFe_2O_4$, and the systematic investigation of nickel content variation to optimize electrochemical performance. In contrast to previous studies that have concentrated on binary composites, this work demonstrates that combining these three materials can result in substantial improvements in C_P and stability, particularly with the PRNC80 composite showing superior performance. The synthesis approach—a combination of auto-combustion for $NiCoFe_2O_4$ and chemical oxidative polymerization for PPy—is both cost-effective and scalable, making it suitable for broader industrial applications.

The methodology used in this research improves upon previous techniques in several important ways. The auto-combustion synthesis of $NiCoFe_2O_4$ is simpler and more cost-effective compared to conventional solid-state reactions, which typically require higher temperatures and longer reaction times. Auto-combustion enables the formation of highly crystalline ferrite particles at lower temperatures, thus reducing energy consumption and making the process more environmentally friendly. The use of chemical oxidative polymerization for PPy ensures a uniform coating over the $rGO/NiCoFe_2O_4$ binary composite, promoting better interaction between the materials. This contrasts with the more complex and less scalable electrochemical polymerization methods employed in some earlier studies. The inclusion of rGO creates a robust, conductive framework that facilitates electron transport while preventing the aggregation of $NiCoFe_2O_4$ particles—an issue frequently encountered in traditional supercapacitor electrodes.

This work focuses on the synthesis and characterization of ternary composite electrodes made from PPy, rGO, and $NiCoFe_2O_4$, with varying nickel content. The nickel-to-cobalt ratio was systematically adjusted in increments of 20%, producing a series of composites labeled PRNC0, PRNC20, PRNC40, PRNC60, PRNC80, and PRNC100. The main objective of this study was to investigate the synergistic effects of these materials and examine how varying the nickel content impacts the electrochemical performance of the composites.

To fabricate the composites, $rGO/NiCoFe_2O_4$ was first synthesized using an auto-combustion method, followed by the incorporation of PPy through a chemical oxidative polymerization process. Of the composites tested, PRNC80 exhibited the highest C_P of

742.85 F/g at a scan rate of 10 mV/s. This enhanced performance is attributed to the optimized nickel content and the synergistic interactions between PPy, rGO, and $NiCoFe_2O_4$. The superior electrochemical performance observed in PRNC80 is largely due to its enhanced conductivity, pseudocapacitive behavior, and redox activity, coupled with the porous structure of the composite that facilitates effective ion diffusion.

The potential of PPy/rGO/$NiCoFe_2O_4$ ternary composites is shown by this work, especially PRNC80, as highly promising electrode materials for advanced supercapacitors. The study underscores the significance of optimizing material composition to enhance electrochemical properties, contributing to the development of efficient and scalable electrode materials for future energy storage applications.

6.2 Characterization Techniques

XRD analysis of the powdered samples of the synthesized PPy/rGO composite was performed using a BRUKER diffractometer. This technique allowed us to investigate the crystallographic structure of the composite. The surface morphology of the composites was examined using a JEOL SEM. FTIR spectra were obtained with a Perkin-Elmer infrared spectrophotometer, providing insights into the functional groups present in the composite. For electrochemical experiments, the METHROM NOVA software was utilized, enabling precise control and analysis of the electrochemical measurements conducted in our study.

6.3 Result and Discussion

6.3.1 Structural and surface characterizations

Figure 6.1 displays the XRD spectra for the PRNC composites, confirming the formation and crystallinity of the synthesized materials. The broad peak in the range of $2\theta = 20–42°$ observed in all samples is characteristic of polypyrrole (PPy) and indicates its amorphous nature. This observation aligns with previously reported studies, such as those by Saira Ishaq et al., where PPy exhibited similar broad diffraction patterns due

to its disordered structure.

Distinct and sharp diffraction peaks corresponding to the formation of $NiCoFe_2O_4$ are observed at $2\theta = 30.08°$, 35.45°, 42.91°, 57.00°, and 62.69°, representing the (220), (311), (400), (511), and (440) crystallographic planes, respectively. These peaks confirm the successful formation of the spinel ferrite structure of $NiCoFe_2O_4$ across all samples. These peaks' clarity and intensity demonstrate the high crystallinity of the $NiCoFe_2O_4$ phase, which remains consistent throughout the series of PRNC composites[130].

Furthermore, a noticeable peak at $2\theta = 26.41°$ is observed in all samples, corresponding to the (002) plane of reduced graphene oxide (rGO). The presence of this peak confirms that the rGO maintains its characteristic structure within the composite, suggesting that the synthesis process does not affect the integrity of rGO within the material.

The crystallite sizes were calculated using the Debye-Scherrer equation, and the d-spacing values were determined using Bragg's law. The d-spacing values, presented in Table 6.1, range from 2.10 Å to 2.21 Å across the PRNC composites. These values suggest minimal variation in the interplanar spacing, indicating that the nickel content does not significantly alter the basic crystal structure of $NiCoFe_2O_4$.

The crystallite size, however, shows more variation with the nickel content. PRNC40 exhibited the largest crystallite size of 8.17 nm, while PRNC100 demonstrated the smallest crystallite size of 3.56 nm. The decreasing crystallite size with increasing nickel content suggests that the nickel-to-cobalt ratio may influence the nucleation and growth of $NiCoFe_2O_4$ crystallites, potentially impacting the electrochemical behavior of the composite.

The lattice constant (a_0) was also calculated for each composite, ranging from 8.354 Å to 8.378 Å, with slight variations observed across the different PRNC compositions. The small changes in lattice constant indicate minor distortions in the crystal lattice, which are likely due to the varying amounts of nickel incorporated into the $NiCoFe_2O_4$ structure.

In addition, the FWHM of the diffraction peaks was analyzed. A smaller FWHM value corresponds to a higher degree of crystallinity, while broader peaks indicate smaller crystallite sizes and possibly more structural defects. For instance, PRNC40 showed a narrow peak with an FWHM of 0.182°, reflecting its larger crystallite size and higher

crystallinity, while PRNC100 had the broadest peak with an FWHM of 0.269°, correlating with its smaller crystallite size and potentially higher defect density.

Despite the variations in nickel content, the XRD patterns demonstrate that the spinel ferrite structure of $NiCoFe_2O_4$ remains stable across all samples. The consistent presence of the characteristic $NiCoFe_2O_4$ diffraction peaks indicates that the crystal structure is preserved, even with changes in the nickel-to-cobalt ratio. The slight variations in crystallite size and peak intensities suggest that the interaction between $NiCoFe_2O_4$, rGO, and PPy may vary slightly with different compositions, but the overall structure remains intact.

The XRD results confirm the successful synthesis of the PPy/rGO/$NiCoFe_2O_4$ composite, with clear evidence of the crystalline $NiCoFe_2O_4$ spinel structure and the retained structure of rGO. Despite slight variations in nickel content, the crystalline phase remains intact, and the changes in crystallite size and lattice constant reflect the composite's adaptability. These structural characteristics, particularly the smaller crystallite size and higher defect density in PRNC100, could be crucial in improving these materials' electrochemical performance in energy storage applications[131], [132], [133].

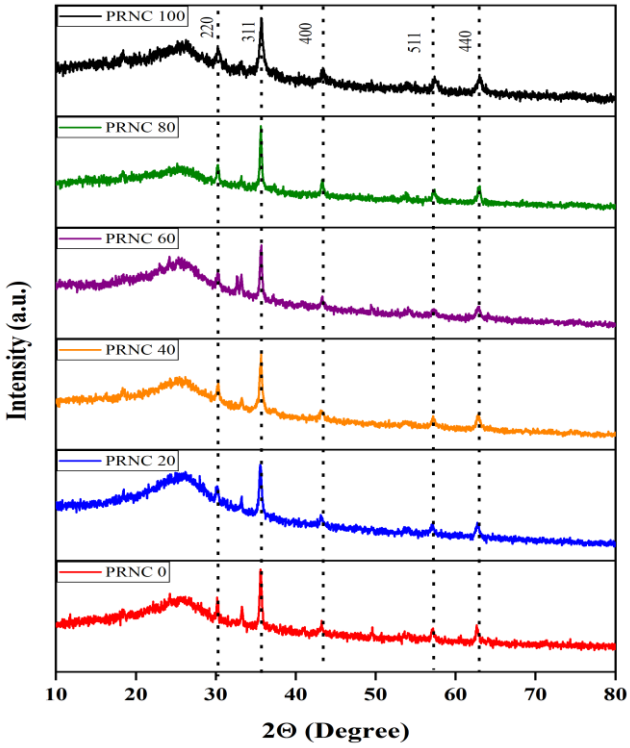

Figure 6.1: XRD of ternary composites PPy/rGO/$NiCoFe_2O_4$

Table 6.1: X-ray Diffraction (XRD) Parameters for PPy/rGO/$NiCoFe_2O_4$ Composites

Composite	2θ (Degree)	d-Spacing (Å)	Crystallite Size (nm)	Lattice Constant (a_0) (Å)	FWHM (Degree)
PRNC0	35.45	2.13	5.05	8.354	0.231
PRNC20	35.45	2.21	7.84	8.378	0.196
PRNC40	35.45	2.16	8.17	8.372	0.182
PRNC60	35.45	2.10	7.41	8.360	0.210
PRNC80	35.45	2.15	4.72	8.366	0.253
PRNC100	35.45	2.12	3.56	8.359	0.269

6.3.2 Morphological characterization

The FESEM images in Figure 6.2 provide detailed insights into the morphological features of the PRNC series composites, showcasing the dispersion and structure of the nanomaterials in each sample. These images highlight the surface characteristics and distribution of $NiCoFe_2O_4$ nanoparticles, rGO, and PPy, which are crucial for the composites' electrochemical performance. In the PRNC0 composite (Fig. 6.2a-b), a highly porous and interconnected structure is visible, with $NiCoFe_2O_4$ nanoparticles dispersed across the rGO sheets. The particle sizes range from 50-80 nm, and the porous structure is beneficial for enhancing electrolyte interaction, providing a large surface area for electrochemical reactions. For the PRNC20 composite (Fig. 6.2c-d), the overall porous structure is maintained, with a denser packing of the nanostructures. The $NiCoFe_2O_4$ particles range in size from 50-90 nm, and the successful incorporation of PPy is evident from the smoother surface texture. This structure enhances conductivity and mechanical stability, crucial for improving electrochemical performance. The PRNC40 composite (Fig. 6e-f) displays a well-defined porous morphology, with a uniform dispersion of $NiCoFe_2O_4$ nanoparticles across the rGO sheets. The particle sizes range from 50-85 nm, and the presence of PPy contributes to a smoother and more uniform surface, indicating improved interfacial contact between components, which promotes better charge transfer during electrochemical reactions. In the PRNC60 composite (Fig. 6g-h), a compact and dense structure is observed, with $NiCoFe_2O_4$ nanoparticles densely packed within the composite matrix. The particle size ranges from 55-85 nm, and the integration of PPy results in a more cohesive surface. The reduced voids and compact morphology suggest more efficient charge transport while maintaining sufficient porosity for electrolyte penetration. The PRNC80 composite (Fig. 6i-j) reveals a highly porous structure, similar to that of PRNC40, with well-dispersed $NiCoFe_2O_4$ nanoparticles across the composite surface. The particle sizes remain consistent, ranging from 50-85 nm. The presence of PPy is visible, contributing to the uniformity of the surface and enhancing the overall structural stability of the composite. The porous nature of PRNC80 suggests that it has a large surface area, which is advantageous for ion diffusion and charge storage, making it highly suitable for energy storage applications. Finally, the PRNC100 composite (Fig. 6k-l) exhibits a compact yet porous structure, with densely packed $NiCoFe_2O_4$ nanoparticles. The

average particle size is slightly larger, ranging from 55-90 nm, with a smoother surface due to the successful incorporation of PPy. This compact structure may lead to improved charge transport by reducing ion diffusion paths, while the retained porosity ensures sufficient electrolyte access. The PRNC100 composite demonstrates a balance between porosity and compactness, which could enhance both charge storage and mechanical stability. Across all composites in the PRNC series, the sponge-like porous structure is a defining characteristic, with well-dispersed $NiCoFe_2O_4$ nanoparticles embedded within the rGO and PPy matrix. The incorporation of PPy plays a key role in enhancing the electrical conductivity and structural integrity of the composites. The rGO framework supports the dispersion of the $NiCoFe_2O_4$ particles, ensuring effective interaction with electrolytes, which is critical for optimizing electrochemical performance. The FESEM analysis confirms the successful synthesis of the PPy/rGO/$NiCoFe_2O_4$ composites, highlighting uniform nanoparticle distribution, well-defined porous structures, and effective incorporation of PPy. This organized structure, with its combination of porosity and uniform nanoparticle dispersion, contributes to the improved electrochemical performance of the composites, As a result, they make good candidates for applications in improved energy storage[134], [135], [136].

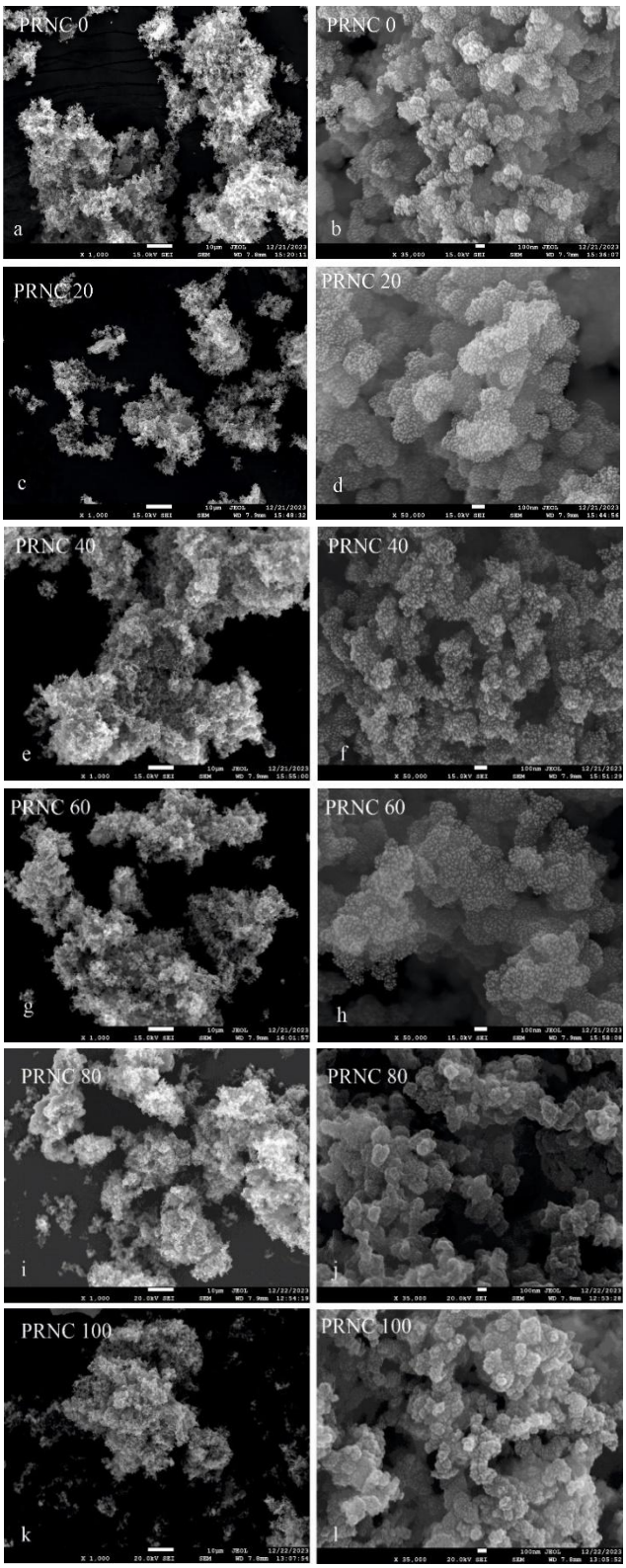

Figure 6.2 FESEM images of ternary composites PPy/rGO/$NiCoFe_2O_4$

6.3.3 Spectroscopic characterization

The FTIR spectra of the PRNC ternary composites, shown in Figure 6.3, provide crucial insights into the structural components and chemical bonds present within the composite materials. The distinct peak at 876 cm^{-1} is attributed to M-O (metal-oxygen) bond vibrations, and the peak at 1041 cm^{-1} corresponds to Fe-O stretching vibrations, which confirm the presence of metal-oxygen bonds from the $NiCoFe_2O_4$ spinel structure. These peaks validate the successful integration of the metal oxides into the composite. In addition to the metal-oxygen vibrations, characteristic polypyrrole (PPy) functional groups are identified in the spectra. Peaks at 1205 cm^{-1}, 1385 cm^{-1}, and 1514 cm^{-1} are attributed to C-H bending, C-N stretching, and =C-H out-of-plane deformation modes, respectively, which are commonly associated with the polypyrrole (PPy) backbone. These peaks reveal that PPy was successfully included into the composite structure, as the vibrational modes corresponding to the polymer's functional groups are clearly observable. The broad absorption band observed around 3000 cm^{-1} is assigned to the O-H stretching vibration, indicative of hydroxyl groups (OH) within the composite. These OH groups likely originate from residual moisture or surface hydroxyl groups on the rGO (reduced graphene oxide) and may contribute to the composite's enhanced hydrophilic properties, promoting better interaction with electrolytes in electrochemical applications. The distinct vibrational modes identified in the FTIR spectrum affirm the successful integration of rGO, PPy, and $NiCoFe_2O_4$ within the ternary composite. The structural stability and electrochemical performance of the composites depend much on the existence of these functional groups and metal-oxygen linkages. Specifically, the metal-oxygen bonds contribute to the redox activity, while the polypyrrole conductive properties improve charge transport and pseudo-capacitance. Additionally, the rGO framework provides a conductive matrix, further supporting ion diffusion and enhancing the composite's overall performance in energy storage devices. The combination of metal-oxygen vibrational modes with the polymer and hydroxyl group modes showcases the structural complexity and versatility of the PRNC composites. This interplay of rGO, PPy, and $NiCoFe_2O_4$ contributes to the synergistic effects observed in the composite, where each component plays a distinct

role in improving the composite's electrochemical capabilities[137], [138], [139].

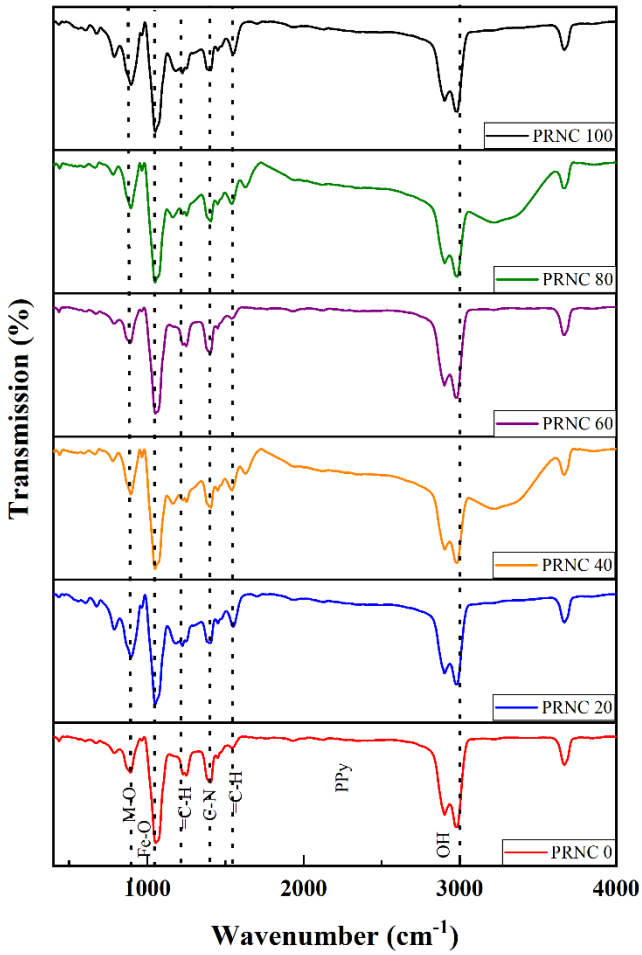

Figure 6.3: FTIR of ternary composites PPy/rGO/$NiCoFe_2O_4$

Table 6.2: FTIR Vibrational Modes and Bond Assignments for PPy/rGO/$NiCoFe_2O_4$ Composites

Wavenumber (cm^{-1})	Vibrational Mode	Assigned Bond or Group
876	Metal-Oxygen Vibration	M-O ($NiCoFe_2O_4$)
1041	Metal-Oxygen Vibration	Fe-O ($NiCoFe_2O_4$)
1205	C-H Bending	Polypyrrole (PPy)
1385	C-N Stretching	Polypyrrole (PPy)
1514	=C-H Out-of-plane Deformation	Polypyrrole (PPy)
3000	O-H Stretching	Hydroxyl Groups (rGO, residual moisture)

6.3.4 Electrochemical characteristics

6.3.4.1 CV Analysis

Cyclic voltammetry (CV) profiles, as displayed in Figure 6.4, provide a comprehensive evaluation of the PPy/rGO/$NiCoFe_2O_4$ composites' electrochemical performance. The scan rates varied from 10 mV/s to 100 mV/s, and the tests were conducted in 3M KOH electrolyte throughout a potential range of 0V to 0.7V. The PRNC80 composite had the highest C_P of all the series at a scan rate of 10 mV/s (742.85 F/g). This superior performance is primarily attributed to the optimal composition, where the nickel content enhances both conductivity and charge storage capacity. The polypyrrole (PPy) component provides a porous structure, facilitating electrolyte penetration and charge storage. Moreover, the PPy network supports rapid electron and ion transport, which further improves the electrochemical performance of the material. The PRNC60 composite exhibited a C_P of 715.25 F/g, showcasing similarly high electrochemical activity. The increased nickel content, in conjunction with the synergistic effects of rGO, $NiCoFe_2O_4$, and PPy, results in enhanced conductivity and redox activity. The presence of PPy contributes significantly to the uniformity of the composite, allowing efficient electrolyte access and improving charge transport capabilities. This composite demonstrates excellent electrochemical properties, closely following the performance of PRNC80. In the PRNC40 composite, a C_P of 691.42 F/g was recorded. This strong electrochemical response stems from the balanced interaction between the conductive rGO, the redox-active $NiCoFe_2O_4$, and the porous network of PPy. The effective integration of these components results in high capacitance, with pronounced redox peaks visible across the CV profiles, indicative of efficient charge storage and retrieval processes. The PRNC20 composite demonstrated a C_P of 238.5 F/g, reflecting an improvement over PRNC0 due to the higher nickel content. The enhanced nickel presence boosts both conductivity and redox behavior, leading to more defined CV peaks and increased charge storage. However, the overall electrochemical performance remains lower than the composites with higher nickel content, owing to less effective ion diffusion and charge transport in the structure. At the lower end of the series, the PRNC0 composite exhibited a C_P of 153.28 F/g, which, while the lowest in the series, still highlights the composite's stable electrochemical behavior. The CV profiles for

PRNC0 show consistent redox activity, attributed mainly to the redox potential of $NiCoFe_2O_4$ and the conductive properties of rGO. Despite lacking the enhanced charge storage seen in higher-nickel composites, PRNC0 still demonstrates reliable electrochemical properties. Lastly, the PRNC100 composite showed a C_P of 328.75 F/g. While higher than PRNC20 and PRNC0, the specific capacitance does not reach the levels seen in PRNC60, PRNC40, or PRNC80. This is likely due to the larger particle size and denser structure observed in the FESEM images, which restricts ion diffusion and limits electrolyte access. Nonetheless, PRNC100 maintains stable behavior across varying scan rates, confirming its reliable electrochemical performance. Across the PRNC series, all composites exhibit consistent CV profiles, with well-defined redox peaks indicating effective charge storage and retrieval. The synergistic interaction between rGO, $NiCoFe_2O_4$, and PPy shows in the composites' performance since a combination of these components improves conductivity, as the combination of these materials enhances conductivity, redox activity, and overall charge transport capabilities. The highest-performing composites, PRNC80, PRNC60, and PRNC40, stand out due to their well-balanced composition, which optimizes both the conductivity and redox characteristics of the materials[118], [140].

Table 6.3 Specific capacitance by CV

Composite	Specific Capacitance (F/g) (CV)
PRNC0	153.28
PRNC20	238.5
PRNC40	691.42
PRNC60	715.25
PRNC80	742.85
PRNC100	328.75

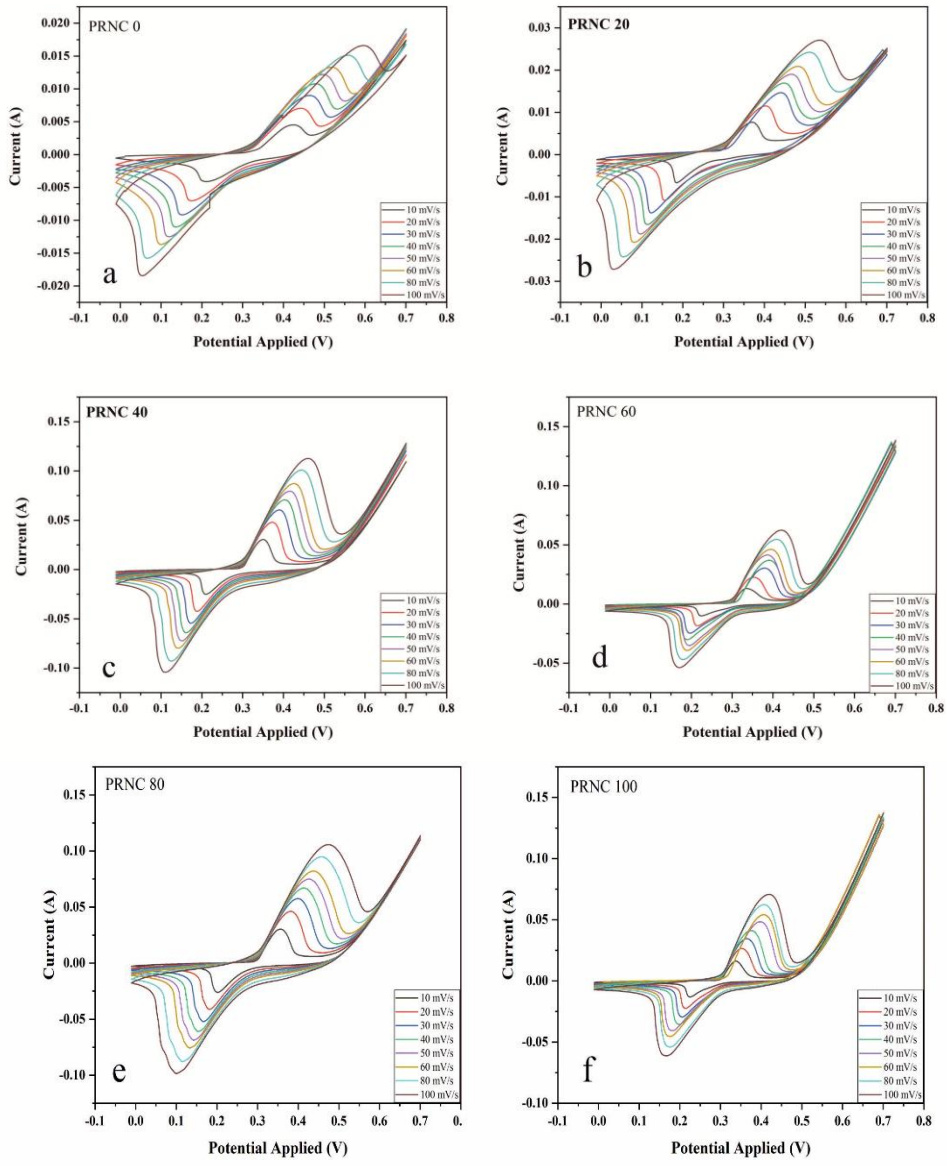

Figure 6.4: CV of ternary composites PPy/rGO/NiCoFe2O4

6.3.4.2 GCD Analysis

Galvanostatic charge-discharge (GCD) examinations were performed at current densities of 1, 2, 4, and 6 A/g, as shown in Figure 6.5. The GCD curves provide critical insights into the electrochemical performance of the PPy/rGO/$NiCoFe_2O_4$ composites. As the current density increases, the discharge time decreases, reflecting the kinetics of the charge-discharge process. Despite the varying current densities, the consistent shape of the GCD curves for all composites indicates ideal capacitive behavior, confirming

the efficiency and stability of the materials under different operational conditions. Among the composites, PRNC80 exhibited the highest C_P of 585.5 F/g at a 1 A/g current density. This enhanced performance is primarily due to the well-balanced composition of the composite, where PPy provides a porous structure that facilitates easy electrolyte access, and rGO ensures excellent conductivity. The $NiCoFe_2O_4$ component contributes redox activity, and the combination of these materials results in superior charge storage capacity. The GCD curves for PRNC80 show extended discharge times, reflecting its high energy storage capability. For the PRNC60 composite, a C_p of 562 F/g was recorded. This composite also demonstrates excellent electrochemical properties, supported by the synergistic interaction between PPy, rGO, and $NiCoFe_2O_4$. The porous network formed by PPy allows for efficient ion diffusion, while rGO enhances electron transport. The GCD curves maintain a consistent shape across all current densities, reflecting the stability of the material under different charging and discharging conditions. The PRNC40 composite showed a C_P of 550 F/g at 1 A/g, indicating its strong electrochemical performance. The effective combination of rGO, $NiCoFe_2O_4$, and PPy results in a well-structured composite that supports efficient charge storage and retrieval. The GCD curves of PRNC40 display uniformity, suggesting stable capacitive behavior across various current densities. For the PRNC20 composite, a C_P of 220 F/g was observed. While lower than PRNC40, PRNC60, and PRNC80, this composite still demonstrates stable electrochemical behavior, as seen in its GCD profiles. The reduction in performance is likely due to the lower nickel content, which limits charge transport and reduces redox activity. The PRNC0 composite exhibited the lowest C_P of 157.25 F/g. The GCD curves for this composite show shorter discharge times, reflecting its reduced charge storage capacity compared to the other composites in the series. However, the stable shape of the curves across varying current densities confirms the reliability of PRNC0 for applications requiring consistent but lower energy storage. Lastly, the PRNC100 composite showed a C_p of 252.5 F/g, which, while higher than PRNC20 and PRNC0, is still significantly lower than PRNC60 and PRNC80. The reduced electrochemical performance is likely due to the denser structure and larger particle sizes observed in the FESEM images, which limit ion diffusion and electrolyte access. Despite this, the GCD curves for PRNC100 maintain a consistent shape, indicating stable charge-discharge behavior. Across the

PRNC series, the GCD curves display nearly identical behavior, with consistent charge-discharge cycles that reflect ideal capacitive properties. The highest specific capacitances were observed in PRNC80, PRNC60, and PRNC40, with PRNC80 standing out as the best performer in both cyclic voltammetry (CV) and GCD tests. This highlights the importance of an optimal combination of PPy, rGO, and $NiCoFe_2O_4$ in achieving superior electrochemical performance [114], [141].

Table 6.4: Specific capacitance by GCD

Composite	Specific Capacitance (F/g) (GCD)
PRNC0	157.25
PRNC20	220
PRNC40	550
PRNC60	562
PRNC80	585.5
PRNC100	252.5

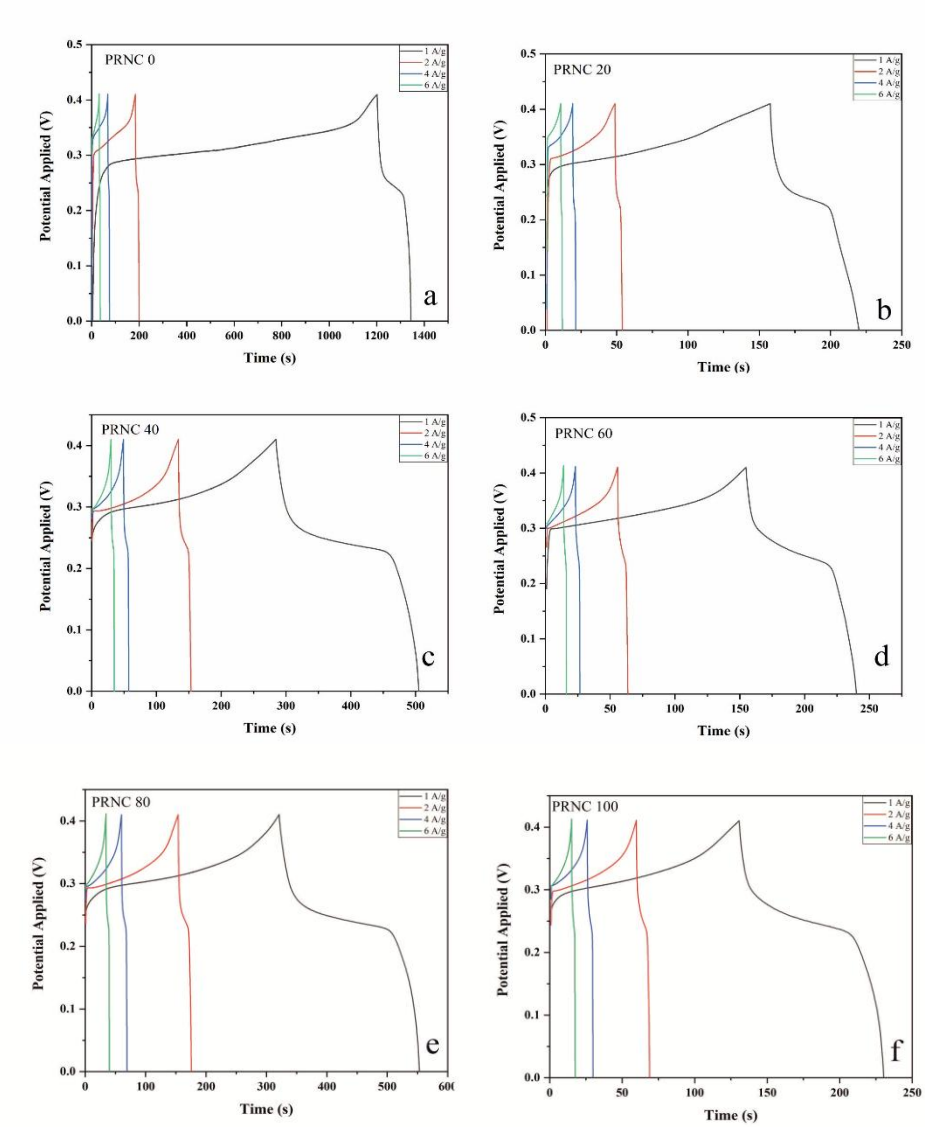

Figure 6.5: GCD of ternary composites PPy/rGO/NiCoFe2O4

6.3.4.3 EIS Analysis

Electrochemical Impedance Spectroscopy (EIS) was performed on the PPy/rGO/$NiCoFe_2O_4$ composites using a 3M KOH solution, covering a frequency range from 10^5 to 10^{-1} Hz, with Nyquist plots shown in Figure 8. The EIS analysis reveals critical insights into the charge transport and resistive properties of the composites. The Nyquist plots for all samples show a distinct semicircle in the high-frequency region, indicative of charge transfer resistance (Rct) at the electrode-

electrolyte interface. Additionally, a linear portion in the low-frequency region indicates Warburg resistance, suggesting controlled ion diffusion in the electrolyte. The impedance at low frequencies reflects the internal resistances and slower charge transfer processes within the material, while at higher frequencies, the reduced impedance reflects enhanced charge movement, improving conductivity. The Nyquist plot for PRNC0 exhibits a large semicircle, indicative of high Rct, and a relatively steep linear segment at low frequencies, characteristic of Warburg diffusion resistance. The equivalent circuit fitting revealed a series resistance (Rs) of approximately 2.31 Ω and a charge transfer resistance (Rct) of 152.4 Ω. The large value of Rct reflects a slower charge transfer process, which is consistent with the lower electrochemical performance observed in the CV and GCD measurements. The Nyquist plot for PRNC20 displays a similarly large semicircle in the high-frequency region, suggesting considerable charge transfer resistance. The Rs for PRNC20 was measured at 1.92 Ω, while the Rct was 134.2 Ω. Although the charge transfer resistance is slightly lower than PRNC0, it still indicates significant resistance to charge transfer, affecting its overall electrochemical performance. In PRNC40, the Nyquist plot shows a smaller semicircle compared to PRNC0 and PRNC20, indicating improved charge transfer properties. The Rs was measured at 1.74 Ω, and the Rct was reduced to 89.5 Ω, reflecting enhanced electron transfer at the electrode-electrolyte interface. The linear region is more vertical, suggesting better capacitive behavior, which correlates with the improved electrochemical performance observed in CV and GCD tests. The PRNC60 composite displayed a relatively small semicircle in the high-frequency region, indicative of low Rct. The Rs was measured at 1.66 Ω, while the Rct was further reduced to 74.8 Ω, highlighting efficient charge transfer. The steep slope in the low-frequency region reflects enhanced ion diffusion, which is consistent with its high specific capacitance and strong electrochemical performance. The Nyquist plot for PRNC80 demonstrates the smallest semicircle among the composites, indicating minimal charge transfer resistance. The Rs for PRNC80 was recorded at 1.52 Ω, and the Rct was as low as 65.3 Ω, confirming superior electron and ion transport. The near-vertical slope in the low-frequency region highlights ideal capacitive behavior and efficient ion diffusion, corresponding to the highest specific capacitance values seen in CV and GCD results. For PRNC100, the Nyquist plot shows a moderate-sized

semicircle, larger than those of PRNC80 but smaller than PRNC20 and PRNC0. The Rs was 1.86 Ω, and the Rct was 109.4 Ω, suggesting intermediate charge transfer resistance. The slope in the low-frequency region reflects moderate capacitive behavior, although not as pronounced as in PRNC80 or PRNC60. This is consistent with the intermediate electrochemical performance observed for PRNC100. The EIS analysis confirms that PRNC80 exhibits the lowest series and charge transfer resistance, contributing to its superior electrochemical performance. The lower Rct values in PRNC60 and PRNC40 also correlate with their strong performance. In contrast, PRNC0 and PRNC20 have significantly higher Rct values, indicating substantial resistance to charge transfer, which limits their overall electrochemical efficiency. In all cases, the presence of the Warburg region (linear segment at low frequencies) indicates diffusion-controlled processes, essential for understanding how well ions are transported within the material. The equivalent circuits used to model the impedance data were constructed using ZSimps, representing the electrochemical system's behavior with components such as resistors (R) and constant phase elements (CPE) to account for the non-ideal capacitive behavior [126], [142], [143].

Table 6.5: Series resistance and charge transfer resistance

Composite	Series Resistance (Rs) (Ω)	Charge Transfer Resistance (Rct) (Ω)
PRNC0	2.31	152.4
PRNC20	1.92	134.2
PRNC40	1.74	89.5
PRNC60	1.66	74.8
PRNC80	1.52	65.3
PRNC100	1.86	109.4

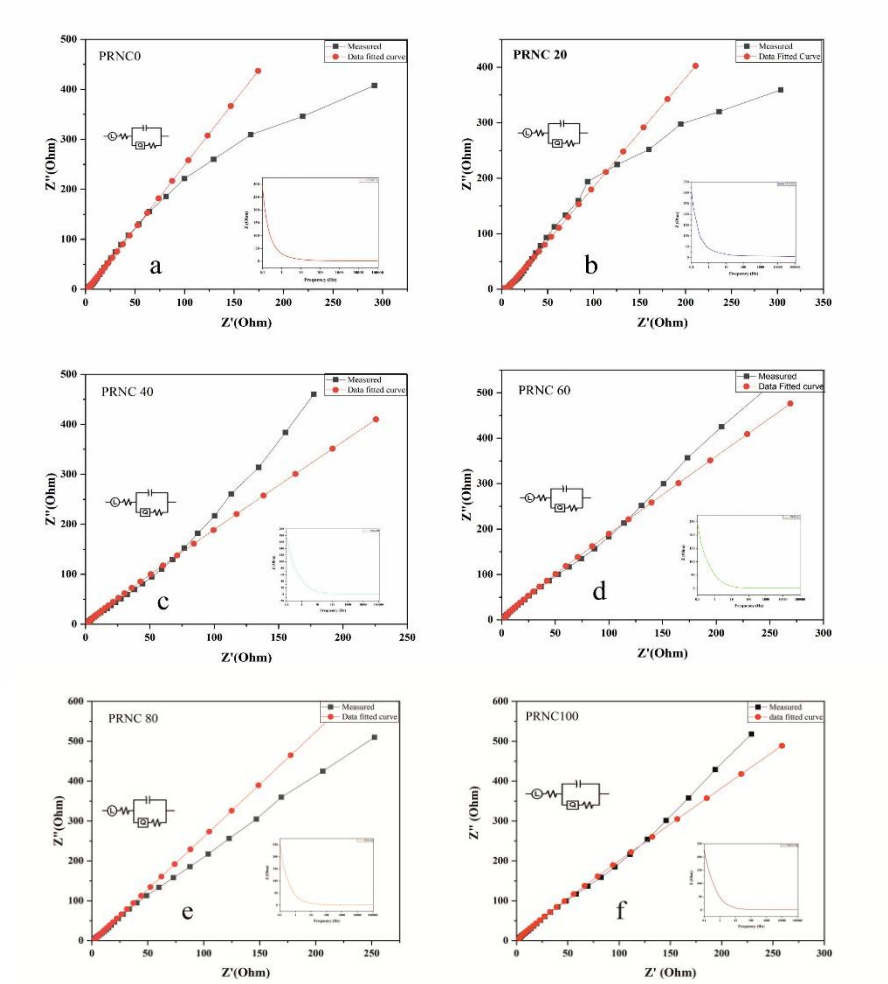

Figure 6.6: EIS of ternary composites PPy/rGO/NiCoFe2O4 (equivalent circuit, Freq vs real part, and Nyquist curve)

6.3.5 Energy density and power density measurements

The electrochemical performance of the PPy/rGO/$NiCoFe_2O_4$ composites was further analyzed by calculating their energy density (Ed) and power density (Pd) from the galvanostatic charge-discharge (GCD) data. These parameters are crucial for evaluating the composites' suitability in practical energy storage systems, where energy density reflects how much energy can be stored per unit mass, and power density indicates how quickly that energy can be delivered.

Among the composites, PRNC80 demonstrated the highest specific capacitance of 585.5 F/g, corresponding to an energy density of 32.19 Wh/kg and a power density of

1234.6 W/kg at a current density of 1 A/g. This combination of high energy and power density makes PRNC80 an excellent candidate for high-performance supercapacitor applications, capable of both rapid charge-discharge cycles and substantial energy storage. PRNC60 and PRNC40 also showed strong performance, with energy densities of 30.92 Wh/kg and 30.26 Wh/kg, and power densities of 1196.8 W/kg and 1172.5 W/kg, respectively. While slightly lower than PRNC80, these values indicate efficient charge storage and transport, likely due to improved electrode conductivity and increased electroactive sites. In contrast, PRNC100, PRNC20, and PRNC0 displayed lower specific capacitances (252.5, 220, and 157.25 F/g, respectively), which resulted in reduced energy densities of 13.89, 12.1, and 8.64 Wh/kg, although their power densities remained reasonably high (987.3, 951.2, and 875.1 W/kg, respectively). These results are consistent with the EIS data, which showed higher internal resistance and slower charge transfer for these composites. Overall, the trends in energy and power density closely follow the specific capacitance results, highlighting the critical role of nickel content and the effective integration of $NiCoFe_2O_4$ within the rGO matrix. PRNC80, in particular, offers a well-balanced combination of high energy storage and fast charge-discharge capability, making it the most promising material for practical supercapacitor applications.

Table 6.6: Energy and power density of ternary composites PPy/rGO/$NiCoFe_2O_4$ Calculation

Composite	C_p (F/g)	E_d (Wh/kg)	P_d (W/kg)
PRNC0	157.25	8.64	875.1
PRNC20	220	12.1	951.2
PRNC40	550	30.26	1172.5
PRNC60	562	30.92	1196.8
PRNC80	585.5	32.19	1234.6
PRNC100	252.5	13.89	987.3

Specific capacitance by using cyclic voltammetry was calculated by Equation (1).

$$C_p = \frac{dQ}{mdV} = \frac{idt}{mdV} = \frac{\bar{\imath}}{mv} = \frac{1}{2mv(V_1 - V_2)} \int_{V_1}^{V_2} i(V)dV \quad (1)$$

$$S = \int_{V1}^{V2} i(V)dV \quad (2)$$

Specific capacitance by using GCD was calculated by equation 328,29.

$$C_P = \frac{I\Delta t}{m.V} \quad (3)$$

Eq. 4 and 5 were used to ascertain the E_d and P_d of the material, respectively.

$$E_d = \frac{C_p(\Delta V)^2}{2} \quad (4)$$

$$P_d = \frac{E}{\Delta t} \quad (5)$$

Table 6.7: Comparison of PPy/rGO/$NiCoFe_2O_4$ and rGO/$NiCoFe_2O_4$ with previously reported

Electrode material	Galvanic charge discharge/scan rate	Electrolyte	Specific capacitance (Fg-1)	References
Ppy/GO/ZnO	1Ag-1	1M Na2SO4	94.6	[142]
CNT/PPy/MnO2	20 mVs-1	1 M Na2SO4	281	[143]
PANI-Graphene-CNT	0.5 Ag-1	PVA-H3PO4	890	[144]
PEDOT-GO/CNTs	10 mVs-1	1 M KCl	104	[117]
Ppy-GO/CNTs	10 mVs-1	1 M KCl	143.6	[117]
PPy/rGO/$NiCOFe_2O_4$	10 mVs-1	3 M KOH	742.85	Present work

6.4 Conclusion

This work synthesised a series of ternary composites of PPy/rGO/$NiCoFe_2O_4$ and methodically assessed their possible use as high-performance electrode materials for supercapacitors. By varying the nickel content from 0 to 100%, we were able to investigate the effects of composition on the electrochemical performance of these composites. The results from XRD, FTIR, FESEM, and electrochemical characterization techniques such as CV, GCD, and EIS have provided comprehensive insights into the structural and electrochemical properties of the prepared materials. Among the composites, PRNC80 demonstrated the best electrochemical performance, exhibiting a C_p of 742.85 F/g in CV measurements and an E_d of 32.19 Wh/kg with a P_d

of 1234.6 W/kg in GCD tests. The enhanced performance of PRNC80 can be attributed to the optimal balance of nickel content, which facilitated efficient charge transfer, improved ion diffusion, and enhanced redox activity. PRNC60 and PRNC40 also showed competitive electrochemical behavior, with C_p of 715.25 F/g and 691.42 F/g, respectively, further demonstrating the effectiveness of the ternary composite system. The EIS study verified that the charge transfer resistance was much reduced in PRNC80, PRNC60, and PRNC40, which correlates well with their high electrochemical performance. In contrast, PRNC0 and PRNC20 exhibited higher charge transfer resistance and lower C_P, limiting their energy storage potential. Overall, the results demonstrate that the incorporation of PPy, rGO, and $NiCoFe_2O_4$ into a ternary composite structure significantly improves the electrochemical properties of the material, making it a strong candidate for next-generation energy storage devices. The synergy between the components provides a robust framework for efficient charge storage and fast electron/ion transport, contributing to the composite's high energy densities and power densities. This work highlights the importance of optimizing material composition to achieve superior performance in supercapacitor applications. The scalable and cost-effective synthesis method employed in this study also underscores the practicality of these composites for commercial energy storage systems. Future research could focus on improving the long-term cyclic stability and further optimizing the synthesis parameters to maximize performance.

Chapter 7
Summary and conclusion

This study was motivated by the need to explore the potential characteristics of composites based on PPy, rGO, and $NiCoFe_2O_4$ for energy storage applications. The primary objective was to develop efficient electrode materials with enhanced electrochemical performance.

rGO was synthesized using a modified Hummer's method and later utilized for composite fabrication. The binary PPy/rGO composite was prepared via a chemical oxidative polymerization process, while the rGO/$NiCoFe_2O_4$ composite was synthesized using a sol-gel auto-combustion technique. To obtain the ternary composite, PPy was incorporated into the rGO/$NiCoFe_2O_4$ system.

A series of six composites was developed by varying the weight percentage of $NiCoFe_2O_4$ (0, 20, 40, 60, 80, and 100 wt%). These materials' morphological and structural characteristics were examined using FTIR, FESEM, and XRD. Using CV, GCD, and EIS, the electrochemical performance was evaluated.

Conclusion

1) An oxidative polymerization method was used to synthesize the PPy/rGO hybrid, which made it easier for the PPy to be evenly distributed in the rGO matrix. The development of a highly porous structure as a result of this homogeneous dispersion improved electrolyte accessibility and ion diffusion, both of which are essential for increasing charge storage capacity. The synthesis parameters were carefully controlled to tailor the composite's morphology, thereby optimizing its electrochemical performance. At a scan rate of 10 mV/s, the binary PPy/rGO composite demonstrated a C_P of 365.1 F/g by electrochemical testing using CV. A C_p of 375 F/g was also demonstrated by GCD tests at a current density of 2 A/g. These findings highlight the effectiveness of this synthesis approach in developing conductive polymer-graphene-based electrode materials with enhanced energy storage capabilities. The study underscores the potential of PPy/rGO composites as efficient and

cost-effective electrode materials for supercapacitor applications.

2) Electrochemical investigations revealed that the binary rGO/$NiCoFe_2O_4$ composite achieved a C_p of 216.5 F/g, as determined by CV. The inclusion of PPy in the ternary composite further enhanced the electrochemical performance, yielding a significantly higher C_p of 664.98 F/g. Similarly, GCD measurements indicated a C_p of 275 F/g for the binary composite, which increased to 720 F/g in the ternary system.

   Additionally, energy and power density calculations demonstrated notable improvements. The binary composite exhibited an energy density of 34.37 Wh/kg with a corresponding power density of 1135.15 W/kg. In contrast, the ternary composite achieved an energy density of 90 Wh/kg and a power density of 1167.14 W/kg, underscoring the superior energy storage capability of the PPy/rGO/$NiCoFe_2O_4$ electrode.

   These findings validate the effectiveness of the proposed synthesis method in developing high-performance composite electrode materials. The approach provides a viable strategy for designing and optimizing advanced supercapacitor electrodes with tailored electrochemical properties, offering the potential for scalable energy storage applications.

3) A series of ternary PPy/rGO/$NiCoFe_2O_4$ composites were synthesized and systematically analyzed to assess their potential as high-performance electrode materials for supercapacitors. By varying the nickel content from 0% to 100%, the influence of composition on electrochemical performance was investigated. Among the tested composites, PRNC80 exhibited the highest electrochemical performance, achieving a specific capacitance of 742.85 F/g in CV measurements. GCD tests further demonstrated its superior energy storage capability, with an energy density of 32.19 Wh/kg and a power density of 1234.6 W/kg. The enhanced performance of PRNC80 is attributed to its optimized nickel content, which facilitated improved charge transfer, efficient ion diffusion, and enhanced redox activity. PRNC60 and PRNC40 also displayed competitive electrochemical properties, with specific capacitances of

715.25 F/g and 691.42 F/g, respectively, reinforcing the effectiveness of the ternary composite system.

EIS analysis revealed significantly lower charge transfer resistance in PRNC80, PRNC60, and PRNC40, correlating well with their superior electrochemical properties. Conversely, PRNC0 and PRNC20 exhibited higher charge transfer resistance and lower specific capacitance, limiting their overall energy storage potential.

These findings confirm that the integration of PPy, rGO, and $NiCoFe_2O_4$ into a ternary composite structure enhances charge storage efficiency and facilitates rapid electron/ion transport, resulting in high energy and power density. Study underscores the significance of optimizing material composition to achieve superior supercapacitor performance. The scalable and cost-effective synthesis method employed further highlights the practicality of these composites for commercial energy storage applications. Future research should focus on improving cyclic stability and refining synthesis parameters to further enhance performance.

Table 7.1: Comparison of all composites

Composite Type	Sample ID	Specific Capacitance (CV) (F/g)	Specific Capacitance (GCD) (F/g)
Binary Composite	PPy/rGO	365.1	375
Binary Series (rGO/$NiCoFe_2O_4$)	RNC80	250	275
Ternary Series (PPy/rGO/$NiCoFe_2O_4$)	PRNC80	742.85	585.5

Future Scope

1) Ppy/rGO/$NiCoFe_2O_4$ composite can be used for supercapacitor applications due to its excellent electrochemical properties. Composite PRNC80 shows the best results among all composites makes it better choice for application.
2) rGO/$NiCoFe_2O_4$ binary composite also shows better results in electrochemical analysis. Especially RNC80 shows best results among binary composites. RNC80

can be used in supercapacitor applications.

3) In future work, the study will focus on:
    a. Developing flexible and wearable supercapacitor electrodes based on the optimized PRNC80 composition, Carbon cloth electrodes that can be used as flexible electrodes.
    b. Scaling up the fabrication process for cost-effective and large-scale production.

Bibliography

[1] N. Shaari, “Chapter 9 - Polymer electrolyte membranes in fuel cell applications,” M. B. T.-R. A. in R. E. T. Jeguirim, Ed. Academic Press, pp. 311–352, 2021.

[2] J. Lim, A. Choi, H. Kim, S. W. Doo, Y. Park, and K. T. Lee, “In situ electrochemical surface modification for high-voltage LiCoO2 in lithium ion batteries,” *J. Power Sources*, vol. 426, pp. 162–168, 2019.

[3] Y. Osada *et al.*, Eds., “Section 2 - Batteries,” Burlington: Academic Press, pp. 421–444, 2001.

[4] V. Cigolotti, M. Genovese, F. Piraino, and P. B. T.-R. M. in C. Fragiacomo Molecular Sciences and Chemical Engineering, “Applications – Stationary | Stationary Energy Storage System: Overview,” Elsevier, 2023.

[5] P. Simon and Y. Gogotsi, “Materials for electrochemical capacitors,” *Nat. Mater.*, vol. 7, no. 11, pp. 845–854, 2008.

[6] A. Muzaffar, M. B. Ahamed, and C. M. Hussain, “Chapter 11 - Electrolyte materials for supercapacitors,” C. M. Hussain and M. B. B. T.-S. S. Ahamed, Eds. Elsevier, pp. 227–254, 2023.

[7] M. A. A. Mohd Abdah, N. H. N. Azman, S. Kulandaivalu, and Y. Sulaiman, “Review of the use of transition-metal-oxide and conducting polymer-based fibres for high-performance supercapacitors,” *Mater. Des.*, vol. 186, p. 108199, 2020,

[8] S. I. Wong, J. Sunarso, B. T. Wong, H. Lin, A. Yu, and B. Jia, “Towards enhanced energy density of graphene-based supercapacitors: Current status, approaches, and future directions,” *J. Power Sources*, vol. 396, pp. 182–206, 2018.

[9] Y. Huang *et al.*, “Nanostructured polypyrrole as a flexible electrode material of supercapacitor,” *Nano Energy*, vol. 22, pp. 422–438, 2016.

[10] S. Kulandaivalu and Y. Sulaiman, “Recent advances in layer-by-layer assembled conducting polymer based composites for supercapacitors,” *Energies*, vol. 12, no. 11, p. 2107, 2019.

[11] H. Zhuo, Y. Hu, Z. Chen, and L. Zhong, “Cellulose carbon aerogel/PPy

composites for high-performance supercapacitor," *Carbohydr. Polym.*, vol. 215, pp. 322–329, 2019.

[12] Y. Tian *et al.*, "Engineering the volumetric effect of Polypyrrole for auto-deformable supercapacitor," *Chem. Eng. J.*, vol. 374, pp. 59–67, 2019.

[13] J. K. Gan, Y. S. Lim, N. M. Huang, and H. N. Lim, "Hybrid silver nanoparticle/nanocluster-decorated polypyrrole for high-performance supercapacitors," *RSC Adv.*, vol. 5, no. 92, pp. 75442–75450, 2015.

[14] M. A. A. M. Abdah, N. A. Rahman, and Y. Sulaiman, "Enhancement of electrochemical performance based on symmetrical poly-(3, 4-ethylenedioxythiophene) coated polyvinyl alcohol/graphene oxide/manganese oxide microfiber for supercapacitor," *Electrochim. Acta*, vol. 259, pp. 466–473, 2018.

[15] Y. Sulaiman, M. K. S. Azmi, M. A. A. M. Abdah, and N. H. N. Azman, "One step electrodeposition of poly-(3, 4-ethylenedioxythiophene)/graphene oxide/cobalt oxide ternary nanocomposite for high performance supercapacitor," *Electrochim. Acta*, vol. 253, pp. 581–588, 2017.

[16] M. A. A. M. Abdah, N. S. M. Razali, P. T. Lim, S. Kulandaivalu, and Y. Sulaiman, "One-step potentiostatic electrodeposition of polypyrrole/graphene oxide/multi-walled carbon nanotubes ternary nanocomposite for supercapacitor," *Mater. Chem. Phys.*, vol. 219, pp. 120–128, 2018.

[17] S. C. Caroline, S. P. Madhusudanan, G. K. Dalapati, and S. K. Batabyal, "Chapter 22 - Energy storage technologies for sustainable development," G. Dalapati, T. Shun Wong, S. Kundu, A. Chakraborty, and S. B. T.-S. and S. B. M. for E. A. Zhuk, Eds. Elsevier, pp. 583–606, 2022.

[18] H. Chai, X. Chen, D. Jia, and W. Zhou, "Electrochemical deposition of Ni(OH)2/CNTs electrode as electrochemical capacitors," *Rare Met.*, vol. 30, no. 1, pp. 85–89, 2011

[19] J. Yan *et al.*, "Advanced Asymmetric Supercapacitors Based on Ni(OH)2/Graphene and Porous Graphene Electrodes with High Energy Density," *Adv. Funct. Mater.*, vol. 22, no. 12, pp. 2632–2641, 2012,

[20] P. Forouzandeh, V. Kumaravel, and S. C. Pillai, "Electrode Materials for Supercapacitors: A Review of Recent Advances," *Catalysts*, vol. 10, no. 9.

2020.

[21] Q. Xiao and X. Zhou, “The study of multiwalled carbon nanotube deposited with conducting polymer for supercapacitor,” *Electrochim. Acta*, vol. 48, no. 5, pp. 575–580, 2003.

[22] L. Ding, X. Zhao, Y. Huang, J. Yan, T. Li, and P. Liu, “Ultra-broadband and covalently linked core–shell CoFe2O4@PPy nanoparticles with reduced graphene oxide for microwave absorption,” *J. Colloid Interface Sci.*, vol. 595, pp. 168–177, 2021.

[23] J. Oh, M. E. Kozlov, B. G. Kim, H.-K. Kim, R. H. Baughman, and Y. H. Hwang, “Preparation and electrochemical characterization of porous SWNT–PPy nanocomposite sheets for supercapacitor applications,” *Synth. Met.*, vol. 158, no. 15, pp. 638–641, 2008.

[24] P. Yang and W. Mai, “Flexible solid-state electrochemical supercapacitors,” *Nano Energy*, vol. 8, pp. 274–290, 2014.

[25] Q. Tang, M. Chen, C. Yang, W. Wang, H. Bao, and G. Wang, “Enhancing the energy density of asymmetric stretchable supercapacitor based on wrinkled CNT@ MnO2 cathode and CNT@ polypyrrole anode,” *ACS Appl. Mater. Interfaces*, vol. 7, no. 28, pp. 15303–15313, 2015.

[26] S. Chabi, C. Peng, Z. Yang, Y. Xia, and Y. Zhu, “Three dimensional (3D) flexible graphene foam/polypyrrole composite: towards highly efficient supercapacitors,” *Rsc Adv.*, vol. 5, no. 6, pp. 3999–4008, 2015.

[27] W. S. Hummers Jr and R. E. Offeman, “Preparation of graphitic oxide,” *J. Am. Chem. Soc.*, vol. 80, no. 6, p. 1339, 1958.

[28] R. Szostak, A. Morais, S. A. Carminati, S. V Costa, P. E. Marchezi, and A. F. Nogueira, “Chapter 10 - Application of Graphene and Graphene Derivatives/Oxide Nanomaterials for Solar Cells,” in *Metal Oxides*, M. B. T.-T. F. of S. O. in N.-G. S. C. Lira-Cantu, Ed. Elsevier, pp. 395–437, 2018.

[29] B. Xu *et al.*, “Reduced graphene oxide as a multi-functional conductive binder for supercapacitor electrodes,” *Energy Storage Mater.*, vol. 12, pp. 128–136, 2018.

[30] B. Lobato, V. Vretenár, P. Kotrusz, M. Hulman, and T. A. Centeno, “Reduced graphite oxide in supercapacitor electrodes,” *J. Colloid Interface Sci.*, vol. 446,

pp. 203–207, 2015.

[31] S. Rasul, A. Alazmi, K. Jaouen, M. N. Hedhili, and P. Costa, “Rational design of reduced graphene oxide for superior performance of supercapacitor electrodes,” *Carbon N. Y.*, vol. 111, pp. 774–781, 2017.

[32] A. Kumar, N. Kumar, Y. Sharma, J. Leu, and T. Y. Tseng, “Synthesis of Free-Standing Flexible rGO/MWCNT Films for Symmetric Supercapacitor Application,” *Nanoscale Res. Lett.*, vol. 14, no. 1, p. 266, 2019.

[33] J. Jayachandiran *et al.*, “Synthesis and Electrochemical Studies of rGO/ZnO Nanocomposite for Supercapacitor Application,” *J. Inorg. Organomet. Polym. Mater.*, vol. 28, no. 5, pp. 2046–2055, 2018.

[34] R. Kumar and R. Thangappan, “Electrode material based on reduced graphene oxide (rGO)/transition metal oxide composites for supercapacitor applications: a review,” *Emergent Mater.*, vol. 5, no. 6, pp. 1881–1897, 2022.

[35] A. Mishra *et al.*, “Comparative electrochemical analysis of rGO-FeVO4 nanocomposite and FeVO4 for supercapacitor application,” *Appl. Surf. Sci.*, vol. 488, pp. 221–227, 2019.

[36] K. O. Abdulwahab, M. M. Khan, and J. R. Jennings, “Ferrites and ferrite-based composites for energy conversion and storage applications,” *Crit. Rev. Solid State Mater. Sci.*, pp. 1–49.

[37] V. V Jadhav, R. S. Mane, and P. V Shinde, “Basics of Ferrites: Structures and Properties BT - Bismuth-Ferrite-Based Electrochemical Supercapacitors,” V. V Jadhav, R. S. Mane, and P. V Shinde, Eds. Cham: Springer International Publishing, pp. 37–45, 2020.

[38] C. R. Mariappan *et al.*, “Synthesis and electrochemical properties of rGO/polypyrrole/ferrites nanocomposites obtained via a hydrothermal route for hybrid aqueous supercapacitors,” *J. Electroanal. Chem.*, vol. 845, pp. 72–83, 2019.

[39] B. Jeevanantham, D. Vignesh, M. K. Shobana, T. Pazhanivel, R. Thangappan, and S. Kavita, “Theoretical and Experimental Insights of Magnesium-doped Cobalt Ferrites for Supercapacitor Applications,” *Electrochim. Acta*, vol. 470, p. 143309, 2023

[40] C. Shen, Y. Xie, B. Zhu, M. Sanghadasa, Y. Tang, and L. Lin, “Wearable

woven supercapacitor fabrics with high energy density and load-bearing capability," *Sci. Rep.*, vol. 7, no. 1, p. 14324, 2017,

[41] F. Manteghi, S. H. Kazemi, M. Peyvandipour, and A. Asghari, "Preparation and application of cobalt oxide nanostructures as electrode materials for electrochemical supercapacitors," *RSC Adv.*, vol. 5, no. 93, pp. 76458–76463, 2015.

[42] D. Hulicova-Jurcakova, A. M. Puziy, O. I. Poddubnaya, F. Suárez-García, J. M. D. Tascón, and G. Q. Lu, "Highly stable performance of supercapacitors from phosphorus-enriched carbons," *J. Am. Chem. Soc.*, vol. 131, no. 14, pp. 5026–5027, 2009.

[43] L. L. Zhang, R. Zhou, and X. S. Zhao, "Graphene-based materials as supercapacitor electrodes," *J. Mater. Chem.*, vol. 20, no. 29, pp. 5983–5992, 2010.

[44] L. Hu *et al.*, "Highly conductive paper for energy-storage devices," *Proc. Natl. Acad. Sci.*, vol. 106, no. 51, pp. 21490–21494, 2009.

[45] C. Li, H. Bai, and G. Shi, "Conducting polymer nanomaterials: electrosynthesis and applications," *Chem. Soc. Rev.*, vol. 38, no. 8, pp. 2397–2409, 2009.

[46] K. Jurewicz, S. Delpeux, V. Bertagna, F. Beguin, and E. Frackowiak, "Supercapacitors from nanotubes/polypyrrole composites," *Chem. Phys. Lett.*, vol. 347, no. 1–3, pp. 36–40, 2001.

[47] H. An *et al.*, "Polypyrrole/carbon aerogel composite materials for supercapacitor," *J. Power Sources*, vol. 195, no. 19, pp. 6964–6969, 2010.

[48] R. Kötz and M. Carlen, "Principles and applications of electrochemical capacitors," *Electrochim. Acta*, vol. 45, no. 15–16, pp. 2483–2498, 2000.

[49] G. Zhang and X. W. Lou, "General solution growth of mesoporous NiCo2O4 nanosheets on various conductive substrates as high-performance electrodes for supercapacitors," *Adv. Mater.*, vol. 25, no. 7, pp. 976–979, 2013.

[50] C. Meng, C. Liu, L. Chen, C. Hu, and S. Fan, "Highly flexible and all-solid-state paperlike polymer supercapacitors," *Nano Lett.*, vol. 10, no. 10, pp. 4025–4031, 2010.

[51] G. Ma, H. Peng, J. Mu, H. Huang, X. Zhou, and Z. Lei, "In situ intercalative polymerization of pyrrole in graphene analogue of MoS2 as advanced electrode

material in supercapacitor," *J. Power Sources*, vol. 229, pp. 72–78, 2013.

[52] Y.-T. Weng, C.-B. Tsai, W.-H. Ho, and N.-L. Wu, "Polypyrrole/carbon supercapacitor electrode with remarkably enhanced high-temperature cycling stability by TiC nanoparticle inclusion," *Electrochem. commun.*, vol. 27, pp. 172–175, 2013.

[53] V. Branzoi, F. Branzoi, and L. Pilan, "Characterization of electrodeposited polymeric and composite modified electrodes on cobalt based alloy," *Mater. Chem. Phys.*, vol. 118, no. 1, pp. 197–202, 2009.

[54] R. Ullah, N. Khan, R. Khattak, M. Khan, M. S. Khan, and O. M. Ali, "Preparation of Electrochemical Supercapacitor Based on Polypyrrole/Gum Arabic Composites," *Polymers*, vol. 14, no. 2. 2022.

[55] M. Zhu *et al.*, "Highly Flexible, Freestanding Supercapacitor Electrode with Enhanced Performance Obtained by Hybridizing Polypyrrole Chains with MXene," *Adv. Energy Mater.*, vol. 6, no. 21, p. 1600969, 2016.

[56] B. Yue, C. Wang, X. Ding, and G. G. Wallace, "Polypyrrole coated nylon lycra fabric as stretchable electrode for supercapacitor applications," *Electrochim. Acta*, vol. 68, pp. 18–24, 2012.

[57] A. Yavuz, N. Ozdemir, and H. Zengin, "Polypyrrole-coated tape electrode for flexible supercapacitor applications," *Int. J. Hydrogen Energy*, vol. 45, no. 38, pp. 18876–18887, 2020.

[58] Y. Huang, M. Zhu, Z. Pei, Y. Huang, H. Geng, and C. Zhi, "Extremely Stable Polypyrrole Achieved via Molecular Ordering for Highly Flexible Supercapacitors," *ACS Appl. Mater. Interfaces*, vol. 8, no. 3, pp. 2435–2440, 2016.

[59] J. Lee *et al.*, "Polypyrrole Films with Micro/Nanosphere Shapes for Electrodes of High-Performance Supercapacitors," *ACS Appl. Mater. Interfaces*, vol. 9, no. 38, pp. 33203–33211, 2017.

[60] D. P. Dubal, S. V Patil, A. D. Jagadale, and C. D. Lokhande, "Two step novel chemical synthesis of polypyrrole nanoplates for supercapacitor application," *J. Alloys Compd.*, vol. 509, no. 32, pp. 8183–8188, 2011.

[61] C. emsp14N emsp14R Rao, A. emsp14K Sood, K. emsp14S Subrahmanyam, and A. Govindaraj, "Graphene: the new two-dimensional nanomaterial,"

Angew. Chemie Int. Ed., vol. 48, no. 42, pp. 7752–7777, 2009.

[62] K. S. Novoselov *et al.*, "Electric field effect in atomically thin carbon films," *Science (80-.).*, vol. 306, no. 5696, pp. 666–669, 2004.

[63] M. J. Allen, V. C. Tung, and R. B. Kaner, "Honeycomb carbon: a review of graphene," *Chem. Rev.*, vol. 110, no. 1, pp. 132–145, 2010.

[64] I. M. De la Fuente Salas, Y. N. Sudhakar, and M. Selvakumar, "High performance of symmetrical supercapacitor based on multilayer films of graphene oxide/polypyrrole electrodes," *Appl. Surf. Sci.*, vol. 296, pp. 195–203, 2014.

[65] X. Fan, Z. Yang, and N. He, "Hierarchical nanostructured polypyrrole/graphene composites as supercapacitor electrode," *RSC Adv.*, vol. 5, no. 20, pp. 15096–15102, 2015.

[66] J. Li, H. Xie, and Y. Li, "Fabrication of graphene oxide/polypyrrole nanowire composite for high performance supercapacitor electrodes," *J. Power Sources*, vol. 241, pp. 388–395, 2013.

[67] A. T. Smith, A. M. LaChance, S. Zeng, B. Liu, and L. Sun, "Synthesis, properties, and applications of graphene oxide/reduced graphene oxide and their nanocomposites," *Nano Mater. Sci.*, vol. 1, no. 1, pp. 31–47, 2019.

[68] X. Guo, N. Bai, Y. Tian, and L. Gai, "Free-standing reduced graphene oxide/polypyrrole films with enhanced electrochemical performance for flexible supercapacitors," *J. Power Sources*, vol. 408, pp. 51–57, 2018.

[69] J. Li and H. Xie, "Synthesis of graphene oxide/polypyrrole nanowire composites for supercapacitors," *Mater. Lett.*, vol. 78, pp. 106–109, 2012.

[70] Y. Liu, Y. Zhang, G. Ma, Z. Wang, K. Liu, and H. Liu, "Ethylene glycol reduced graphene oxide/polypyrrole composite for supercapacitor," *Electrochim. Acta*, vol. 88, pp. 519–525, 2013.

[71] R. Xu *et al.*, "Highly conductive, twistable and bendable polypyrrole–carbon nanotube fiber for efficient supercapacitor electrodes," *RSC Adv.*, vol. 5, no. 28, pp. 22015–22021, 2015.

[72] Y. Su and I. Zhitomirsky, "Asymmetric electrochemical supercapacitor, based on polypyrrole coated carbon nanotube electrodes," *Appl. Energy*, vol. 153, pp. 48–55, 2015.

[73] X. Lu *et al.*, “Polypyrrole/carbon nanotube nanocomposite enhanced the electrochemical capacitance of flexible graphene film for supercapacitors,” *J. Power Sources*, vol. 197, pp. 319–324, 2012.

[74] V. Vignesh, K. Subramani, M. Sathish, and R. Navamathavan, “Electrochemical investigation of manganese ferrites prepared via a facile synthesis route for supercapacitor applications,” *Colloids Surfaces A Physicochem. Eng. Asp.*, vol. 538, pp. 668–677, 2018.

[75] A. E. Elkholy, F. E.-T. Heakal, and N. K. Allam, “Nanostructured spinel manganese cobalt ferrite for high-performance supercapacitors,” *RSC Adv.*, vol. 7, no. 82, pp. 51888–51895, 2017.

[76] S. Sahoo, S. Dhibar, G. Hatui, P. Bhattacharya, and C. K. Das, “Graphene/polypyrrole nanofiber nanocomposite as electrode material for electrochemical supercapacitor,” *Polymer (Guildf).*, vol. 54, no. 3, pp. 1033–1042, 2013.

[77] J. Liu, J. An, Y. Ma, M. Li, and R. Ma, “Synthesis of a Graphene-Polypyrrole Nanotube Composite and Its Application in Supercapacitor Electrode,” *J. Electrochem. Soc.*, vol. 159, no. 6, p. A828, 2012.

[78] S. Biswas and L. T. Drzal, “Multilayered Nanoarchitecture of Graphene Nanosheets and Polypyrrole Nanowires for High Performance Supercapacitor Electrodes,” *Chem. Mater.*, vol. 22, no. 20, pp. 5667–5671, 2010.

[79] J. Cao *et al.*, “Three-dimensional graphene oxide/polypyrrole composite electrodes fabricated by one-step electrodeposition for high performance supercapacitors,” *J. Mater. Chem. A*, vol. 3, no. 27, pp. 14445–14457, 2015.

[80] T. Qian, C. Yu, S. Wu, and J. Shen, “A facilely prepared polypyrrole–reduced graphene oxide composite with a crumpled surface for high performance supercapacitor electrodes,” *J. Mater. Chem. A*, vol. 1, no. 22, pp. 6539–6542, 2013.

[81] A. Moyseowicz, K. Pająk, K. Gajewska, and G. Gryglewicz, “Synthesis of Polypyrrole/Reduced Graphene Oxide Hybrids via Hydrothermal Treatment for Energy Storage Applications,” *Materials*, vol. 13, no. 10, 2020.

[82] H. Fu, Z. Du, W. Zou, H. Li, and C. Zhang, “Carbon nanotube reinforced polypyrrole nanowire network as a high-performance supercapacitor

electrode," *J. Mater. Chem. A*, vol. 1, no. 47, pp. 14943–14950, 2013.

[83] B. Wang, J. Qiu, H. Feng, and E. Sakai, "Preparation of graphene oxide/polypyrrole/multi-walled carbon nanotube composite and its application in supercapacitors," *Electrochim. Acta*, vol. 151, pp. 230–239, 2015.

[84] Y. Chen, J. Li, L. Tan, Q. Li, X. Zhang, and H. Xu, "Electrodeposition of polypyrrole/functionalized-multiwalled carbon nanotubes composite and its application in supercapacitors," *Electrochim. Acta*, vol. 258, pp. 43–50, 2017.

[85] P. Li *et al.*, "Carbon nanotube-polypyrrole core-shell sponge and its application as highly compressible supercapacitor electrode," *Nano Res.*, vol. 7, no. 2, pp. 209–218, 2014.

[86] B. Mordina, R. Kumar, N. S. Neeraj, A. K. Srivastava, D. K. Setua, and A. Sharma, "Binder free high performance hybrid supercapacitor device based on nickel ferrite nanoparticles," *J. Energy Storage*, vol. 31, p. 101677, 2020.

[87] W. Raza, G. Nabi, A. Shahzad, N. Malik, and N. Raza, "Electrochemical performance of lanthanum cerium ferrite nanoparticles for supercapacitor applications," *J. Mater. Sci. Mater. Electron.*, vol. 32, no. 6, pp. 7443–7454, 2021.

[88] A. Soam *et al.*, "Synthesis of Nickel Ferrite Nanoparticles Supported on Graphene Nanosheets as Composite Electrodes for High Performance Supercapacitor," *ChemistrySelect*, vol. 4, no. 34, pp. 9952–9958, 2019.

[89] N. B. Thakare, F. C. Raghuwanshi, V. S. Kalyamwar, and Y. S. Tamgadge, "Reduced graphene oxide-ZnO composites based gas sensors: A review," in *AIP Conference Proceedings*, vol. 1953, 2018.

[90] S. M. Alshehri, J. Ahmed, A. N. Alhabarah, T. Ahamad, and T. Ahmad, "Nitrogen-Doped Cobalt Ferrite/Carbon Nanocomposites for Supercapacitor Applications," *ChemElectroChem*, vol. 4, no. 11, pp. 2952–2958, 2017.

[91] K. H. Kenari, A. Bahari, and M. S. Lashkenari, "Widely improved supercapacitance properties of zirconium-cobalt ferrite nanoparticles by N-doped graphene oxide as an electrode in supercapacitor," *J. Energy Storage*, vol. 74, p. 109274, 2023.

[92] S. A. Al Kiey, R. Ramadan, and M. M. El-Masry, "Synthesis and characterization of mixed ternary transition metal ferrite nanoparticles

comprising cobalt, copper and binary cobalt–copper for high-performance supercapacitor applications," *Appl. Phys. A*, vol. 128, no. 6, p. 473, 2022.

[93] L. Saleh Ghadimi, N. Arsalani, I. Ahadzadeh, A. Hajalilou, and E. Abouzari-Lotf, "Effect of synthesis route on the electrochemical performance of CoMnFeO4 nanoparticles as a novel supercapacitor electrode material," *Appl. Surf. Sci.*, vol. 494, pp. 440–451, 2019.

[94] T. V. Thu *et al.*, "Graphene-MnFe2O4-polypyrrole ternary hybrids with synergistic effect for supercapacitor electrode," *Electrochim. Acta*, vol. 314, pp. 151–160, 2019.

[95] L. Zhao, "Carbon nanofibers with radially grown graphene sheets derived from electrospinning for aqueous supercapacitors with high working voltage and energy density," *Nanoscale*, vol. 5, pp. 4902–4909, 2013.

[96] Q. Bao, "Graphene–polymer nanofiber membrane for ultrafast photonics," *Adv. Funct. Mater.*, vol. 20, pp. 782–791, 2010.

[97] Y. Wang, "Supercapacitor Devices Based on Graphene Materials," *J. Phys. Chem. C*, vol. 113, pp. 13103–13107, 2009.

[98] M. D. Stoller, S. Park, Y. Zhu, J. An, and R. S. Ruoff, "Graphene-Based Ultracapacitors," *Nano Lett.*, vol. 8, pp. 3498–3502, 2008.

[99] J. Yan, "Rapid microwave-assisted synthesis of graphene nanosheet/Co3O4 composite for supercapacitors," *Electrochim. Acta*, vol. 55, pp. 6973–6978, 2010.

[100] D. Bloor, R. Hercliffe, C. Galiotis, and R. Young, *Electronic properties of polymers and related compounds*, New York: Springer-Verlag, 1979.

[101] D. Zha, P. Xiong, and X. Wang, "Strongly coupled manganese ferrite/carbon black/polyaniline hybrid for low-cost supercapacitors with high rate capability," *Electrochim. Acta*, vol. 185, pp. 218–228, 2016.

[102] W. K. Chee, "Performance of Flexible and Binderless Polypyrrole/Graphene Oxide/Zinc Oxide Supercapacitor Electrode in a Symmetrical Two-Electrode Configuration," *Electrochim. Acta*, vol. 157, pp. 88–94, 2015.

[103] N. I. Zaaba et al., "Synthesis of Graphene Oxide using Modified Hummers Method: Solvent Influence," *Procedia Eng.*, vol. 184, pp. 469–477, 2017.

[104] H. A. Abdul Bashid, "Electrodeposition of Polypyrrole and Reduced Graphene Oxide onto Carbon Bundle Fibre as Electrode for Supercapacitor," *Nanoscale Res. Lett.*, vol. 12, p. 246, 2017.

[105] J. Kwon et al., "Facile hydrothermal synthesis of cubic spinel AB2O4 type MnFe2O4 nanocrystallites and their electrochemical performance," *Appl. Surf. Sci.*, vol. 413, pp. 83–91, 2017.

[106] S. Bose, "In-situ synthesis and characterization of electrically conductive polypyrrole/graphene nanocomposites," *Polymer*, vol. 51, pp. 5921–5928, 2010.

[107] F. Wu et al., "Reduced graphene oxide (RGO) modified spongelike polypyrrole (PPy) aerogel for excellent electromagnetic absorption," *J. Mater. Chem. A*, vol. 3, no. 27, pp. 14358–14369, 2015.

[108] A. Patterson, "The Scherrer formula for X-ray particle size determination," *Phys. Rev.*, vol. 56, p. 978, 1939.

[109] F. Zhou et al., "A facile low-temperature synthesis of highly distributed and size-tunable cobalt oxide nanoparticles anchored on activated carbon for supercapacitors," *J. Power Sources*, vol. 273, pp. 945–953, 2015.

[110] M. Toupin et al., "Charge storage mechanism of MnO2 electrode used in aqueous electrochemical capacitor," *Chem. Mater.*, vol. 16, pp. 3184–3190, 2004.

[111] K. Wang et al., "Mesoporous carbon nanofibers for supercapacitor application," *J. Phys. Chem. C*, vol. 113, pp. 1093–1097, 2009.

[112] P. Xiong et al., "Design and synthesis of ternary cobalt ferrite/graphene/polyaniline hierarchical nanocomposites for high-performance supercapacitors," *J. Power Sources*, vol. 245, pp. 937–946, 2013.

[113] H. Wang et al., "Ni(OH)2 nanoplates grown on graphene as advanced electrochemical pseudocapacitor materials," *J. Am. Chem. Soc.*, vol. 132, pp. 7472–7477, 2010.

[114] M. M. Costa, G. F. M. Pires Júnior, and A. S. B. Sombra, “Dielectric and impedance properties studies of the lead-doped (PbO)-Co_2Y type hexaferrite ($Ba_2Co_2Fe_{12}O_{22}$ (Co_2Y)),” *Mater. Chem. Phys.*, vol. 123, no. 1, pp. 35–39, 2010.

[115] I. L. Lera, S. Khasnabis, L. M. Wangatia, O. E. Femi, and P. C. Ramamurthy, “Polypyrrole@polyaniline-reduced graphene oxide nanocomposite support material and cobalt for the enhanced electrocatalytic activity of nickel phosphide

microsphere towards alkaline urea oxidation," *Mater. Res. Express*, vol. 8, no. 9, 2021.

[116] S. R. Sivakkumar, J. M. Ko, D. Y. Kim, B. C. Kim, and G. G. Wallace, "Performance evaluation of CNT/polypyrrole/MnO_2 composite electrodes for electrochemical capacitors," *Electrochim. Acta*, vol. 52, no. 25, pp. 7377–7385, 2007.

[117] H. Zhou and G. Han, "One-step fabrication of heterogeneous conducting polymers-coated graphene oxide/carbon nanotubes composite films for high-performance supercapacitors," *Electrochim. Acta*, vol. 192, pp. 448–455, 2016.

[118] M. Cui, L. Wei, S. J. Park, and S. Kim, "Electrochemical behaviors of binder-free CoFe-layered double-hydroxide-decorated hexagonal-flower-like $NiCo_2O_4$ as electrode for supercapacitors," *J. Alloys Compd.*, vol. 940, p. 168875, 2023.

[119] K. H. Kim, M. Yang, K. M. Cho, Y. S. Jun, S. B. Lee, and H. T. Jung, "High quality reduced graphene oxide through repairing with multi-layered graphene ball nanostructures," *Sci. Rep.*, vol. 3, 2013.

[120] I. Kotutha, E. Swatsitang, W. Meewassana, and S. Maensiri, "One-pot hydrothermal synthesis, characterization, and electrochemical properties of rGO/$MnFe_2O_4$ nanocomposites," *Jpn. J. Appl. Phys.*, vol. 54, 2015.

[121] S. D. Dhas, P. S. Maldar, M. D. Patil, M. R. Waikar, R. G. Sonkawade, and A. V. Moholkar, "Sol-gel synthesized nickel oxide nanostructures on nickel foam and nickel mesh for a targeted energy storage application," *J. Energy Storage*, vol. 47, p. 103658, 2022.

[122] M. Liu *et al.*, "Hierarchical composites of polyaniline-graphene nanoribbons-carbon nanotubes as electrode materials in all-solid-state supercapacitors," *Nanoscale*, vol. 5, no. 16, pp. 7312–7320, 2013.

[123] K. L. Routray and S. Saha, "Graphene nanoplatelets anchored into Ag-doped spinel $CoFe_2O_4$ nanohybrid: Synthesis, structural, electrical, superior dielectric, and room temperature-induced ferromagnetism performance for high-frequency device application," *Diam. Relat. Mater.*, vol. 141, p. 110680, 2024.

[124] S. Ramesh, K. Karuppasamy, Y. Haldorai, A. Sivasamy, H. S. Kim, and H. S. Kim, "Hexagonal nanostructured cobalt oxide @ nitrogen-doped multiwalled

carbon nanotubes/polypyrrole composite for supercapacitor and electrochemical glucose sensor," *Colloids Surf. B Biointerfaces*, vol. 205, p. 111840, 2021.

[125] B. Li, Y. Fu, H. Xia, and X. Wang, "High-performance asymmetric supercapacitors based on MnFe2O4/graphene nanocomposite as anode material," *Mater. Lett.*, vol. 122, pp. 193–196.

[126] A. Md Jani *et al.*, "Morphological and electrochemical properties of hybridized PPy/rGO composites," *Mater. Today: Proc.*, vol. 4, pp. 5138–5145, 2017.

[127] A. Jain *et al.*, "Fabrication of polypyrrole gas sensor for detection of NH3 using an oxidizing agent and pyrrole combinations: Studies and characterizations," *Heliyon*, vol. 9, 2023.

[128] V. Sharma, Y. Jain, M. Kumari, R. Gupta, S. K. Sharma, and K. Sachdev, "Synthesis and characterization of graphene oxide (GO) and reduced graphene oxide (rGO) for gas sensing application," *Macromol. Symp.*, vol. 376, no. 1, 2017.

[129] T. V. Thu *et al.*, "Graphene-MnFe2O4-polypyrrole ternary hybrids with synergistic effect for supercapacitor electrode," *Electrochim. Acta*, vol. 314, pp. 151–160, 2019.

[130] S. Ishaq *et al.*, "Facile synthesis of ternary graphene nanocomposites with doped metal oxide and conductive polymers as electrode materials for high-performance supercapacitors," *Sci. Rep.*, vol. 9, 2019.

[131] T. Ma *et al.*, "Facile synthesis of hierarchically porous rGO/MnZn ferrite composites for enhanced microwave absorption performance," *Synth. Met.*, vol. 265, 2020.

[132] L. P. Lingamdinne *et al.*, "Preparation and characterization of porous reduced graphene oxide based inverse spinel nickel ferrite nanocomposite for adsorption removal of radionuclides," *J. Hazard. Mater.*, vol. 326, pp. 145–156, 2017.

[133] W. Wang, Q. Hao, W. Lei, X. Xia, and X. Wang, "Ternary nitrogen-doped graphene/nickel ferrite/polyaniline nanocomposites for high-performance supercapacitors," *J. Power Sources*, vol. 269, pp. 250–259.

[134] G. Yu *et al.*, "Enhancing the supercapacitor performance of graphene/MnO2 nanostructured electrodes by conductive wrapping," *Nano Lett.*, vol. 11, pp. 4438–4442, 2011.

[135] K. V. Sankar and R. K. Selvan, "The preparation of MnFe2O4 decorated flexible graphene wrapped with PANI and its electrochemical performances for hybrid supercapacitors," *RSC Adv.*, vol. 4, pp. 17555–17566.

[136] Y. Ren, J. Wang, X. Huang, and J. Ding, "The synthesis of polypyrrole@Mn3O4/reduced graphene oxide anode with improved coulombic efficiency," *Electrochim. Acta*, vol. 186, pp. 345–352.

[137] X. Sun, H. Zhang, L. Zhou, X. Huang, and C. Yu, "Polypyrrole-coated zinc ferrite hollow spheres with improved cycling stability for lithium-ion batteries," *Small*, vol. 12, pp. 3732–3737.

[138] P. Xiong, "Ternary manganese ferrite/graphene/polyaniline nanostructure with enhanced electrochemical capacitance performance," *J. Power Sources*, vol. 266, pp. 384–392.

[139] D. P. Dubal and R. Holze, "All-solid-state flexible thin film supercapacitor based on Mn3O4 stacked nanosheets with gel electrolyte," *Energy*, vol. 51, pp. 407–412.

[140] A. Moyseowicz, A. Śliwak, E. Miniach, and G. Gryglewicz, "Polypyrrole/iron oxide/reduced graphene oxide ternary composite as a binderless electrode material with high cyclic stability for supercapacitors," *Compos. B Eng.*, vol. 109, pp. 23–29, 2017.

[141] S. D. Dhas *et al.*, "Sol-gel synthesized nickel oxide nanostructures on nickel foam and nickel mesh for a targeted energy storage application," *J. Energy Storage*, vol. 47, p. 103658, 2022.

[142] T. N. J. I. Edison *et al.*, "A novel binder-free electro-synthesis of hierarchical nickel sulfide nanostructures on nickel foam as a battery-type electrode for hybrid-capacitors," *Fuel*, vol. 276, p. 118077, 2020.

[143] F. Wu, A. Xie, M. Sun, Y. Wang, and M. Wang, "Reduced graphene oxide (RGO) modified spongelike polypyrrole (PPy) aerogel for excellent electromagnetic absorption," *J. Mater. Chem. A Mater.*, vol. 3, pp. 14358–14369, 2015.

[144] A. C. Lazanas and M. I. Prodromidis, "Electrochemical impedance spectroscopy─A tutorial," *ACS Meas. Sci. Au*, vol. 3, pp. 162–193, 2023.

List of Publications

I. List of Journal Publications

1) **Ansari Novman Nabeel**, Alok Jain, Kailash Chandra Juglan, Bhagwa, S., & Naeem, S. (2025). Structural, Morphological, and Electrochemical Characterization of Polypyrrole-Enhanced Reduced Graphene Oxide/NiCoFe2O4 Ternary Composite for High-Performance Supercapacitors. Energy Technology. https://doi.org/10.1002/ente.202402142

2) **Ansari Novman Nabeel**, Jain, A., Juglan, K. C., & Naeem, S. (2025). Synthesis and Optimization of Polypyrrole/Reduced Graphene Oxide/Nickel Cobalt Ferrite (PRNC) Ternary Composites for the Application in High-Performance Supercapacitors. *Transactions on Electrical and Electronic Materials*. https://doi.org/10.1007/s42341-025-00633-9

3) **Ansari Novman Nabeel**, Jain, A., Arora, S. K., & Nizeyimana, E. (2025). Synthesis of Binary Nanocomposite Conductive Polypyrrole and Reduced Graphene Oxide as Electrode Materials for High-Performance Supercapacitor. International Journal of Electrochemistry, 2025(1), 3179088. https://doi.org/https://doi.org/10.1155/ijel/3179088

4) **Ansari Novman Nabeel**, Alok Jain, Alharbi, T., Ahmad, A., Husain, D., & Naeem, S. (2025). Synthesis of PPy/rGO/NiCoFe2O4 Ternary Composite and rGO/NiCoFe2O4 Binary Composite Hybrid Materials for the Fabrication of Flexible Carbon Cloth Electrodes for Supercapacitors. Energy Storage, 7(1). https://doi.org/10.1002/est2.70105

5) Alok Jain, **Ansari Novman Nabeel**, Bhagwat, S., Kumar, R., Sharma, S., Kozak, D., Hunjet, A., Kumar, A., & Singh, R. (2023). Fabrication of polypyrrole gas sensor for detection of NH3 using an oxidizing agent and pyrrole combinations: Studies and characterizations. Heliyon, 9(7), e17611. https://doi.org/10.1016/J.HELIYON.2023.E17611

6) **Ansari Novman Nabeel**, Alok Jain, A., Kumar, R., Sharma, S., Li, C., Dwivedi, S. P., Naidu, K. S., Gupta, S., Kumar, A., Abbas, M., & Mohammed, K. A. (2025). Electrochemical properties of PPy/rGO/NiCoFe2O4 composites as advanced electrode materials for supercapacitors: a state-of-the-art review. In Ionics. Springer Science and Business Media Deutschland GmbH. https://doi.org/10.1007/s11581-024-05971-x

II. Book Chapter

1) **Ansari Novman Nabeel**, Alok Jain, A. (2024). Graphene and its perspective application as electrocatalytic materials. In S. Patra, S. K. Shukla, & M. Sillanpää (Eds.), *Electrocatalytic materials* (pp. 67–108). Springer. https://doi.org/10.1007/978-3-031-65902-7_3

III. List of Conferences Participation

1) Presented **Poster presentation** on "Synthesis of Polypyrrole by oxidation method and gas sensing" at the International Conference on Recent Advances in Fundamental and Applied Sciences (RAFAS 2021) held in Lovely Professional University, Punjab.

2) Presented **Oral presentation** on "Synthesis of Polypyrrole reduced graphene composite as an electrode for supercapacitor applications" at international conference on Recent advances in functional material (RAFM 2024) organized by department of physics, Delhi University.

3) Presented **Oral presentation** on "Facile synthesis of Ppy/rGO/NiCoFerrite nanocomposite as electrode material for supercapacitor applications" at the International Conference on Recent Advances in Fundamental and Applied Sciences (RAFAS 2024) held in Lovely Professional University, Punjab.

Publications

1. Publication (Research paper)

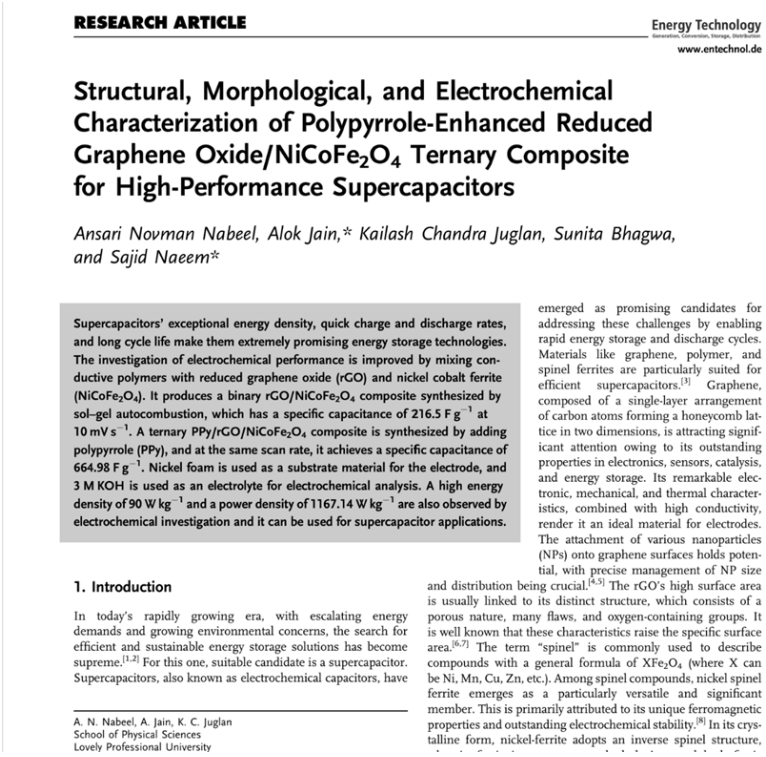

RESEARCH ARTICLE

Energy Technology
www.entechnol.de

Structural, Morphological, and Electrochemical Characterization of Polypyrrole-Enhanced Reduced Graphene Oxide/$NiCoFe_2O_4$ Ternary Composite for High-Performance Supercapacitors

Ansari Novman Nabeel, Alok Jain, Kailash Chandra Juglan, Sunita Bhagwa, and Sajid Naeem**

Supercapacitors' exceptional energy density, quick charge and discharge rates, and long cycle life make them extremely promising energy storage technologies. The investigation of electrochemical performance is improved by mixing conductive polymers with reduced graphene oxide (rGO) and nickel cobalt ferrite ($NiCoFe_2O_4$). It produces a binary rGO/$NiCoFe_2O_4$ composite synthesized by sol–gel autocombustion, which has a specific capacitance of 216.5 F g^{-1} at 10 mV s^{-1}. A ternary PPy/rGO/$NiCoFe_2O_4$ composite is synthesized by adding polypyrrole (PPy), and at the same scan rate, it achieves a specific capacitance of 664.98 F g^{-1}. Nickel foam is used as a substrate material for the electrode, and 3 M KOH is used as an electrolyte for electrochemical analysis. A high energy density of 90 W kg^{-1} and a power density of 1167.14 W kg^{-1} are also observed by electrochemical investigation and it can be used for supercapacitor applications.

1. Introduction

In today's rapidly growing era, with escalating energy demands and growing environmental concerns, the search for efficient and sustainable energy storage solutions has become supreme.[1,2] For this one, suitable candidate is a supercapacitor. Supercapacitors, also known as electrochemical capacitors, have emerged as promising candidates for addressing these challenges by enabling rapid energy storage and discharge cycles. Materials like graphene, polymer, and spinel ferrites are particularly suited for efficient supercapacitors.[3] Graphene, composed of a single-layer arrangement of carbon atoms forming a honeycomb lattice in two dimensions, is attracting significant attention owing to its outstanding properties in electronics, sensors, catalysis, and energy storage. Its remarkable electronic, mechanical, and thermal characteristics, combined with high conductivity, render it an ideal material for electrodes. The attachment of various nanoparticles (NPs) onto graphene surfaces holds potential, with precise management of NP size and distribution being crucial.[4,5] The rGO's high surface area is usually linked to its distinct structure, which consists of a porous nature, many flaws, and oxygen-containing groups. It is well known that these characteristics raise the specific surface area.[6,7] The term "spinel" is commonly used to describe compounds with a general formula of XFe_2O_4 (where X can be Ni, Mn, Cu, Zn, etc.). Among spinel compounds, nickel spinel ferrite emerges as a particularly versatile and significant member. This is primarily attributed to its unique ferromagnetic properties and outstanding electrochemical stability.[8] In its crystalline form, nickel-ferrite adopts an inverse spinel structure,

A. N. Nabeel, A. Jain, K. C. Juglan
School of Physical Sciences
Lovely Professional University

2. Publication (Research paper)

Transactions on Electrical and Electronic Materials
https://doi.org/10.1007/s42341-025-00633-9

Online ISSN 2092-7592
Print ISSN 1229-7607

REGULAR PAPER

Synthesis and Optimization of Polypyrrole/Reduced Graphene Oxide/ Nickel Cobalt Ferrite (PRNC) Ternary Composites for the Application in High-Performance Supercapacitors

Novman Nabeel[1] · Alok Jain[1] · Kailash Chandra Juglan[1] · Sajid Naeem[2]

Received: 10 November 2024 / Revised: 7 January 2025 / Accepted: 14 May 2025
© The Korean Institute of Electrical and Electronic Material Engineers 2025

Abstract
Supercapacitors (SCs) are gaining interest in next-generation energy storage due to their high energy density, fast charge-discharge capabilities, long cycle life, and cost-effectiveness. This investigation shows a scalable and straightforward method for synthesizing a ternary composite electrode composed of polypyrrole (PPy), reduced graphene oxide (rGO), and nickel cobalt ferrite ($NiCoFe_2O_4$). Initially, a binary rGO/$NiCoFe_2O_4$ composite was prepared using an auto-combustion technique, followed by the incorporation of PPy via a chemical oxidative process. A series of composites were created by varying the nickel-to-cobalt ratio, labeled PRNC0, PRNC20, PRNC40, PRNC60, PRNC80, and PRNC100 (PRNC = Polypyrrole Reduced Graphene Oxide Nickel Cobalt Ferrite). Further, XRD, FTIR, and FESEM characterization confirmed successful synthesis and the structural integrity of the composites. Electrochemical evaluations performed via cyclic voltammetry (CV), galvanostatic charge-discharge (GCD), and electrochemical impedance spectroscopy (EIS) on nickel foam electrodes revealed specific capacitances of 153.28, 238.5, 691.42, 275.7, 742.85, and 328.75 F/g for PRNC0, PRNC20, PRNC40, PRNC60, PRNC80, and PRNC100, respectively. GCD measurements provided specific capacitances of 157.25, 562, 550, 220, 585, and 252.5 F/g. The remarkable improvement in capacitance in the ternary composites highlights the synergistic effects of PPy, rGO, and $NiCoFe_2O_4$, indicating this method's potential for developing high-performance supercapacitor electrodes.

Keywords Supercapacitors · Electrodes · rGO · Polymer · $NiCoFe_2O_4$ · Nickel Foam

3. Publication (Research paper)

Wiley
International Journal of Electrochemistry
Volume 2025, Article ID 3179088, 9 pages
https://doi.org/10.1155/ijel/3179088

WILEY

Research Article

Synthesis of Binary Nanocomposite Conductive Polypyrrole and Reduced Graphene Oxide as Electrode Materials for High-Performance Supercapacitor

Ansari Novman Nabeel,[1,2] Alok Jain,[1,2] Sandeep Kumar Arora,[1,2] and Eric Nizeyimana[1,2]

[1]*Lovely Professional University, Phagwara 144401, Punjab, India*
[2]*University of Rwanda, Kigali, Rwanda*

Correspondence should be addressed to Alok Jain; alok.jain@lpu.co.in, Sandeep Kumar Arora; sandeep.16930@lpu.co.in, and Eric Nizeyimana; nizerik@yahoo.fr

Received 29 May 2024; Revised 26 September 2024; Accepted 28 April 2025

Academic Editor: Rajan Jose

Copyright © 2025 Ansari Novman Nabeel et al. International Journal of Electrochemistry published by John Wiley & Sons Ltd. This is an open access article under the terms of the Creative Commons Attribution License, which permits use, distribution and reproduction in any medium, provided the original work is properly cited.

In this study, a polypyrrole/reduced graphene oxide (PPy/rGO) composite material was synthesized through a chemical oxidative process, to tackle the persistent challenge of developing cost-effective and scalable electrode materials with high energy density and excellent charge storage capabilities for supercapacitor applications by integrating polypyrrole with rGO. The rGO was introduced into the polymerization process of polypyrrole. The composite underwent detailed investigation using different characterization techniques. Subsequently, analysis of the electrochemical properties included galvanostatic charge–discharge (GCD), cyclic voltammetry (CV), and electrochemical impedance spectroscopy (EIS). Nickel foam was used as the substrate material for the electrode. The PPy/rGO composite exhibited a remarkable specific capacitance of 365.1 F/g at a scan rate of 10 mV/s, as evidenced by CV, highlighting its excellent electrochemical properties. Moreover, the specific capacitance derived from GCD measurements surpassed expectations, reaching an impressive value of 375 F/g at a current density of 2 A/g. The corresponding energy density and power density for the specific capacitance of 375 F/g are 46.875 Wh/kg and 1140.20 W/kg, respectively. This further highlights the exceptional potential of this composite material

4. Publication (Research paper)

Energy Storage

WILEY

ENERGY STORAGE

RESEARCH ARTICLE

Synthesis of PPy/rGO/$NiCoFe_2O_4$ Ternary Composite and rGO/$NiCoFe_2O_4$ Binary Composite Hybrid Materials for the Fabrication of Flexible Carbon Cloth Electrodes for Supercapacitors

Ansari Novman Nabeel[1] | Alok Jain[1] | Talal Alharbi[2] | Akbar Ahmad[3] | Dilawar Husain[4] | Sajid Naeem[5]

[1]School of Physical Sciences, Lovely Professional University, Phagwara, India | [2]Department of Electrical Engineering, College of Engineering, Qassim University, Buraydah, Saudi Arabia | [3]Faculty of Science and Information Technology, MI College, Male, Maldives | [4]Department of Mechanical Engineering, Maulana Mukhtar Ahmad Nadvi Technical Campus, Malegaon, India | [5]Department of Applied Sciences, Maulana Mukhtar Ahmad Nadvi Technical Campus, Malegaon, India

Correspondence: Alok Jain (alok.jain@lpu.co.in) | Sajid Naeem (sajidnaeem@mmantc.edu.in)

Received: 17 May 2024 | **Revised:** 23 November 2024 | **Accepted:** 14 December 2024

Funding: The authors received no specific funding for this work.

Keywords: conductive polymer | flexible carbon cloth electrode | $NiCoFe_2O_4$ | polypyrrole | reduced graphene oxide | supercapacitors | ternary composite

ABSTRACT

This study presents a simple, scalable approach for synthesizing binary and ternary composites tailored for electrode materials, with a focus on supercapacitor applications. The composites were fabricated by integrating reduced graphene oxide (rGO) with $NiCoFe_2O_4$ metal oxides and the conductive polymer polypyrrole (PPy). The significance of this work lies in the development of supercapacitors, which are highly valued for their superior energy density, fast charge and discharge rates, prolonged life cycle, and cost-effectiveness. The binary composite, rGO/$NiCoFe_2O_4$, was synthesized using a sol–gel auto-combustion method, with carbon cloth serving as the electrode substrate for electrochemical testing. Electrochemical analysis showed that the rGO/$NiCoFe_2O_4$ binary composite exhibited a specific capacitance of 154 F/g at a scan rate of 10 mV/s. The addition of PPy resulted in the formation of the ternary composite, PPy/rGO/$NiCoFe_2O_4$, which demonstrated a markedly improved specific capacitance of 210 F/g under the same conditions, underscoring the synergistic effect of PPy. Furthermore, galvanostatic charge–discharge (GCD) analysis revealed specific capacitance values of 222.5 F/g at 1 A/g and 145 F/g at 2 A/g for the ternary composite, compared to 157.1 F/g and 110 F/g for the binary composite. The findings of this investigation emphasize the significant potential of the PPy/rGO/$NiCoFe_2O_4$ composite for the development of high-performance supercapacitors, leveraging the combined benefits of rGO, $NiCoFe_2O_4$, and PPy for superior energy storage capabilities.

1 | Introduction

The growing need in the contemporary association for sustainable energy has sparked substantial research efforts aimed at developing effective energy storage solutions, incorporating both supercapacitors and batteries [1]. In the past decade, supercapacitors have attracted significant interest owing to their outstanding characteristics; the features include high power density, rapid charge–discharge capabilities, and extended cycle life. These attributes complement the high-energy-density characteristics of batteries [1–3]. Polypyrrole (PPy) is an increasingly popular material for supercapacitors due to its exceptional properties, including high conductivity, long-term environmental stability, eco-friendliness, favorable

5. Publication (Research paper)

Heliyon 9 (2023) e17611

Contents lists available at ScienceDirect

Heliyon

journal homepage: www.cell.com/heliyon

Fabrication of polypyrrole gas sensor for detection of NH_3 using an oxidizing agent and pyrrole combinations: Studies and characterizations

Alok Jain [a], Ansari Novman Nabeel [b], Sunita Bhagwat [c], Rajeev Kumar [d,***], Shubham Sharma [e,f,g,*], Dražan Kozak [h], Anica Hunjet [h,**], Abhinav Kumar [i,****], Rajesh Singh [k,l]

[a] School of Physical Sciences, Lovely Professional University, Phagwara-144411, India
[b] Research Scholar, School of Physical Sciences, Lovely Professional University, Phagwara-144411, India
[c] Department of Physics, Abasaheb Garware College, Savitribai Phule University, Pune-411004, India
[d] School of Mechanical Engineering, Lovely Professional University, Phagwara-144411, India
[e] Deptt. of Mechanical Engg., University Centre for Research and Development (UCRD), Chandigarh University, Mohali, India
[f] School of Mechanical and Automotive Engineering, Qingdao University of Technology, Qingdao, 266520, China
[g] Department of Manufacturing Engineering and Materials Science, Faculty of Mechanical Engineering, Opole University of Technology, Opole, Poland
[h] University of Slavonski Brod, Mechanical Engineering Faculty in Slavonski Brod, Trg Ivane Brlić-Mažuranić 2, HR-35000 Slavonski Brod, Croatia
[i] University Center Varaždin, University North 104, Brigade 3, HR-42 000 Varaždin, Croatia
[j] Department of Nuclear and Renewable Energy, Ural Federal University Named After the First President of Russia, Boris Yeltsin, 19 Mira Street, 620002 Ekaterinburg, Russia
[k] Uttaranchal Institute of Technology, Uttaranchal University, Dehradun 248007, India
[l] Department of Project Management, Universidad Internacional Iberoamericana, Campeche C.P. 24560, Mexico

ARTICLE INFO

Keywords:
Polypyrrole
Monomers
Ferric chloride ($FeCl_3$)
Chemical oxidative polymerization
Conductivity
NH_3 gas response

ABSTRACT

The organic polymer known as Polypyrrole (Ppy) is synthesized when pyrrole monomers are polymerized. Excellent thermal stability, superior electrical conductivity, and environmental stability are all characteristics of Polypyrrole. Chemical oxidative polymerization was used to synthesize Ppy using Ferric chloride ($FeCl_3$) as an oxidizing agent and surfactant CTAB in aqueous solution. Oxidant ($FeCl_3$) to pyrrole varied in different molar ratios (2, 3, 4 and 5). It was found that increasing this ratio up to 4 increases PPy's conductivity. XRD, FTIR, and SEM were used to characterize Ppy. The conductive nature of Ppy was studied by I–V characteristics. The best conductive polymer is studied for the NH_3 gas response.

6. Publication (review paper)

Ionics
https://doi.org/10.1007/s11581-024-05971-x

REVIEW

Electrochemical properties of PPy/rGO/$NiCoFe_2O_4$ composites as advanced electrode materials for supercapacitors: a state-of-the-art review

Ansari Novman Nabeel[1] · Alok Jain[1] · Rajeev Kumar[2] · Shubham Sharma[3,4,5] · Changhe Li[5] · Shashi Prakash Dwivedi[6] · K. Satyam Naidu[7] · Sofia Gupta[8] · Abhinav Kumar[9,10,11] · Mohamed Abbas[12] · Kahtan A. Mohammed[13,14]

Received: 1 October 2024 / Revised: 15 November 2024 / Accepted: 21 November 2024
© The Author(s), under exclusive licence to Springer-Verlag GmbH Germany, part of Springer Nature 2024

Abstract
Due to their high storage capacity, excellent stability, and strong reversibility, supercapacitors are a major focus in current research and development. For a supercapacitor to exhibit these qualities, an effective electrode material is essential. This review explores the synthesis of electrodes using a composite of polypyrrole (Ppy), reduced graphene oxide (rGO), and nickel–cobalt ferrite (Ni-Co ferrite) for supercapacitor applications. The ternary composite exhibits a high specific capacitance of 250 F/g, outperforming binary composites like rGO/$MnFe_2O_4$, which typically achieve a specific capacitance of 147 F/g. Polypyrrole amorphous structure offers ideal voids for charge storage, while the plate-like rGO enhances charge accumulation. The magnetic nature of Ni-Co ferrite further contributes multifunctional properties, enabling applications in microwave absorption and toxic gas sensing for industrial gases like NH_3 and CO. These characteristics make the PPy/rGO/Ni-Co ferrite composite highly suitable for advanced energy storage, environmental monitoring, and flexible electronics applications.

7. Publication (Book Chapter)

Graphene and Its Perspective Application as Electrocatalytic Materials

Ansari Novman Nabeel and Alok Jain

Abstract The growing field of graphene-based electrocatalytic materials has positioned itself at the forefront of electrochemistry research, particularly in the context of electrochemical water-splitting. This pivotal process in sustainable energy conversion involves the generation of hydrogen and oxygen gases through the judicious application of an electric current. Graphene, a two-dimensional carbon allotrope distinguished by remarkable electronic, mechanical, and chemical properties, has emerged as a compelling candidate for advancing the efficiency and efficacy of electrocatalytic materials. This review comprehensively synthesizes the latest advancements and key insights into the utilization of graphene-based materials as electrocatalysts for water-splitting reactions. Delving into the synergistic interplay between graphene and catalytic components, such as metal nanoparticles or metal oxides, researchers have engineered hybrid structures exhibiting superior catalytic activity. The tunability of graphene's electronic properties through functionalization or doping provides a versatile platform for tailoring catalytic performance. The exploration of metal-free catalysts, including specific graphene derivatives, underscores the potential to reduce reliance on expensive and rare metal catalysts, thereby advancing the economic viability of electrochemical water-splitting technologies. As the demand for sustainable energy intensifies, this review endeavors to offer significant insights into the difficulties and obstacles encountered in the field. The collective efforts highlighted in this review showcase the rich landscape of research in graphene-based electrocatalytic materials, offering a foundation for cleaner and more sustainable electrochemical water-splitting processes.

Keywords Graphene · Electrocatalytic materials · Carbon materials · Water splitting · CNT · Metal nanoparticles

List of Conference Participation

1. Conference 1

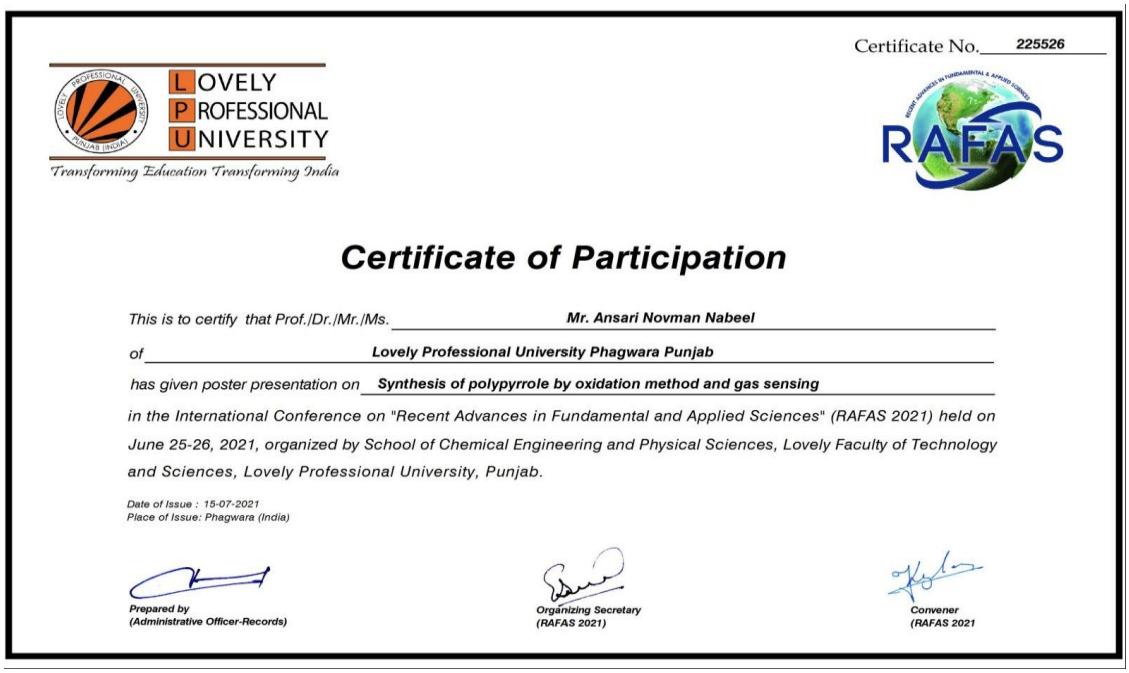

Certificate No. 225526

LOVELY PROFESSIONAL UNIVERSITY
Transforming Education Transforming India

RAFAS

Certificate of Participation

This is to certify that Prof./Dr./Mr./Ms. **Mr. Ansari Novman Nabeel**

of **Lovely Professional University Phagwara Punjab**

has given poster presentation on **Synthesis of polypyrrole by oxidation method and gas sensing**

in the International Conference on "Recent Advances in Fundamental and Applied Sciences" (RAFAS 2021) held on June 25-26, 2021, organized by School of Chemical Engineering and Physical Sciences, Lovely Faculty of Technology and Sciences, Lovely Professional University, Punjab.

Date of Issue : 15-07-2021
Place of Issue: Phagwara (India)

Prepared by
(Administrative Officer-Records)

Organizing Secretary
(RAFAS 2021)

Convener
(RAFAS 2021

2. Conference 2

ATMA RAM SANATAN DHARMA COLLEGE

UNIVERSITY OF DELHI

Accredited Grade 'A++' By NAAC || All India 6th Rank in NIRF (Ministry of Education)

2nd International Conference on

Recent Advances in Functional Materials (RAFM-2024)

Under the aegis of IQAC and DBT (GoI) star college scheme

Certificate of Oral Presentation

This is to certify that Prof./Dr./Mr./Ms.

ANSARI NOVMAN NABEEL MOHAMMAD HAROON

Lovely Professional University, Phagwara, Punjab

has presented his/her research work as oral presentation titled

Synthesis of Polypyrrole and Reduced Graphene composite as an electrode for supercapacitor applications.

in 2nd International Conference on "Recent Advances in Functional Materials" (RAFM-2024) organised by Department of Physics under the aegis of IQAC ARSD College, University of Delhi & DBT (GoI) Star College during March 14-16, 2024 via online mode.

Dr. Manish Kumar
Convener, RAFM-2024

Prof. Vinita Tuli
Coordinator, IQAC

Prof. Gyantosh Kumar Jha
Principal, ARSD College

Certificate No: ARSD/RAFM-2024/OT/029

3. Conference 3

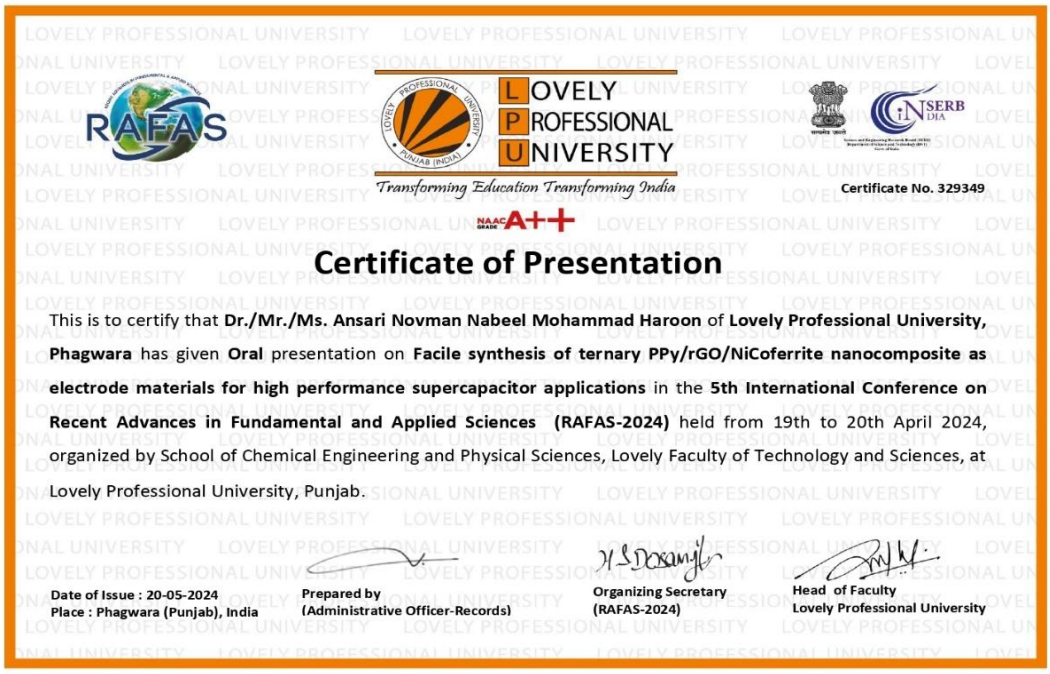

LOVELY PROFESSIONAL UNIVERSITY
Transforming Education Transforming India
NAAC A++
Certificate No. 329349

Certificate of Presentation

This is to certify that **Dr./Mr./Ms. Ansari Novman Nabeel Mohammad Haroon** of **Lovely Professional University, Phagwara** has given **Oral** presentation on **Facile synthesis of ternary PPy/rGO/NiCoferrite nanocomposite as electrode materials for high performance supercapacitor applications** in the **5th International Conference on Recent Advances in Fundamental and Applied Sciences (RAFAS-2024)** held from 19th to 20th April 2024, organized by School of Chemical Engineering and Physical Sciences, Lovely Faculty of Technology and Sciences, at Lovely Professional University, Punjab.

Date of Issue : 20-05-2024
Place : Phagwara (Punjab), India

Prepared by
(Administrative Officer-Records)

Organizing Secretary
(RAFAS-2024)

Head of Faculty
Lovely Professional University